Spring 2008

Modeling and simulations of diphasic composites for development of high energy density dielectrics

Sandeep K. Patil

Department: Materials Science and Engineering

MODELING AND SIMULATIONS OF DIPHASIC COMPOSITES FOR DEVELOPMENT OF HIGH ENERGY DENSITY DIELECTRICS

by

SANDEEP KESHARSINGH PATIL

A DISSERTATION

Presented to the Faculty of the Graduate School of the

MISSOURI UNIVERSITY OF SCIENCE AND TECHNOLOGY

In Partial Fulfillment of the Requirements for the Degree

DOCTOR OF PHILOSOPHY

in

MATERIALS SCIENCE AND ENGINEERING

2008

Approved by:

R. W. Schwartz, Advisor
W. Huebner, Co-Advisor
M. Y. Koledintseva
R. K. Brow
G. Hilmas
J. D. Smith

PUBLICATION DISSERTATION OPTION

This dissertation consists of the following three articles that have been, or will be, submitted for publication as follows:

Pages 21-54 have been submitted to the Journal of Applied Physics.

Pages 55-82 are intended for submission to IEEE Transactions on Dielectric and Insulations.

Pages 83-110 are intended for submission to Journal of Applied Computational Electromagnetics Society Newsletter.

ABSTRACT

This doctoral research is focused on analytical and numerical modeling of diphasic composites for use in high energy density capacitors for pulsed power applications. An analytical model is presented based on an equivalent capacitance/impedance circuit used to express the effective permittivity of a composite dielectric with complex-shaped inclusions as functions of frequency and inclusion volume fraction. Zero-three (0-3) types of composites are investigated using this model. The results of this model are compared with different known effective medium theories (Maxwell Garnett, logarithmic, Bruggeman, series, and parallel mixing rules). Model predictions are also compared with published experimental data and are found to be in good agreement.

Electrostatic field distribution characteristics and energy storage magnitudes for diphasic dielectrics containing high-permittivity inclusions in a low permittivity host phase (0-3 composite) have been evaluated analytically and numerically. Field distribution and energy storage were studied as a function of dielectric contrast (ratio of inclusion to host permittivity) and inclusion volume fraction. Information obtained from these studies was used to consider optimized diphasic dielectric traits that would lead to increases in energy density and breakdown behavior. Results of these simulations were also compared to the Maxwell Garnett (MG) mixing rule and the upper limit of applicability of the MG formulation in terms of inclusion volume fraction was established. It was determined that this limit was a function of the dielectric contrast.

ACKNOWLEDGMENTS

Pursuing a PhD was a dream for me. I always looked up to the people who had the distinction of successful completion of a PhD. This journey towards completion of a PhD would not have been possible without kind help and support of many important people. First and foremost, I would like to thank my advisor Dr. Robert Schwartz. Dr. Schwartz has been very kind and encouraging all along, right from helping me prepare for my qualifier exams to comprehensives, he has been looking after my progress patiently. I would also like to thank my co-advisor Dr. Wayne Huebner who has been my strongest supporter all along. Dr. Huebner has always made sure that my confidence remains high. Both Dr. Schwartz and Dr. Huebner have helped me tremendously with their unstinted support in my research ideas and progress of my PhD.

The one person to whom I am indebted immensely is Dr. Marina Koledintseva. Dr. Marina not only took me under her wings but also helped me understand and grow in the field of electromagnetics. She has been the person who has never shied away from any of my questions. I would also like to express my gratitude to Dr. Eugene Furman of Penn State and Dr. Konstantin Rozanov of Russian Academy of Sciences as several discussions with them helped me navigate my PhD research.

I would also like to thank Dr. Matt O'Keefe for funding my PhD studies. I would like to acknowledge the advice and guidance of my esteemed committee members Dr. Richard Brow, Dr. Gregory Hilmas, Dr. Jeffrey Smith. I would also like to express my appreciation for Dr. Signo Reis, Dr. L. C. Pathak, Dr. Wei Li, Christopher Larson, and Ron Haas for helping me at various stages of my PhD. I would also like to thank my group members Dr. Manoj Narayanan, Xuhui Lu and numerous friends in Rolla who made my stay in Rolla comfortable.

I would like to thank my wife Pradnya for being supportive of me along. She has been my pillar of support and has always had faith in my abilities. Without her contribution it would have been very difficult for me to complete my PhD. I would also like to thank my beloved parents Dr. K. J. Patil and Mrs. Patil, my in-laws Mr. and Mrs. P. Y. Patil and my siblings. Last and not the least, I would like thank the God almighty for showing the way.

TABLE OF CONTENTS

LIST OF ILLUSTRATIONS

SECTION 1

PAPER 1

SECTION 4

LIST OF TABLES

Table Page

1. INTRODUCTION

1.1. IDENTIFICATION AND SIGNIFICANCE OF OPPORTUNITY

Recent advances in dielectric materials have been driven by critical requirements in Department of Defense (DoD) pulsed power and power distribution systems. Electric guns and high power microwave systems require capacitors with 10-500 MJ energy storage capabilities [1, 2] and a rapid discharge rate (nanoseconds to milliseconds). The need for inexpensive, fast response capacitors with high volumetric efficiency (15-30 J/cm^3) has become acute. Dielectric energy density is most appropriately described using Eq. 1

$$U_D = \int_0^{E_{\max}} \varepsilon_o \varepsilon_r E \, dE \qquad (1)$$

In Eq. 1, U_D is the energy density (J/cm^3), ε_r is the relative permittivity (dielectric constant), ε_o is the permittivity of free space and E is the electric field (V/m). From this fundamental equation, it can be seen that to achieve the requisite performance characteristics, dielectric materials with high breakdown strength and permittivity must be developed.

Inorganic ceramic materials (**I**) usually have very high permittivity ($2000 \le \varepsilon_r \le 20{,}000$) but are significantly limited by their low breakdown strength ($E_B < 100$ kV/cm). The other end of the spectrum with regard to these properties is occupied by polymeric materials (**O**). Polymers usually have very high breakdown

strength ($E_B \approx 1-3\cdot 10^8 V/cm$) [3-5] and provide ease of fabrication. However, polymers have considerably lower permittivities ($2 \le \varepsilon_r \le 6$) .

Figure 1.1 shows the current state of the art for pulsed power capacitor materials [6], which have energy storage densities of approximately 1-3 J/cm^3. For comparison, state of the art power electronic capacitors have energy storage densities one order of magnitude lower than pulsed power capacitors. The DoD goal for dielectric materials is to be able to store approximately 30 J/cm^3 at an applied field of around 4 MV/cm. The DoD goal for a packaged capacitor is 10 J/cm^3 considering the loss in energy density that occurs when the dielectric is incorporated in a packaged component.

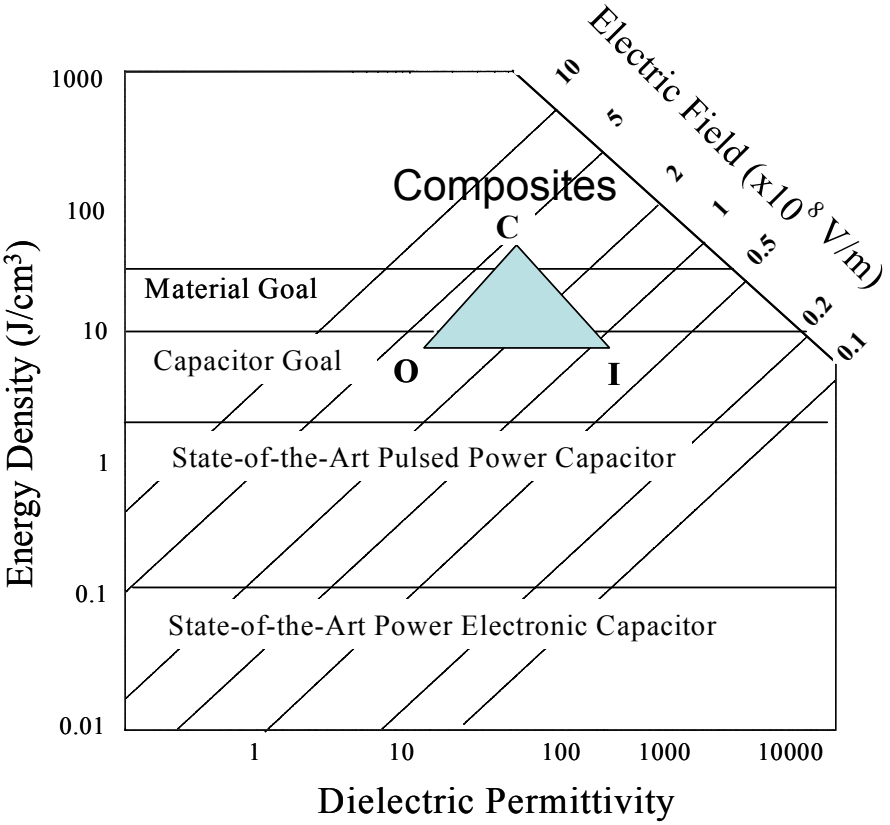

Figure 1.1 Comparison of dielectric materials performance with targeted goals for future applications [6].

Composite dielectrics (**C**) offer the unique opportunity to synergistically combine the high permittivity of inorganic filler materials with the high breakdown strength of an organic polymer host material. Naturally, this route of composite dielectrics has attracted considerable attention [6-17] and the effective permittivities of composite dielectrics have been thoroughly investigated. Along with ceramic-polymer composites, another composite system that has attracted attention are glass-ceramic dielectrics. This system is best described as a continuously connected minor phase (low volume fraction, typically less than 10%) separating the major phase into discrete localized volumes. In this composite dielectric the low permittivity phase is the glass phase with high breakdown strength which is continuously connected and ceramic grains ($BaTiO_3$, $PbTiO_3$) are the high permittivity phase [18-20].

The dielectric properties of composites are controlled by several parameters, including the electrical properties of the filler and host materials, the wetting properties of the host on the filler, since this may impact interfacial polarization response, and other filler properties. The inclusion/filler properties of potential importance are inclusion size, shape, distribution, orientation and volume fraction. Along with these properties, dielectric susceptibility is also significant. Dielectric susceptibility is the index of how susceptible the material is to being polarized by an applied electric field. In addition to these parameters there is a microstructural dependence of dielectric response to applied electric field. Microstructure and dielectric susceptibility govern the electric field splitting that takes place in the composite. For a composite system containing a mixture of insulating phases, the electric lines of flux will tend to distribute themselves according to the relative susceptibilities of the constituent phases and their microstructures. This

should either lead to property enhancement or dilution in multiphase mixtures. Modeling composite electrical response can provide an avenue to fundamentally understand the impact of tailoring the properties of the individual phases on the possible enhancement of energy density. Modeling of composites also affords the opportunity to develop guiding principles for the design of future dielectrics. It is the goal of this research effort that many interesting qualitative characteristics identified by modeling will be generic for broader classes of composite dielectric systems. Considering the opportunity afforded by composites, advancement in theoretical understanding of the local electrical response of composites is critical.

1.2. DIELECTRIC COMPOSITE NOMENCLATURE

The properties of mixtures of phases depend on the distribution of the components [21]. The concept of "connectivity" is useful in classifying different types of mixtures. The foundation of this nomenclature has emerged from the work done in the area of piezoelectric transducers [22] and the nomenclature is based on the fact that any phase in a mixture may be self-connected in zero, one, two or three dimensions. Thus, randomly dispersed and separated particles have a connectivity of 0, whereas the medium surrounding them has a connectivity of 3. A disc containing a rod-shaped phase extending between its major surfaces has connectivity of 1 with respect to the rods and of 3 with respect to the intervening phase. A mixture consists of two phases which are in the form of layers organized one on top of each other would have connectivity of 2-2. Figure 1.2 shows the classification of dielectric composites based on the connectivity of the phases.

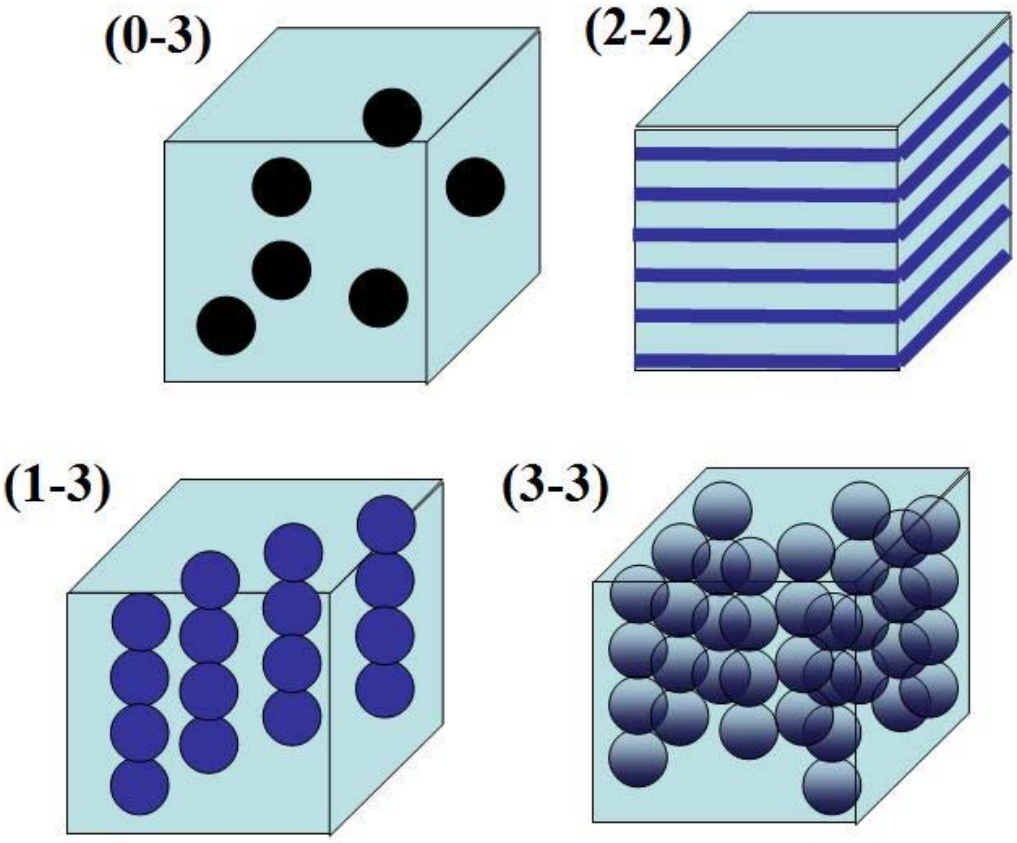

Figure 1.2 Dielectric composites classification based on the connectivity of individual phases.

The real world dielectric composites that represent this classification are listed as below:

- Isolated organic or oxide particles dispersed in a polymer matrix: 0-3
- Laminated sheets of organics bonded to an inorganic: 2-2
- Particles aligned in chains within a silicone or epoxy matrix: 1-3
- Glass-ceramic systems: (e.g. Corning ware): 3-3

Composite connectivity strongly influences energy storage and breakdown strength. When an electric field is applied across a heterophasic dielectric, the lines of flux will tend to concentrate in the phase with greatest dielectric susceptibility (dielectric

constant). The average dielectric constant for such diphasic composites depends critically upon the relative values of susceptibility, the volume concentration of the higher susceptibility phase, and the manner of mixing of the two phases, specifically the extent to which the lower susceptibility component interrupts effective flux passage [23]. The key factor is the electrostatic field distribution in the composite, which includes electric field enhancement in the phase with lower permittivity and electrical field penetration in the phase with high permittivity.

1.3. THEORETICAL FOUNDATION

1.3.1 The Philosophy of Homogenization of Mixtures. Understanding the properties of a multi-phase material via the homogenization of electrical properties has been an area of intense mathematical research since the 1850's [24-32]. The process of homogenization has been persistently viewed as an averaging procedure**.**

For example, when the density of matter is calculated, a division of mass by volume gives density. In case of a mixture, calculation of density still just requires that the total mass be divided by total volume. Irrespective of structural scale, the geometrical distribution of the components that compose the sample does not matter. This makes homogenization of the density of a mixture appear simply like an averaging procedure.

Electrical properties, however, cannot be homogenized using the same approach as density. Stated precisely, homogenization of heterogeneous materials can be defined as a process leading to prediction of macroscopic response with fewer parameters than needed for a full description of the original object [4]. For example, heterogeneous dielectric bodies can be accurately described with a single *effective permittivity (* ε_{eff}).

The homogenization process can only be applied under specific circumstances that depend on a consideration of the length scales that characterize the heterogeneity. The microstructure of snow is a classic example. If snow is viewed from a very long distance (more than few meters away) as is seen in Figure 1.3, it appears uniform and homogenous. However, on closer examination (optical microscopic examination), as can be seen from Figure 1.3 (b), the same uniform and homogenous structure appears to be clearly heterogeneous, with ice grains and air pores present as distinct sub regions. Two parameters contribute to this homogenization; one is the distance of the observer from the snow and the other is the wavelength of light that carries the observation signal. In Figure 1.3 (a), a distinct heterogeneous microstructure still exists, but in a homogenized way. A relevant parameter in homogenization problems is the ratio between the size of the inhomogenities and the wavelength of the electromagnetic field that is used. If this ratio is much smaller than unity, the medium appears homogenous to the wave. However, when the particle size is of the order of the wavelength, the particles start to scatter radiation and then concepts of average parameters, such as ε_{eff}, lose their usability [2]. The utility, and limitations, of mixing theories to predict effective properties became apparent with the advent of microwave communication. Because microwave signals are able to travel long distances and their wavelength ($200\,\mu m$ – few mm) is much greater than snow heterogeneities (less than $100\,\mu m$) , by proper application of mixing theories, it became possible to predict the amount of ice and water in snow cover.

Mixing theories have a similar role to play in the field of composite dielectrics as they could give critical insight into the selection of constituent phases and volume

fractions suitable for increased effective permittivities, which is one of the key factors in the design of composites with increased energy density.

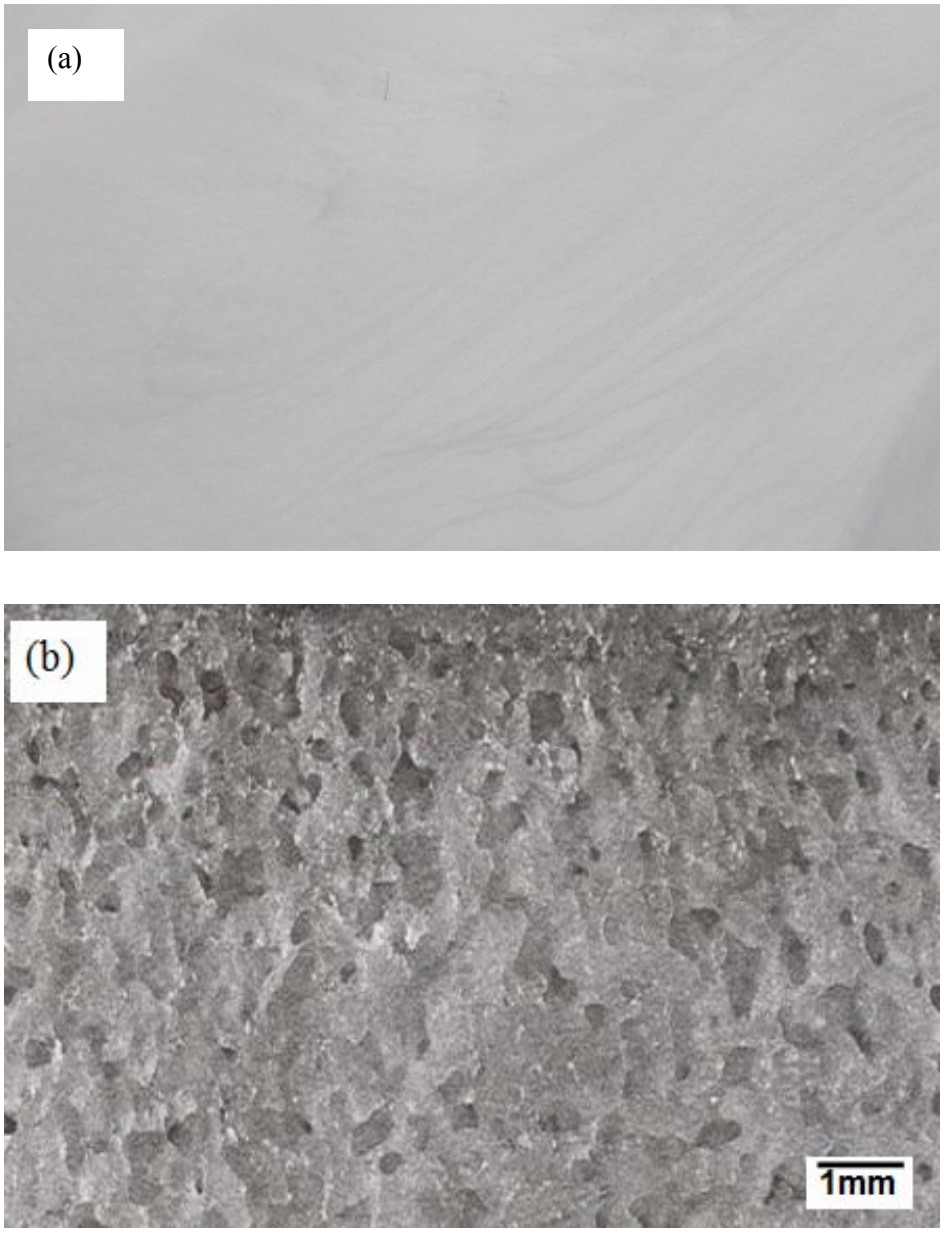

Figure 1.3 Snow image from a distant view and an optical micrograph of vertical cut seasonal snow layer [24].

1.3.2. Development of Analytical Mixing Theories. The first quantitative studies regarding the dielectric properties of mixtures or conglomerates of different materials began to emerge around the mid-1800s. Poisson's theory of magnetism helped Octavio F. Mossotti formulate equations for the effect of a dielectric inclusion on its environment [25]. Clausius studied the relative effective dielectric constant ε_r of a collection of molecules and showed that the ratio $\frac{\varepsilon_r - 1}{\varepsilon_r + 2}$ is proportional to number of molecules in the unit volume [26]. In later literature, an equation containing this ratio was referred to as the Clausius Mossotti relation. In 1864, J. C. Maxwell unified electricity and magnetism and discovered the electromagnetic nature of light, which opened possibilities to connect the optical and dielectric properties of matter. Lorentz developed an extensive theory of the refractive index of matter assuming that the density of matter is determined by the density of rigid molecules. This resulted in the famous work which later came to be known as the Lorenz-Lorentz formula [27-29]. Lord Rayleigh calculated the effective material permittivity of a mixture based on spherical or cylindrical inclusions in a rectangular lattice and his results gave a connection to the properties of inclusions and a macroscopic medium [30]. Maxwell Garnett was the first to derive the now famous relation between the effective dielectric constant of a medium with metal spheres possessing specific optical properties and occupying random positions in a host medium [31]. This formalism, which also describes volume fraction effects, has been modified several times and also extended to insulating inclusions in an insulating host medium.

There have been other scientists who have worked on homogenization theories, the most prominent being Bruggeman, Ketteler, Havelock, and Lichtenecker.

Bruggeman's work led to a new mixing approach with mixing rules that were qualitatively different than earlier homogenization principles [32]. In the area of material science, Bruggeman's theory also carries the name of *effective medium theory* (EMT).

The foundation of effective medium theory is to focus on one particular inclusion and to replace the surrounding random medium by an effective homogeneous medium. The effective medium is determined self-consistently by taking into account the fact that any other inclusion could have been chosen [24, 32-35]. EMT is a technique meant to bridge the gap between a detailed description of the fine grained features of the heterostructure, and a macroscopic description, which treats the composite as a completely homogenous entity [36]. Weiner proposed form factors for inclusions with cylindrical and lamellar shape [37]. Rushman and Striven used these form factors to explain the impact of porosity on the dielectric constant of barium titanate [38]. Further experimental evidence for the Weiner mixing rule and its ability to take into account porosity was confirmed by Kingery in 1960 [39].

The empirically derived logarithmic mixing rule is widely applied for fitting experimental data [40]. The logarithmic mixing rule was proposed by Lichtenecker and calculates effective permittivity by taking averages of logarithms of permittivities and volume fraction of constituent phases. Payne et al. in 1973 proposed the brick wall model as an approximation for predicting the effective dielectric properties of composite microstructures [23]. Payne has also presented a detailed account of the history of mixing theories, their origin and inadequacies. The central idea of a brick wall model is that microstructure can be approximated by a brick wall model if the boundary phase is continuously connected. Figure 1.4. presents this method of approximation of the

microstructure. The brick wall model assumes cubes of major phases which are separated by an intergranular boundary phase and identified two extreme cases based on dielectric susceptibility ratios.

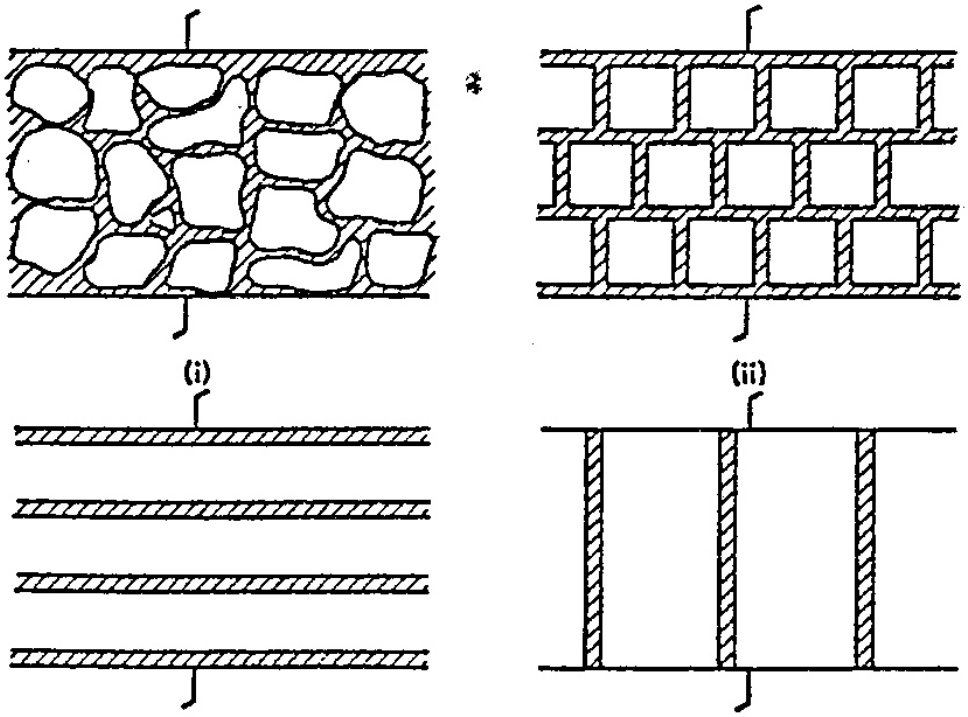

Figure 1.4 Two extreme cases of brick wall model. (i) series mixing and (ii) parallel mixing [23]

These two extreme cases assume that if both phases are insulators, the lines of flux will preferentially concentrate in the phase with highest dielectric susceptibility (χ). Under this assumption:

- When $\chi_1 >> \chi_2$ the lines of flux prefer the major phase and the low susceptibility boundaries normal to the flux path are important. This reduces the brick wall model to a series mixing rule, as given in expression below:

$$\frac{1}{\varepsilon_{eff}} = \frac{\nu_1}{\varepsilon_1} + \frac{\nu_2}{\varepsilon_2} \tag{2}$$

- For the other extreme of $\chi_2 >> \chi_1$ the lines of flux concentrate in the minor phase and brick wall model simplifies to parallel mixing rule.

$$\varepsilon_{eff} = \nu_1 \cdot \varepsilon_1 + \nu_2 \cdot \varepsilon_2 \tag{3}$$

Payne also used an equivalent circuit approach to predict the effective properties as a function of frequency for these extreme cases. The equivalent circuits approach was first suggested by J. C. Maxwell for a simplified system (dielectric layers) and was extended by Payne to the brick wall case with primary focus on a dispersive diphasic series capacitor.

1.3.3 Numerical Modeling of Composites. Analytical modeling of composites started in the mid 1850's and has significantly added to our understanding of diphasic systems. In contrast, numerical modeling has only recently started to gain ground within the past two decades, assisted by advances in simulation techniques [36].

Typically, in the numerical approaches the dielectric composite is sliced into small cells and the electrostatic fields are solved in a finite number of points. The most prominent among these have been Monte Carlo simulations (MC) [41], finite element method (FEM) [42, 43], finite difference method [44] and boundary integration method [45, 46]. Wakino et al. reported modeling effective permittivity by using combined FEM with MC simulations [41]. Ang et al. presented results for modeling the dielectric constant and loss of composites that consist of phase A with different shapes (circles and triangles) distributed in a square matrix phase B. They investigated the shape attributes in

2-dimensions and also calculated the electric field distribution as a function of distance through the 2 dimensional composite. They also investigated the quantitative impact of inclusion shape on the local electric field distribution in diphasic composites.

It is noteworthy to consider the contribution of Sareni et al., who through the use of numerical analysis techniques calculated the effective dielectric constant of periodic composites [45], then random composites [47]. These authors also analyzed the complex effective permittivity of a lossy composite material [48]. Myroshnychenko et al. [36] have exhaustively developed an algorithm for estimation of the complex permittivity of two-dimensional, diphasic statistically isotropic heterostructures, and compared their results with different effective medium approaches. They investigated electric field distribution in 2D composites with two cases of percolating and non-percolating systems using FEM simulations and compared the results to EMT theories. Since their studies were in two dimensions, the permittivity predictions were investigated as a function of surface fractions. In these studies, the geometric shape of the inclusion was restricted to spheres and discs and inclusions were randomly distributed in the host matrix. They found the complex effective permittivity deviated markedly from that of the predictions of simple mixture rules and EMT. They found that the electrostatic field distribution was governed by the inclusion proximity and relative orientation of the closest neighbor. They also stressed the need for performing 3D simulations and their studies were for very low dielectric contrast cases (less than 2) and fixed surface fraction. An investigation of the electrostatic field distribution as a function of dielectric contrast and inclusion volume fraction is still needed.

1.3.4. Difficulties and limitations in Mixing Theories. The simplest Maxwell Garnett formulation is for a mixture of a host material with relative permittivity ε_h and spherical inclusions with relative permittivity ε_s as given by:

$$\varepsilon_{efMG} \cong \varepsilon_h + \frac{3 f_s \varepsilon_h (\varepsilon_s - \varepsilon_h)/(\varepsilon_s + 2\varepsilon_h)}{1 - f_s (\varepsilon_s - \varepsilon_h)/(\varepsilon_s + 2\varepsilon_h)}, \tag{4}$$

where $f_s = \frac{V_S}{V_\Sigma}$ is the volume fraction of spherical inclusions in the total mixture. Here is V_S represented volume of inclusion phase and V_Σ represents the total volume of the composite. Maxwell Garnett theory, which has been the most widely used mixing theory, has inherent limitations in terms of predicting the effects of inclusion size. Maxwell Garnett theory is satisfactory only when exact interparticle interactions are not significant, *i.e.*, for low concentrations of inclusions in a dielectric host [49]. MG theory is applicable for inclusions of any arbitrary ellipsoidal shape, including spheres, spheroids, cylinders, and disks, through the introduction of depolarization factors [50]. However, any arbitrary shape of an inclusion cannot be accurately taken into account, other than by approximating the shape by the closest ellipsoidal shape. This limits the applicability of the MG theory [51] and suggests an opportunity for development of mixing theory that is free from inclusion size dependence and shape limitations.

It has been reported that the Maxwell Garnett (MG) formulation for diphasic dielectrics can be applied up to 10% volume fraction of inclusions, that is, for comparatively dilute mixtures [52]. Most mixing rules assume that the lines of electric flux are *not distorted* by the particles, and hence, there are inherent limitations in

accurately predicting the energy storage capabilities of composites [53]. However, for heterogeneous composites, the electric lines of flux will tend to distribute according to the permittivity ratio of the host and the inclusion phases, as discussed earlier. Local inhomogeneities in electric field distribution, *i.e.*, field enhancement in the low permittivity phase and field penetration in the high permittivity phase, are not taken into account by classical mixing theories, leading to errors in prediction of dielectric response.

Effective Medium Theories are based on an assumption that the local electric and magnetic fields are the same in the volume occupied by each component of the composite material. Stated otherwise, the energy density is homogenous by construction, which is not the case in real world systems. Also, EMT do not allow for correlations between the inclusions, i.e., it assumes that each inclusion is surrounded by the same effective medium. Thus, such an approach is applicable only when inclusion volume fractions are dilute and the approach breaks down when dielectric phase contrast values are high [36].

The commonly utilized empirical approach to predict effective permittivity of composites is the logarithmic mixing rule. This mixing rule is popular with experimentalists and several authors have justified its existence on the grounds that it appears to fit experimental data. First and foremost, the logarithmic mixing rule is purely based on volume fractions and individual phase permittivities. It does not account for inclusion shape, orientation, or size and can be termed an averaging procedure, instead of a mixing rule based on a physical foundation. It has also been pointed out in the literature that fitting of experimental data by the logarithmic rule could simply be fortuitous [23]. Table 1.1, summarizes the analytical mixing theories that have been developed, their advantages and disadvantages from the period 1850 through 2002.

TABLE 1.1 Analytical Mixing Theories

Sr. No	Contributors	Year	Mixing Rule in Nutshell	Uniqueness/ Advantages	Limitations
1.	O.F. Mossotti R. Clausius[25,26]	1850/ 1879	$\frac{\varepsilon_r - 1}{\varepsilon_r + 2} \propto$ No of molecules in unit volume	(a) First quantitative expression (b) Applicable to gases	(a) Not applicable for all solids (b) Only applicable to high symmetry ionic structures that are non polar
2.	Lorenz-Lorentz [27-29]	1880	(a) First to introduce local electric field calculation (b) Introduced idea of "depolarization"	Co-related refractive index with dielectric constant	(a) Broad based approach (b) Specific issues not addressed
3.	Rayleigh [30]	1892	Studied spherical and cylindrical inclusions in ordered rectangular lattice	Extended the approach to conductivity of heat	Study was restricted to two shape of inclusions
4.	J. C. Maxwell Garnett [31]	1904	(a) First well defined approach identifying all specifics in diphasic system (b) Dipole moment based approach	(a) Solid electrostatic foundation (b) Concept of averaging of electric field introduced	(a)Applicable to dilute inclusion volume fractions (b) Electric field perturbation at high inclusion volume fraction not accounted for
5.	Lichtenecker [40]	1909	(a) Simple approach, (b) Purely based on permittivity and volume fraction of constituent phases	Ease of application	(a) Doubtful physical origin (b) Its an averaging procedure

TABLE 1.1 Analytical Mixing Theories Cont.

Sr. No	Contributors	Year	Mixing Rule in Nutshell	Uniqueness/ Advantages	Limitations
6.	D.A.G. Bruggeman [24, 32-35]	1930	Technique meant to bridge gap between detailed description of fine grained features with macroscopic description	(a) Applicable for dense composites (b) Electrostatic interaction accounted in specific V_f range	(a) Inhomogenities in local electric field not accounted (b) Inclusion shape not accounted
7.	O. Weiner [37]	1957	Introduced form factors for ellipsoid shape and lamellar shape	Suitable for 0-3 composites	Other possible shapes of inclusions not considered
8.	D. A. Payne [23]	1973	(a) First attempt to broadly consider all possible microstructures and types of dielectric mixtures (0-3, 2-2, 3-3) (b) Brick wall model introduced based on dielectric susceptibility and additional proof for series and parallel mixing theories presented	Equivalent circuit approach to understand frequency dependence of effective permittivity	(a) Assumption that all inclusions are of similar shape (b) Multiple inclusions cannot be modeled
9.	K. Wakino [41]	1993/ 2002	Modification of logarithmic mixing rule	Random distribution of inclusions considered	(a) No shape characteristics considered (b) Physical origin is not strong

In this research, the limitations of mixing rules are addressed through development of a mixing rule paradigm that accounts for particle shape and other effects over a broader range of volume fractions.

1.4 RESEARCH OBJECTIVE

This research is focused on diphasic dielectric composites for high energy density storage applications in pulsed power and power distribution systems. Composite materials are particularly attractive because they can synergistically combine high permittivity with high breakdown strength of the individual phases. Energy density, which captures permittivity and dielectric breakdown strength as vital material parameters, dominates this research challenge. Avenues for increasing the effective permittivity and breakdown strength may be found by gaining fundamental understanding of the response of diphasic dielectrics to an applied electric field. Improved understanding of these characteristics will ultimately lead to dielectrics with increased energy storage densities. Current research is centered on improving the understanding of dielectric composite response through analytical modeling, numerical simulations and experimental work. Three research themes have been explored in this research.

The first research area deals with analytical modeling of the effective permittivity of diphasic dielectrics. An analytical model to express the effective permittivity of a composite dielectric with complex-shape inclusions has been formulated. There is a need for a mixing theory applicable to all composites, whether 0-3, 2-2 or other uniform composite. Herein, an equivalent capacitance model for calculating effective permittivity was developed. The foundational approach developed in this model is that of the discretization of the inhomogeneous dielectric body. The composite dielectric is

discretized into partial parallel-plate capacitor elements, and the total equivalent capacitance of the structure is calculated. The effective permittivity of the composite dielectric is then obtained from this equivalent capacitance. The specific case of a diphasic dielectric body containing a high-permittivity *spherical* inclusion enclosed in a parallelepiped (in particular, a cube) having a lower permittivity has been evaluated. The results of modeling based on the developed approach are compared with results obtained using Maxwell Garnett theory, Bruggeman mixing rule, logarithmic mixing rule for effective permittivity and experimental results identified in the literature. The significance of this model lies in the fact that, unlike the traditional mixing theories, the new model facilitates study of the effect of inclusion size, shape, and proximity, as well as volume fraction.

The objective of the second focus of this work was to further expand the analytical model developed in the first research area to account for the complex permittivities of the two phases. By developing a mixing theory that can account for the complex permittivity behavior of the constituent phases, the dielectric response of the composite may be explored as a function of alternating electric field (i.e., the frequency dependence of the composite may be studied).

The third research theme involved analytical as well as numerical modeling of electrostatic field distribution and energy storage in diphasic dielectrics. This research aimed to comprehensively analyze the impact of field distribution on energy storage and breakdown strength of composites. These investigations utilized an analytical formulation based on the Maxwell Garnett (MG) mixing rule and numerical simulations based on boundary element method (BEM) software. The electric field distribution was

studied as a function of dielectric contrast and volume fraction of phases. Key insights with respect to selection of constituent phases have been identified. The upper limit of applicability of the MG formulation in terms of the inclusion volume fraction was also established and was found to be function of dielectric contrast.

PAPER

1. PREDICTION OF EFFECTIVE PERMITTIVITY OF DIPHASIC DIELECTRICS USING AN EQUIVALENT CAPACITANCE MODEL

S. K. Patil[1], M. Y. Koledintseva[2], R.W. Schwartz[1] and W. Huebner[1]
[1]*Department of Materials Science & Engineering and*
[2]*Department of Electrical and Computer Engineering,*
Missouri University of Science and Technology, Rolla MO 65409 USA

ABSTRACT: An analytical model based on an equivalent capacitance circuit for expressing a static effective permittivity of a composite dielectric with complex-shaped inclusions is presented. The dielectric response of 0-3 composites is investigated using this model. The geometry of the capacitor containing a composite dielectric is discretized into partial parallel-plate capacitor elements, and the effective permittivity of the composite is obtained from the equivalent capacitance of the structure. First, an individual cell (a high-permittivity spherical inclusion enclosed in a lower permittivity parallelepiped) of a diphasic dielectric is considered. The capacitance of this cell is modeled as a function of inclusion radius/volume fraction. The proposed approach is extended over a periodic three-dimensional structure comprised of multiple individual cells. The results of modeling are compared with results obtained using different effective medium theories, including Maxwell Garnett, logarithmic, Bruggeman, series, and parallel mixing rules. It is found that the model predictions are in good agreement with the experimental data. The equivalent capacitance model may be applied to composites containing inclusions of any geometry and size. Though the method presented is at static electric field, it can be easily generalized for prediction of frequency-dependent effective permittivity.

Keywords: Dielectric composites, electric field distribution, energy storage, equivalent capacitance

I. INTRODUCTION

The effective properties of dielectric mixtures have been investigated for more than 100 years, with the earliest known reference for prediction of effective dielectric constant of a mixture being attributed to Poisson.[1] Rayleigh calculated the effective permittivity of a mixture based on spherical or cylindrical inclusions in a rectangular lattice and his results provided a connection between the properties of the mixture and the properties of the inclusions and macroscopic medium.[2] One of the classical and most widely used formulations to calculate effective permittivity of dilute mixtures is the Maxwell Garnett (MG) theory,[3-6] which was first formulated for spherical inclusions.

The Maxwell Garnett theory was also extended for ellipsoidal inclusions (spheroids, cylinders and disks).[3] The theory is also applicable for inclusions of any arbitrary ellipsoidal shape (spheroids, cylinders, and disks) through introduction of depolarization factors. The table of depolarization factors can be found for example in paper.[7] However, an arbitrary inclusion shape cannot be accurately accounted for, other than by approximation by the closest ellipsoidal shape.[8]

There have been numerous other models developed to predict the effective permittivity of composites. To account for non-ellipsoidal shapes, Weiner proposed form factors for inclusions with cylindrical and lamellar shape.[9] Rushman *et al*., used these form factors to explain the impact of porosity upon the dielectric constant of barium titanate.[10] Experimental evidence for the Weiner mixing rule and its applicability to porous dielectrics was confirmed by Kingery in 1960.[11]

Bruggeman's effective medium theory (EMT) is better suited for denser composites than the MG rule.[12] The effective medium is determined self-consistently by taking into account the fact that any other inclusion could have been chosen. However, EMT does not allow for correlation between the inclusions, i.e., it assumes that each inclusion is surrounded by the same effective medium.[13] Bruggeman extended diphasic mixing to the study of dense composites, taking into account electrostatic interactions.

The empirically derived logarithmic mixing rule is also used for description of effective properties of composites.[14] In many cases it appears to fit experimental data; however in some cases it may be fortuitous, as has been pointed out by Payne.[15]

This paper is focused on the development of a simple analytical model to predict the effective permittivity of a dielectric composite that is valid for any volume fraction of inclusions, and can be applied to inclusions *of any shape*. The model presented herein is based on the discretization of a dielectric body of any shape into simple parallel plate partial capacitor elements. By using this approach, actual inclusion shapes can be accounted for. The effective permittivity is then calculated based on the capacitance of the appropriate equivalent circuit.

The specific example of this approach presented in this paper is a geometrically isotropic (spherical) inclusion of higher permittivity in a host dielectric of lower permittivity. The host dielectric is a parallelepiped, in particular, a cube. This structure is called "an individual cell" (or just "a cell"). The capacitance of a cell is modeled as a function of the radius or volume fraction of the inclusion. The approach is subsequently extended over a periodic three-dimensional structure with multiple individual cells. This is analogous to the extensively studied epoxy/$BaTiO_3$ systems, for which substantial

experimental data is available.[16-22] Recently, 0-3 high-permittivity polymer-based composites have been increasingly investigated for both comparatively low-energy embedded capacitor technology, [16-21] and for high-energy density applications for pulsed power capacitors. [22]

Results of the equivalent capacitance approach that is developed here are compared with computations based on the MG mixing theory, Bruggeman's mixing rule, logarithmic mixing rule and recently reported experimental results. The mathematical formulation for the equivalent capacitance model is presented below in Section II, results for the model are presented in Section III with comparison to the MG model, and conclusions regarding the utility of the model are presented in Section IV.

II. MATHEMATICAL FORMULATION

A. ONE INDIVIDUAL CAPACITOR CELL

A general diphasic slab with a three-dimensional periodic structure of inclusions is subdivided into individual cells (cubes), each of which contains one inclusion of a higher permittivity surrounded by a host material of a lower permittivity. Fig. 1 shows the basic building block of the composite and its three-dimensional translation. The structure that is modeled is thus an ordered composite. Modeling of random composites is readily facilitated.

First, consider an individual cell with an inclusion of an isotropic shape, i.e., a sphere placed at the center of the cube. The inclusion size is varied from 0.1 μm to 0.54 μm within a host phase cube of dimension 1.1 μm. In the present model, it is assumed that both the inclusion and host are linear isotropic and homogeneous dielectric materials.

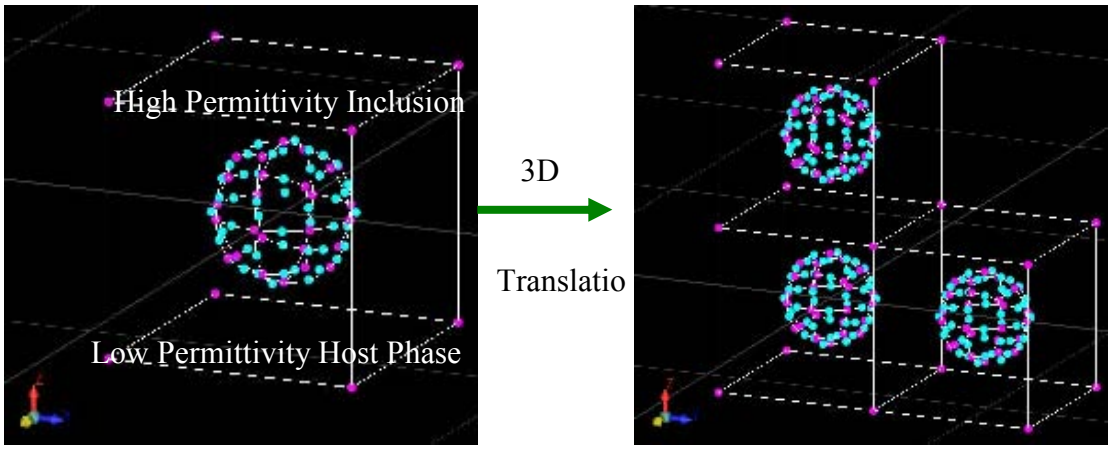

FIG. 1. Basic building block of composite sphere enclosed in a cube and its 3-D translation in x, y, z directions.

A homogeneous static electric field is applied along the vertical dimension of the cell. Then, any cell is an individual capacitor with inhomogeneous contents, and it can be discretized into parallel and series parallel-plate partial capacitors with capacitances given by:

$$C_p = \frac{\varepsilon_o \varepsilon_p A_p}{d_p}, \qquad (1)$$

where $\varepsilon_o = 8.854 \cdot 10^{-12}$ F/m is the vacuum permittivity, ε_p is the relative permittivity of a dielectric in a partial capacitor, A_p is an area of the partial capacitor plates, and d_p is the thickness of the partial capacitor. The resultant capacitance of a whole cell can be calculated using an appropriate equivalent circuit model.

Fig. 2 shows how the discretization process is implemented for a basic cubic building block with a spherical inclusion. This figure also shows a planar projection of

the three-dimensional (3D) view. The individual cell is divided into partial capacitors (numbered 1-7), and the corner capacitors around the sphere labeled as C_d. An equivalent circuit for this structure is shown in Fig. 3. Below, explicit formulae for calculating these partial capacitances are given. C_1 and C_2 are the capacitances on the left and the right sides of the inclusion. If the structure is symmetrical, C_1 and C_2 are identical, and linearly decrease as the radius of the inclusion increases. These capacitances may be calculated according to:

$$C_1 = C_2 = \frac{\varepsilon_0 \varepsilon_h (a_c / 2 - r) b_c}{d_c}, \tag{2}$$

where ε_h is the relative permittivity of the host material, a_c b_c and d_c are the length, width, and height of the individual cell (for the particular case of a cube, $a_c = b_c = d_c$), and r is the radius of the inclusion. The partial capacitances C_3 and C_4 are associated with the elements located on the top and the bottom of the inclusion, and their values are calculated as:

$$C_3 = C_4 = \frac{2\varepsilon_0 \varepsilon_h (2 b_c r)}{d_c - 2r}. \tag{3}$$

The partial capacitors C_6 and C_7 are not seen in this planar view – they are located in front and behind the sphere, but can be seen in a three-dimensional Fig.2. Their values are calculated as:

$$C_6 = C_7 = \frac{\varepsilon_0 \varepsilon_h (b_c - 2r)}{2}. \tag{4}$$

Fig. 2 also shows the discretization approach utilized for the corner shape and inclusion sphere. The capacitance of the corner capacitor elements is calculated using elemental slices parallel to the cell's electrode planes.

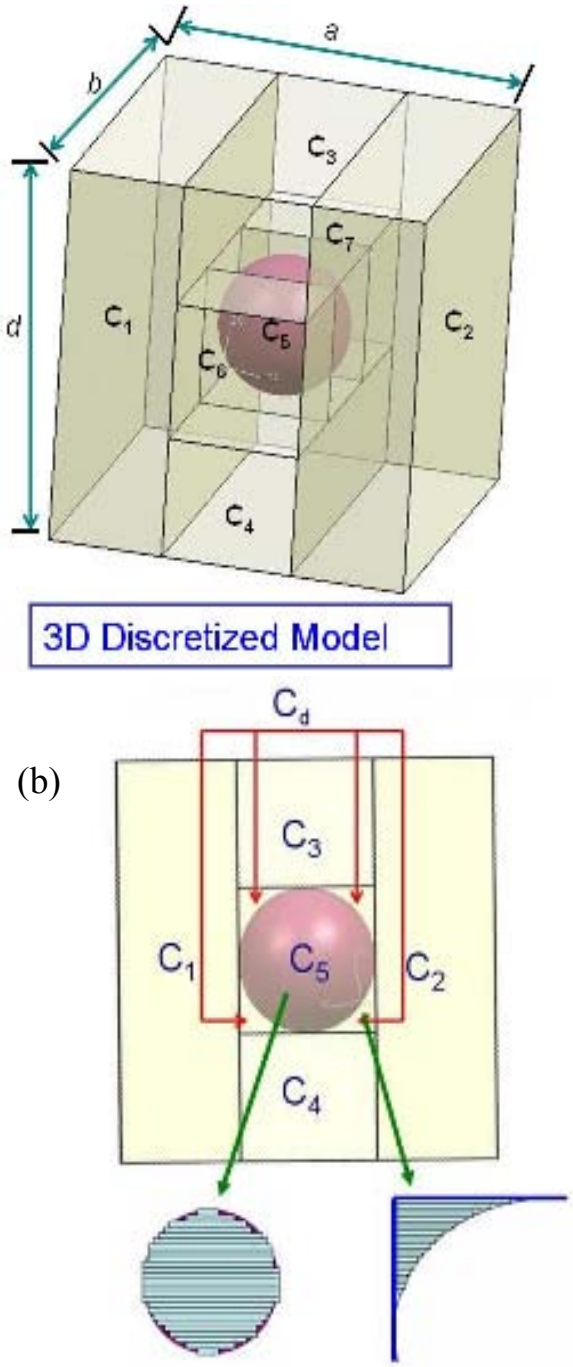

FIG. 2. 3- D view of discretized diphasic dielectric body and 2-D planar view of discretized diphasic dielectric body showing discretization pathway for corner shape and inclusion sphere.

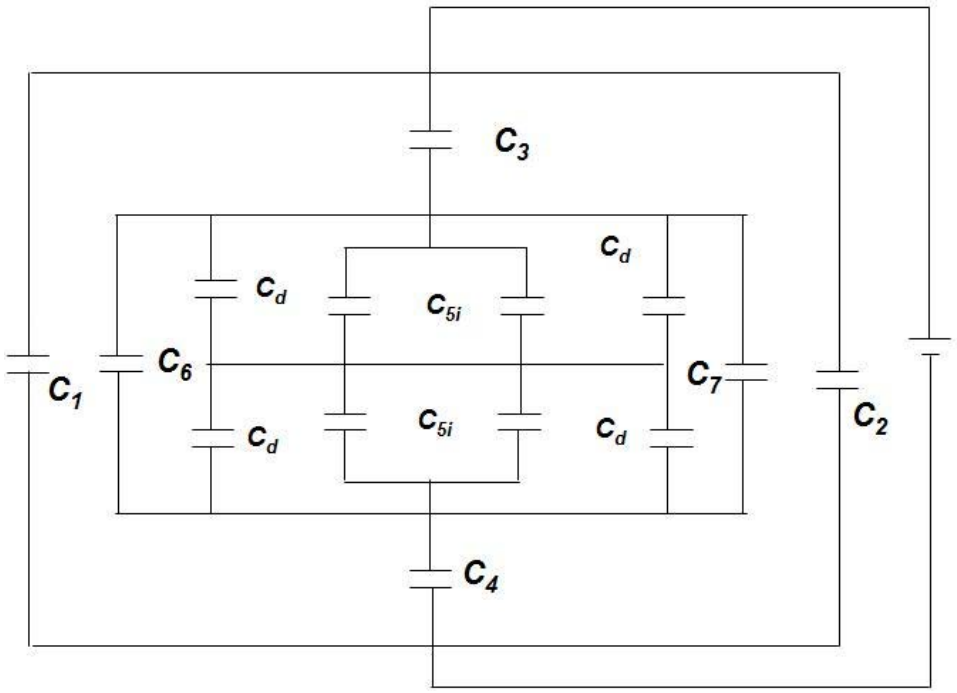

FIG. 3. Diphasic dielectric represented by an equivalent circuit.

These partial capacitors are connected in series, and the integration over the space of the corners is then used to evaluate the total capacitance of these volumes (see the derivation in *Appendix A*).The total capacitance for all four corner elements- two bottom and two top $(i = 1...4)$ is:

$$C_d = \frac{\varepsilon_o \varepsilon_h r \pi}{2} \frac{1}{\frac{1}{\sqrt{\frac{4}{\pi} - 1}} \arctan\left[\frac{1}{\sqrt{\frac{4}{\pi} - 1}}\right]}, \tag{5}$$

To calculate the capacitance of the high-permittivity sphere, it is convenient to cut it into thin parallel slices, and consider the series connection of these elements, corresponding to the slices. As shown in *Appendix B*, the integration procedure yields the

capacitance of the quarters of the dielectric sphere C_{5_i}, $(i = 1...4)$ which is the same as for the total sphere:

$$C_5 = C_{5_i} = \frac{\varepsilon_0 \varepsilon_i \pi \cdot r}{2 \int_0^{\pi/2} \frac{d\theta}{\cos(\theta)}}. \tag{6}$$

To assure convergence of the integral in the denominator, zero in the integration was substituted by 10^{-7}. Since the capacitor elements C_5, C_6, C_7 and C_d are all in parallel (see Fig. 2), and they are in series with C_3 and C_4, the equivalent capacitance for the central region of the cube is:

$$C_{eq1} = \frac{1}{\frac{1}{C_3} + \frac{1}{C_4} + \frac{1}{C_5 + C_6 + C_7 + C_d}}, \tag{7}$$

This capacitance C_{eq1}, as shown in Fig. 2, in its turn, is parallel with the left and right capacitors C_1 and C_2, and therefore, the total equivalent capacitance is:

$$C_{cell} = C_1 + C_2 + C_{eq1}, \tag{8}$$

Then, assuming a homogeneous dielectric fills the space between the cell capacitor plates, the effective permittivity can be calculated from the expression for total capacitance C_{cell} of the cell as:

$$\varepsilon_{eff}^{'} = \frac{C_{cell} d_c}{\varepsilon_o a_c b_c}, \tag{9}$$

The effective permittivity ($\varepsilon_{eff}^{'}$) captures the shape of the inclusion, and there are no restrictions on the inclusion size. In general, the shape of an inclusion can be arbitrary, though different integration schemes are required. For example, ellipsoidal, tetrahedral and other straight-line geometries would be relatively straightforward, while arbitrary curvilinear shapes would require special discretization schemes.

B. N^3 INDIVIDUAL CAPACITOR CELLS

The equivalent capacitance model may be extended for the case of multiple inclusions to test for consistency of single as well as multiple inclusion structures. Considered here is a case when there are N inclusions in the form of spheres along any of three dimensions of the total capacitor. This means that there are N^3 elemental capacitor cells in the structure under consideration. The capacitor cells in vertical branches are connected in series, while all the branches are connected in parallel, as shown in Fig. 4. This means that the capacitance in any branch is

$$C_{branch} = \frac{C_{cell}}{N}. \tag{10}$$

Because there are N^2 vertical branches, the total capacitance is:

$$C_{\Sigma} = \frac{C_{cell}}{N} \cdot N^2 = NC_{cell}. \tag{11}$$

An individual cell capacitance C_{cell} is calculated as in Section II. A and C_{Σ} is total capacitance of the composite. If the dimensions of the total capacitor are $a, b,$ and d, then the dimensions of an individual cell are, respectively:

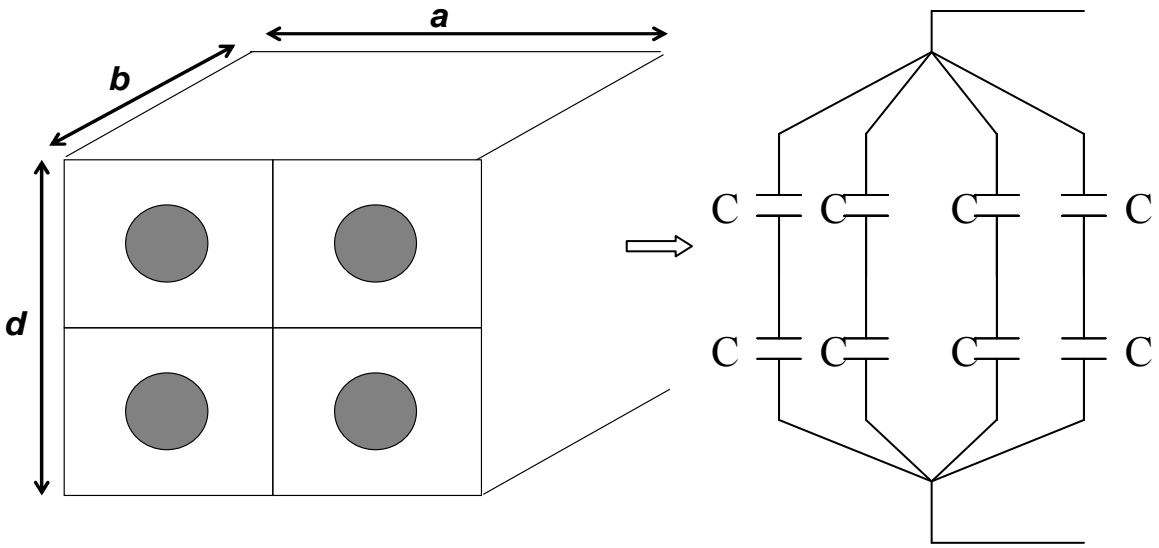

FIG. 4. Discretization pathway for N^3 capacitor cells.

$$\begin{aligned} a_c &= a / N; \\ b_c &= b / N; \\ d_c &= d / N. \end{aligned} \tag{12}$$

Then, the effective permittivity of an inhomogeneous dielectric inside the total capacitor can be calculated as:

$$\varepsilon_{eff}^{'} = \frac{C_{\Sigma} d}{a\ b\ \varepsilon_o}. \tag{13}$$

The effective permittivity of an inhomogeneous dielectric obtained using the method presented above may be compared with the well-known homogenization technique based on the Maxwell Garnett (MG) mixing rule. The simplest formulation is for a mixture of a host material with relative permittivity ε_h and spherical inclusions with relative permittivity ε_s, as given by:[3, 4, 9]

$$\varepsilon_{efMG} \cong \varepsilon_h + \frac{3 f_s \varepsilon_h (\varepsilon_s - \varepsilon_h)/(\varepsilon_s + 2\varepsilon_h)}{1 - f_s (\varepsilon_s - \varepsilon_h)/(\varepsilon_s + 2\varepsilon_h)}, \tag{14}$$

where $f_s = \frac{V_S}{V_\Sigma}$ is the volume fraction of spherical inclusions in the total mixture and V_s is the volume of inclusion and V_Σ is the total volume of the composite.

It is also informative to compare the equivalent capacitance model to the formula for the logarithmic mixing rule, given by:

$$\varepsilon_{eff\ Logarithmic} \cong V_h \cdot \log \varepsilon_h + V_i \log \varepsilon_i, \tag{15}$$

and to the formula for the Bruggeman mixing rule, given by:

$$\frac{\varepsilon_i - \varepsilon'_{eff}}{\varepsilon_i - \varepsilon_h} = \frac{1 - V_i}{\sqrt[3]{\varepsilon_h / \varepsilon_{eff}}}, \tag{16}$$

Here, V_h and ε_h are the volume fraction and permittivity of the host phase, respectively, and V_i and ε_i are the volume fraction and permittivity of the inclusion phase, respectively.

III. RESULTS AND DISCUSSION

The first calculation is for the capacitance of a cube containing one spherical inclusion placed in the center of the cube. The inclusion is a high-permittivity dielectric, in particular, barium titanate (BT), with relative permittivity assumed to be $\varepsilon_i = 1900$.

The cube surrounding the BT sphere is a low-permittivity phase, for example, with relative permittivity $\varepsilon_h = 4$ (polyamides, epoxy etc). The cube has the following dimensions: $a_c = b_c = d_c = 1.1$ μm. This size is chosen to imitate a real structure of a polymer ceramic dielectric. The radius of the sphere is varied, and, hence, the volume fraction of the inclusion is also varied. For this capacitor structure, the maximum inclusion volume fraction is approximately 52.3 %. The electric field applied is in the vertical direction, as dictated by the equivalent capacitance model outlined above. The capacitance of this structure is calculated according to the formulae presented in Section II.A. The analytical software MAPLE 10 was used to carry out the computations presented below.

C_1-C_2: The capacitance of elements C_1 and C_2 are equal, since both capacitors have the same low permittivity ε_h, the same area, and the same thickness. The capacitance data for both capacitors C_1 and C_2 as a function of the radius of the inclusion is plotted in Fig. 5 (a). Capacitances C_1 and C_2 show a linear decrease as the inclusion radius increases. This is an expected result, since with increasing inclusion radius; there is a linear decrease in the area of the capacitor plates, while its thickness remains constant.

C_3-C_4: The capacitances of capacitors C_3 and C_4 are also equal; as these partial capacitors located on top and bottom of the spherical inclusion, have the same area and thickness. The capacitance data for both capacitors C_3 and C_4 as a function of radius of the inclusion is plotted in Fig. 5 (b). It is seen that when the inclusion radius is small ($r \leq 0.2 \mu m$), there is a minimal increase in capacitance (0.01-0.1 $\cdot 10^{-14}$ F). This is because

the area of the capacitor "plates" remains small (area < 0.4 μm^2), while the thickness of the dielectric remains relatively high (d ≥ 0.6μm).

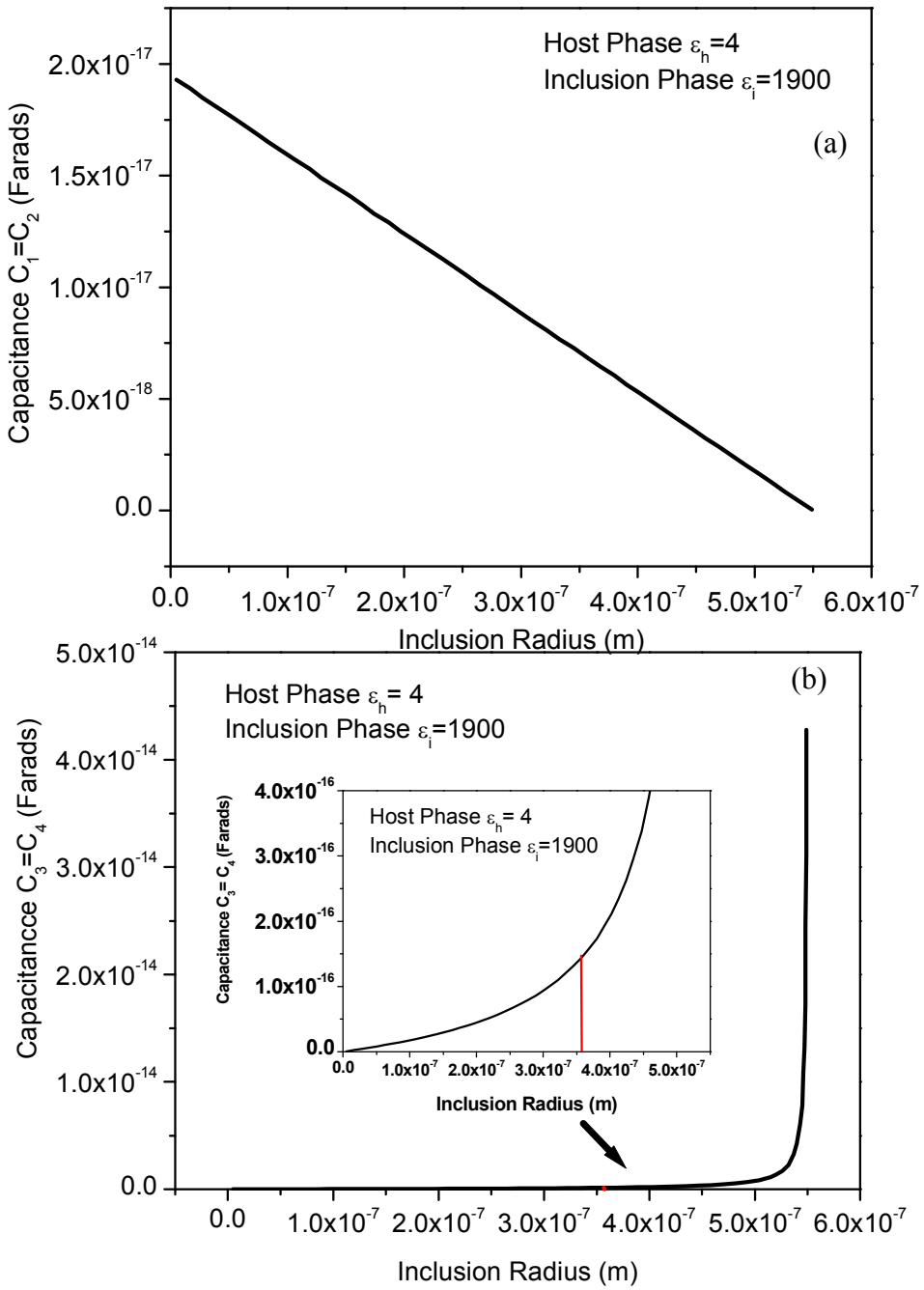

FIG. 5. Magnitude of capacitances of capacitor elements C_1, C_2, C_3 and C_4 as a function of inclusion radius (r).

After the radius becomes approximately 1/3 of the cell dimension, the area of capacitor increases, the thickness concurrently decreases, and there is a rapid increase in capacitance as $\propto r^3$. It is observed that beyond the inclusion radius of 0.53 μm, there is a rapid increase in the capacitances of C_3 and C_4. When inclusions start touching the top and bottom of the host phase cube the corresponding capacitances go to infinity. In computations, it is assumed that the thickness of the dielectric layers for C_3 and C_4 is at least 1% of the inclusion radius. Therefore, this model is applicable till the inclusion radii are about 0.5445 μm.

C_d: The capacitance of the corner elements depend on the shape of the inclusion. There is a linear increase in this capacitance with inclusion radius, as shown in Fig. 6 (a).This capacitance C_d becomes significant, when the radius of the inclusion increases.

C_5: The capacitor C_5 is constituted of the high-permittivity phase. The capacitance data for capacitor C_5 as a function of inclusion radius is plotted in Fig. 6 (b). There is a linear increase in C_5 as the radius of the inclusion increases, which is an expected result.

C_6-C_7: The capacitances C_6 and C_7 located in front and back of the inclusion show a linear decrease in the capacitance with increasing inclusion radius, similar to the behavior of C_1 and C_2.

Fig. 7 (a) shows that capacitance C_6 (and C_7 as well) decreases as a function of inclusion radius. This is because the area of the corresponding capacitor "plates" decreases linearly with increase in inclusion radius.

C_Σ: The total equivalent capacitance for the diphasic composite as a function of inclusion radius is plotted in Fig. 7 (b), and it shows a trend similar to that for the partial

capacitances C_3 and C_4, since at larger inclusion radii ($r \geq 0.4 \mu m$) these two capacitances dominate.

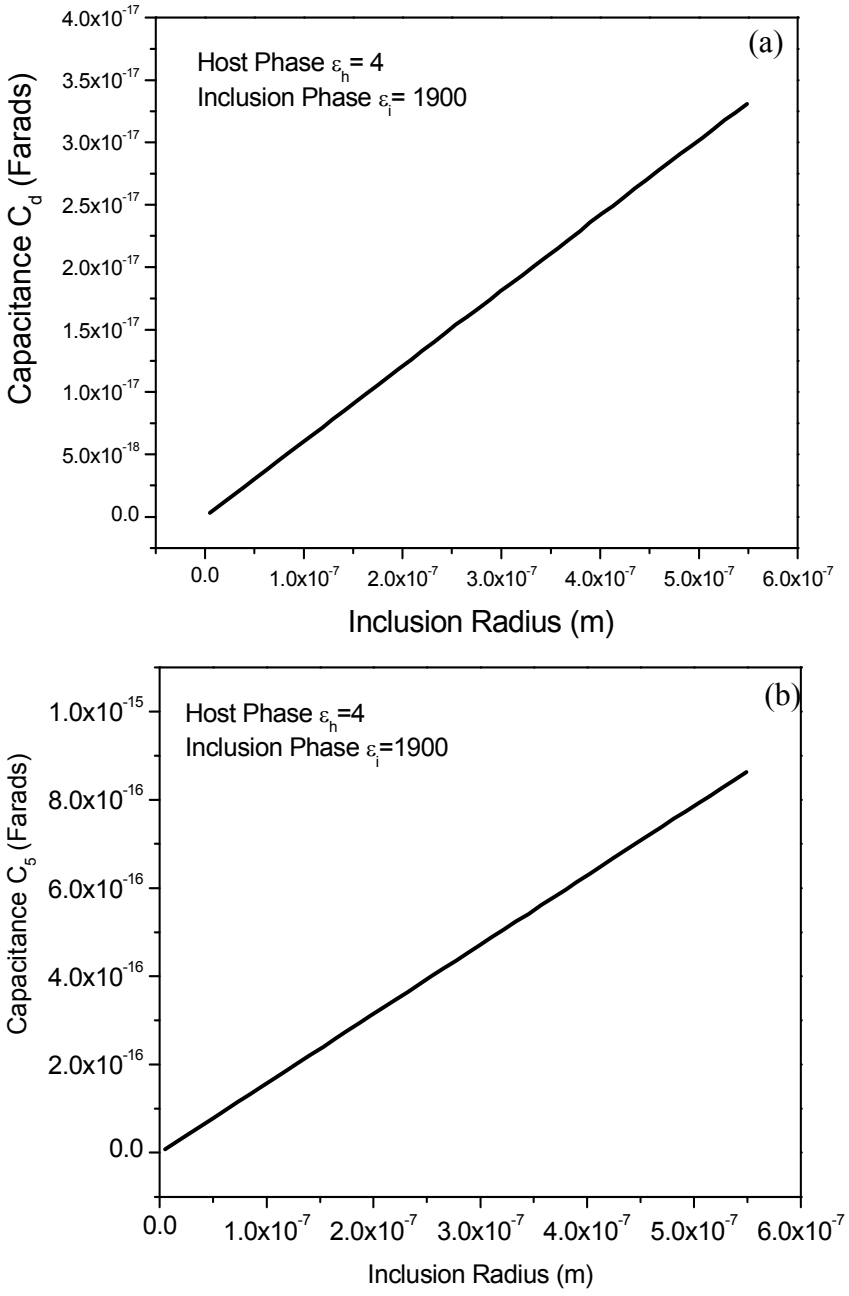

FIG. 6. Magnitude of capacitances of capacitor elements C_d and C_5 as a function of inclusion radius (r).

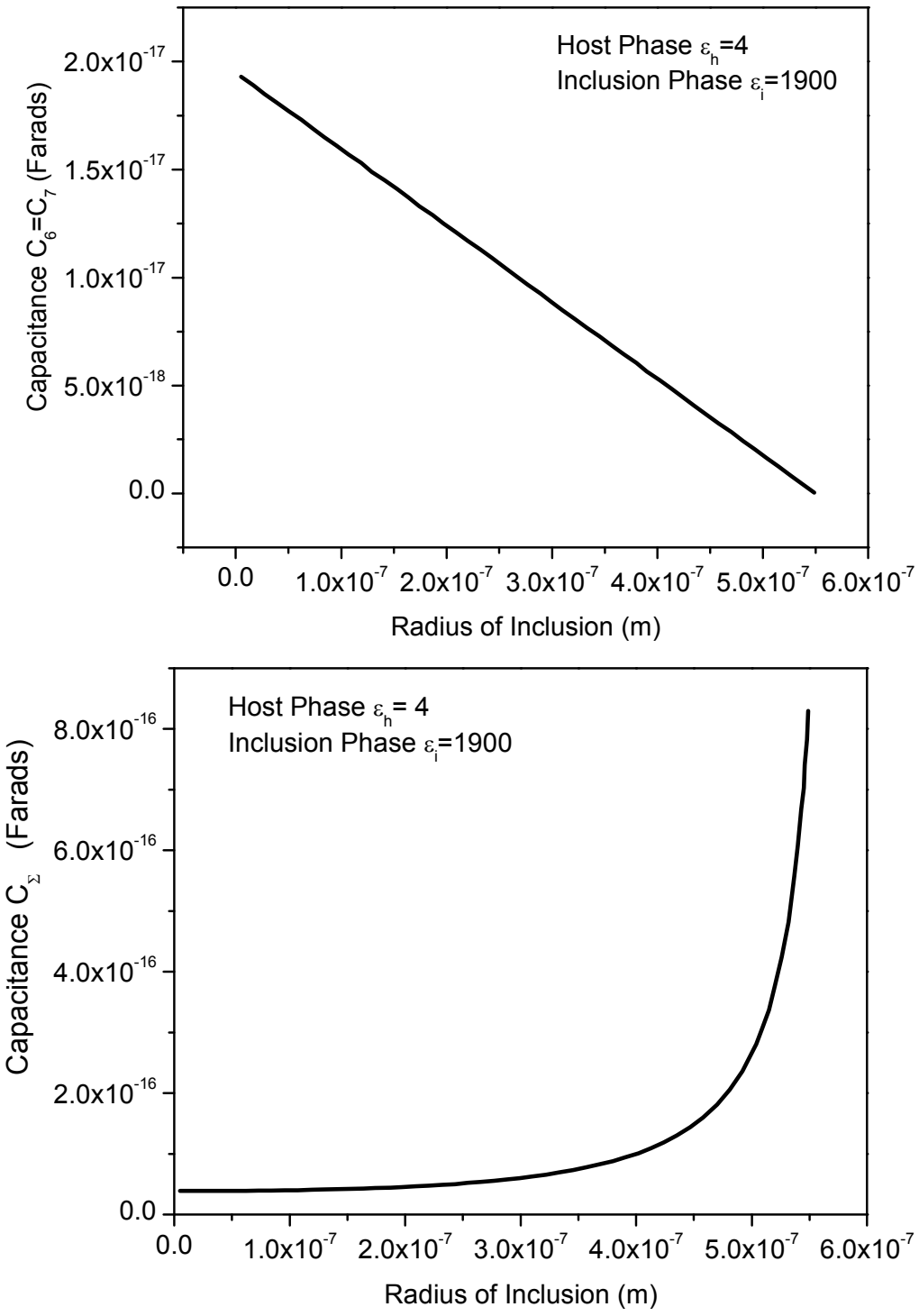

FIG. 7. Magnitude of capacitances of capacitor elements C_6, C_7 and C_Σ as a function of inclusion radius (r).

The effective permittivity of the composite, calculated through the total capacitance, is illustrated in Fig. 8. According to the equivalent capacitance model, the predicted effective permittivity for the inclusion volume fraction range of 0 to 35% increases from 4 to 15. The predicted permittivity for inclusion volume fraction variation from 35 to 52% increases from 15 to 80. When the radius of the spherical inclusions is approximately 1/3 of the cell dimension, the rate of the effective permittivity increase becomes greater. The calculated maximum permittivity is around 80 for a volume fraction of approximately 52% and a dielectric contrast (*ratio of permittivity of inclusion phase to permittivity of host)* of 300.

Fig. 8 also shows the effective permittivity as a function of inclusion radius for the same composite calculated using the Maxwell Garnett mixing rule, logarithmic rule, and Bruggeman formulation. The trend shown by the equivalent circuit capacitance model is similar to that for the other mixing rules. However the slope of the dependence equivalent capacitor model becomes steeper as the inclusion radius approaches its limiting point (r> $0.54\,\mu m$). The equivalent capacitance model results lie between the logarithmic rule, which overestimates the effective permittivity, and the Bruggeman model predictions.

The equivalent capacitance model was also tested for multiple inclusions as opposed the single inclusion case reported above. A composite system with the same host cube dimensions but with 1000 high permittivity inclusions is considered. The total capacitor dimensions are the same as in the previous example with one spherical BT inclusion in host ($a = b = d = 1.1\ \ \mu m$). In the equivalent capacitance model, the total structure contains 1000 individual cells.

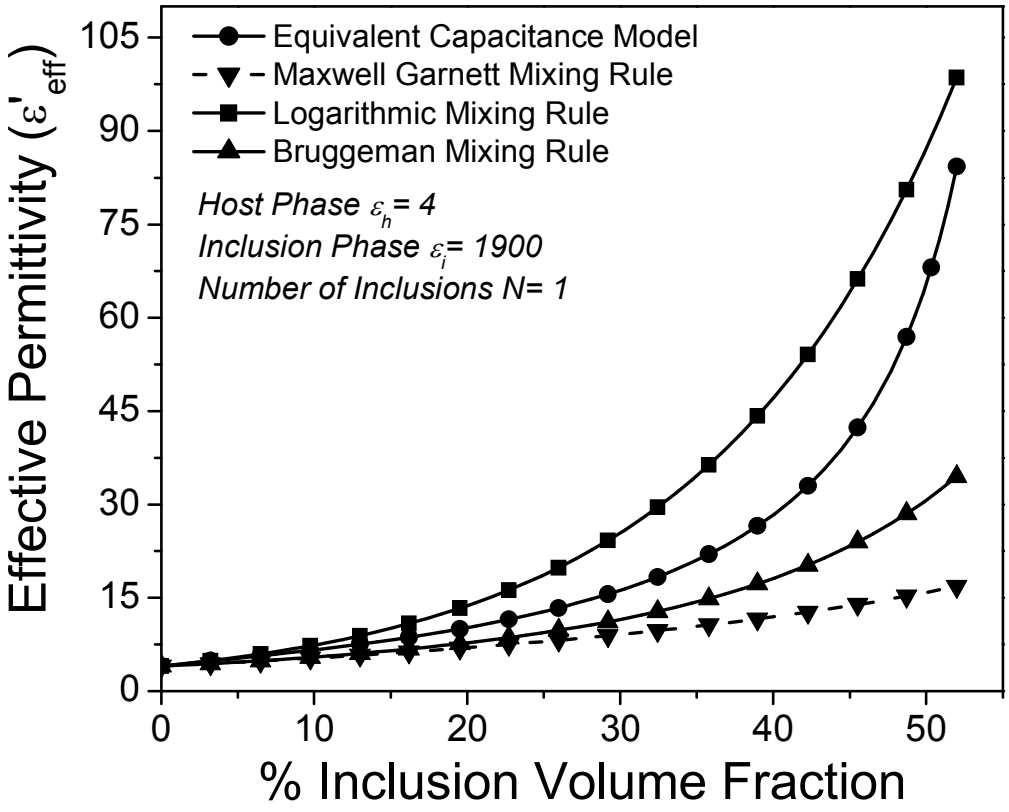

FIG. 8. Effective permittivity of composite predicted by equivalent capacitance model as a function of inclusion volume fraction for N=1 inclusions and its comparison to predictions of Maxwell Garnett mixing theory, Bruggeman mixing rule and Logarithmic mixing rule.

The maximum radius of each inclusion is 10 times smaller than in the previous single cell example. In this particular case, the inclusion size is reduced and is varied from 10 nm to a maximum 54 nm, as opposed to the earlier case when the single inclusion size was varied from 0.1 μm to 0.54 μm. This structure is an ordered nanoscale composite. It has been verified that the predictions of the equivalent capacitance model for the multiple inclusion case remain identical to the single inclusion case. The model

suggests consistent results for analogous volume fraction no matter how many inclusions of the same shape are present. The results are independent of inclusion size, but they capture inclusion shape.

In a parallelepiped with a homogeneous static electric field applied along one of its dimensions, there is a continuous linear variation of the electrostatic potential along this direction.[23] That is why cutting the structure into parallel-plane slices and applying rules for calculating equivalent series and parallel capacitances allows for taking into account local electric field present within this slices. The model satisfies all boundary conditions for electric field and potential between the partial capacitor elements. The accuracy of these computations depends on how fine the discretization is, and the discretization is defined by the shape of inclusions.

The equivalent capacitance model is validated by comparison with experimental data for two different diphasic dielectric systems, both of which contain BT in a polymeric host (i.e., similar dielectric contrast and volume fractions to those studied). It should be pointed out that the permittivity of BT powder is highly sensitive to the grain size[24-28] and it has been reported that coarse grain BT (20-50 μm) shows $\varepsilon_r = 1500 - 2000$ at room temperature, whereas the permittivity for fine-grained BT (~1 μm) is 3500-4000. As the grain size decreases below 1 μm, the permittivity is most likely to be around 950-1200.

The first system experimentally investigated by Chiang *et al.*[29] contains cyanoresin as a host phase ($\varepsilon_h = 21$) and barium titanate (BT) with grain size less than 2 μm as the inclusion phase. Because the exact data on inclusion permittivity has not been reported,[29] in the present model, the BT permittivity is assumed to be

approximately $\varepsilon_i = 3800$, in accordance with the permittivity of BT of grain size less than $2\,\mu m$. In this case, the dielectric contrast is 180. The volume fraction of the inclusion phase in the equivalent circuit model is varied between 0 and 52 vol%. Fig. 9(a) shows the experimental effective permittivity as a function of the inclusion volume fraction for this system, as well as the dependencies calculated based on different models.

The second experimental system[30] to which the equivalent capacitance model is compared contains polypropylene as a host phase ($\varepsilon_h = 2.2$) and BT as an inclusion phase ($\varepsilon_i = 3800$). In this case, the dielectric contrast is ~ 1700. Using these parameters, the effective permittivity as a function of the inclusion volume fraction is shown in Fig. 9 (b).

The computations based on the equivalent capacitance model agree with the experimental data, with the first set of experimental data for inclusion volume fraction less than 40 % having a discrepancy of not more than 15% (Chiang data; Fig. 9(a)). As is seen Fig. 9 (b), for the 40 % inclusion volume fraction the maximum discrepancy does not exceed 25%.

The equivalent capacitance model agrees satisfactorily with experimental data. The equivalent capacitance model also agrees well with the Bruggeman predictions, especially for the first case of the lower dielectric contrast. The equivalent capacitance model provides a better fit to the experimental results than the MG and logarithmic mixing rules. The discrepancy between experimental data and the model prediction can arise from numerous factors. Some of the reasons are the following. The equivalent capacitance model has been developed for an ordered system, while the real-world composites have inclusions randomly dispersed in the host phase.

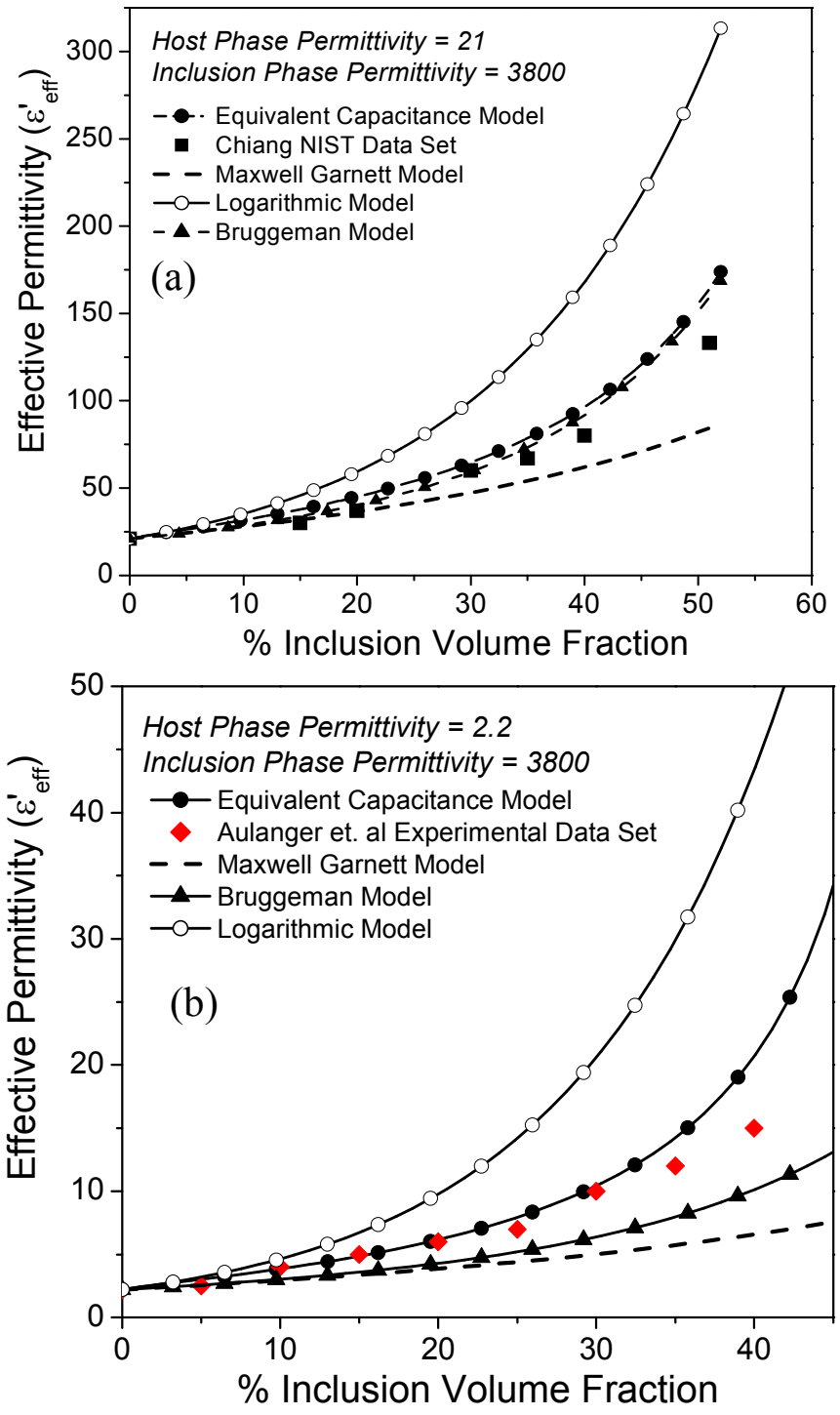

FIG. 9. Effective permittivity of the diphasic composite as predicted by equivalent capacitance model and its comparison to experimental data with host phase permittivity of 21and 2.2.

Although the reported experimental systems are for 0-3 composites, the actual inclusion shape in these composite might not be exactly spherical.

An equivalent capacitance model has also been applied to model diphasic structures in which the inclusion volume fraction is higher than in the previously considered cases ($V_f > 90\%$). The results of modeling using the equivalent capacitance model have been compared to the results of two known mixing rules: series and parallel mixing.[1] These two models were used by Payne[1] to study the effective permittivity of real-world composites, such as liquid phase sintered BT. The composites in these models are represented as layered structures, either series or parallel, depending on the ratio of permittivities of phases. If the inclusion phase has a significantly higher permittivity than the host (dielectric contrast ≥ 10), a series mixing rule may be used to predict the effective permittivity of the composite, due to local electric field behavior. If the inclusion phase has a lower permittivity than the host, a parallel mixing rule may be used to predict the effective permittivity of the structure.

Fig. 10 (a) shows a comparison of the predicted effective permittivity of a dielectric composite as a function of inclusion volume fraction for the series mixing rule and equivalent capacitance model. The system modeled in this case is a diphasic mixture of titania ceramics ($\varepsilon_1 = 100$) containing intergranular boundary phase of aluminosilicate ($\varepsilon_2 = 8$). The second system considered is a diphasic mixture of TiO_2 ($\varepsilon_1 = 100$) and Mg_2TiO_4 ($\varepsilon_2 = 22$). This system is modeled using the parallel mixing rule, which is also compared to the equivalent capacitance model in Fig. 10 (b). The predictions of the equivalent capacitance model match the series and parallel mixing rules for the appropriate composite structures.

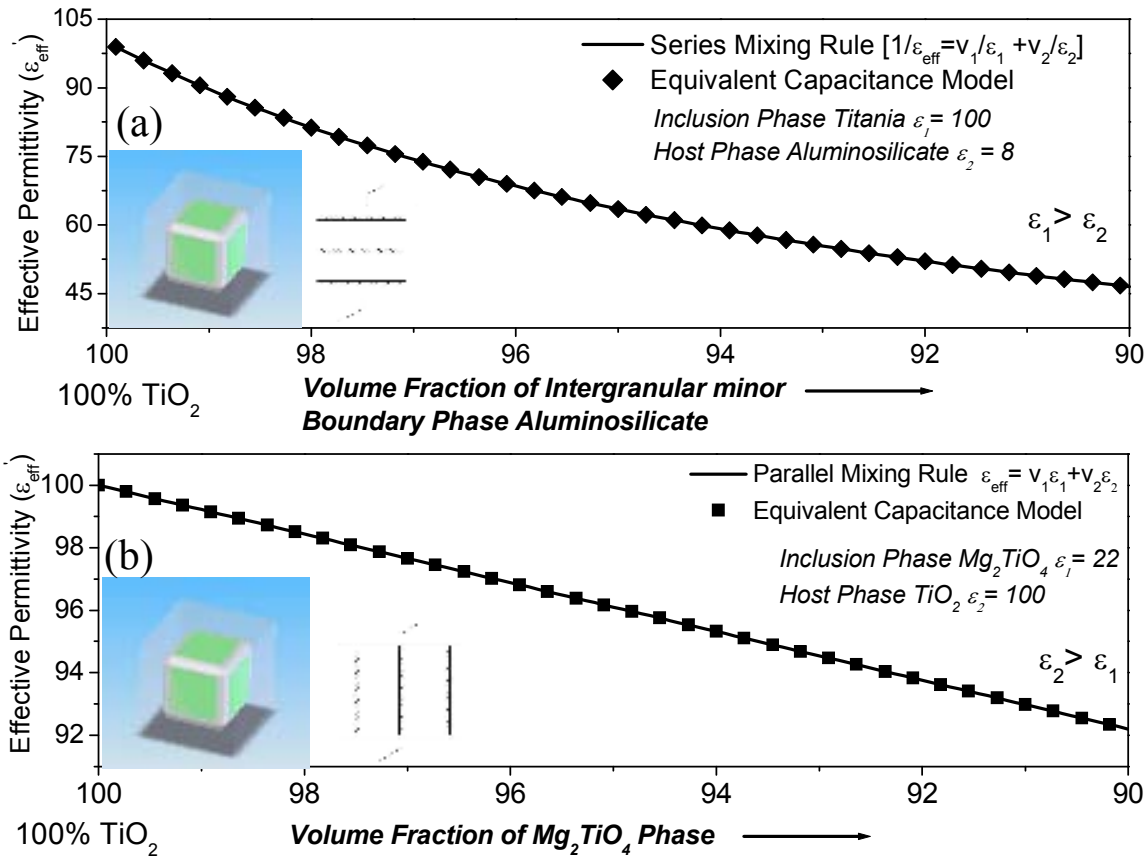

FIG. 10. Comparison of effective permittivity predictions of series and parallel mixing rule with equivalent capacitance model.

These mixing rules represent limiting cases of the more general equivalent capacitance model. This implies that the equivalent capacitance model may be used to describe effective permittivity of a wide range of diphasic dielectric microstructures.

IV. CONCLUSIONS

An equivalent capacitance model to estimate the static effective permittivity of a composite mixture based on discretizing a dielectric body into partial capacitor elements was presented. The model was demonstrated for a system consisting of high-permittivity

spherical inclusion(s) in a cube of a lower permittivity phase (e.g., a 0-3 composite), as well as for a periodic system of such individual cells. The predictions of the equivalent capacitance model agree well with experimental data obtained from the literature. The results of computations show that the classical Maxwell Garnett and equivalent capacitance models diverge at inclusion volume fractions greater than approximately 10%, since the MG model is valid for only dilute mixtures. The present model based on discretization of the dielectric volume has no inherent restrictions on inclusion volume fraction, size, or shape, and is applicable to any structure subjected to an applied homogeneous static electric field.

Effective permittivity predictions by the equivalent capacitance model match the limiting case series and parallel mixing rules. This implies that the equivalent capacitance model is applicable to a wide range of composite microstructures. Extension of the equivalent capacitance model to predict frequency-dispersive relative permittivity of composites has also been developed by including loss in the model, assigning partial resistances along with the partial capacitances (RC-circuits). This extension of the model is described in a separate paper. The equivalent capacitance model, may also be extended to the case of randomly dispersed inclusions.

V. ACKNOWLEDGMENTS

This work was supported through a MURI program sponsored by the Office of Naval Research under Grant No. N000-14-05-1-0541.

VI. REFERENCES

[1] S. D. Poisson, in *Mem. Acad. Sc.* Paris. **5:247** (1821); See also L. K. H. Ven Beck, Prog. Diel., 7, 71 (1967); See also D. A. Payne, Ph.D. Thesis, The Pennsylvania University, 1973.

[2] L. Rayleigh, *Philosophical Magazine.*, **44,** 28 (1897); See also T. C. Choy, *Effective Medium Theory, Principles and Applications* (Oxford University Press, Oxford, 1999).

[3] J. C. M. Garnett, in *Trans. of the Royal Society,* London, Ser. B **203**, 385 (1904); See also H. Frohlich, *Theory of Dielectrics,* 2nd ED. (Oxford University, London, 1958); See also P.S. Neelakanta, *Handbook of Electromagnetic Materials* (CRC Press, Boca Raton, FL, 1995).

[4] R. Landauer, in *Electrical Transport and Optical Properties of Inhomogeneous Media,* edited by J. C. Garland and D.B. Tanner, AIP Conference Proceedings, No.40 (American Institute of Physics, New York, 1978).

[5] D. J. Bergman and D. Stroud, in *Solid State Physics*, edited by H. Ehrenreich and D. Turnbull (Academic, New York, 1992), Vol. 46, pp. 178-320.

[6] A. Sihvola, E*lectromagnetic Mixing Formulas and Applications* (IEE, London, UK, 1999).

[7] M. Y. Koledintseva, J. Wu, J. Zhang, J. L. Drewniak, and K. N. Rozanov, in *Proc. IEEE Symp. Electromag. Compat.*, Santa Clara, CA, 2004, Vol. 1, pp. 309-314.

[8] J. Avelin and A. Sihvola, Microw. Opt. Technol. Lett., **32**, 60 (2002).

[9] O. Weiner, Abh. *Sachs.Akad.Wiss*. **32,** 509 (1912) See also D. A. Payne, Ph.D. Thesis, The Pennsylvania University, 1973.

[10] D. F. Rushman and M. A. Striven, *Proc. Phys. Soc*., **59,** 1011 (1947).

[11] W. D. Kingery, *Introduction to Ceramics,* (John Wiley and Sons, New York, 1960).

[12]D. A. G. Bruggeman, Ann. Phys. (Leipzig) **24**, 636 (1935); See also B. Sareni, L. Krahenbuhl, A. Beroual, C. Brosseau, J. Appl. Phys. **83**, 3288 (1998).

[13] V. Myroshnychenko and C. Brosseau, J. Appl. Phys, **97**, 044101 (2005).

[14] K. Lichtenecker, Phys. Z., **10**, 1005 (1909); See also P.S. Neelakanta, *Handbook of Electromagnetic Materials* (CRC Press, Boca Raton, FL, 1995).

[15] D. Payne, *Tailoring Multiphase and Composite Ceramics*, *Material Science Research*. **20,** edited . R. E. Tressler, G. L. Messing, C. G. Pantano (Plenum Press 1987), Vol. 20, pp. 413-431.

[16] C. J. Dias and D. K. Das-Gupta, IEEE Trans. Dielect. Electr. **3**, 707 (1996).

[17] C. J. Dias and D. K. Das-Gupta, Key Engineering Materials, **92**, 217 (1994).

[18] Y. Bai, Z. Y. Cheng, V. Bharti, H. S. Xu, and Q. M. Zhang, Appl. Phys. Lett. **76**, 3804 (2000).

[19] Y. Rao, S. Ogitani, P. Kohl, and C. P. Wong, J. Appl. Polym. Sci., **83**, 1084 (2002).

[20] C. Huang and Q. M. Zhang, Adv. Funct. Mater. **14**, 501 (2004).

[21] Y. Rao, S. Ogitani, Paul Kohl, and C. P. Wong, *Electronic Components and Technology Conference,* 2000*,* pp. 183-187.

[22] B. Chu, X. Zhou, K. Ren, B. Neese, M. Lin, Q. Wang, F. Bauer and Q. M. Zhang, Science, **313**, 334, (2006).

[23]S. V. Marshall, R. E. Du Broff, and G.G. Skitek, *Electromagnetic Concepts and Applications*, (4th ed., Prentice Hall, NJ, 1996).

[24] G. Arlt, D. Henning, and G. de With, J. Appl. Phys. **58**, 1619 (1985).

[25] G. Arlt, J. Mater. Res. **25**, 2655 (1990).

[26] G. Arlt, Ferroelectrics. **104**, 217 (1990).

[27] K. Uchino, E.Sadanaga, and T. Hirose, J. Am. Ceram. Society, vol. 72, 1555 (1989).

[28] R. Waser, Ferroelectrics, vol. 15, 39 (1997).

[29] C. Chiang and R. Popielarz, Ferroelectrics **275**, 1, (2002).

[30]E. Aulagner, J. Guilet, G. Seytre, C. Hantouche, P. Le Gonidec and G. Tezulli, IEEE Symp. Conduction and Breakdown in Solid Dielectrics. (1995), Vol. 1, pp. 423-427.

APPENDIX A

Calculation of the Corner Capacitance

Consider the corner capacitor elements, as shown in Fig. 11. Their dimensions are characterized by parameters b and d. "$b = 2r$" is equal to the diameter of the sphere, as the cube dimension in which inclusion sphere is enclosed. "d" is the thickness of the plates. The angle θ is measured from the horizontal direction, and $d\theta$ is an increment. The area of the corner capacitors can be calculated using 3D visualization, as illustrated in Fig. 11 and Fig. 12. The area of the discretized corner plate can be calculated from Figure 12. Thus, an expression for the area of the discretized corner capacitor plate may be written:

$$S = 2r^2 - \frac{\pi \cdot r^2 \cos^2 \theta}{2} \tag{A1}$$

From the triangle Δ EDO, the length ED is

$$l(ED) = r \cdot \sin(d\theta), \tag{A2}$$

As the angle $d\theta$ is very small,

$$l(ED) \approx rd\theta, \tag{A3}$$

From the triangle Δ ECD, the incremental thickness dh of any discretized plate can be found as:

$$dh = l(EC) = r\cos\theta \cdot d\theta, \tag{A4}$$

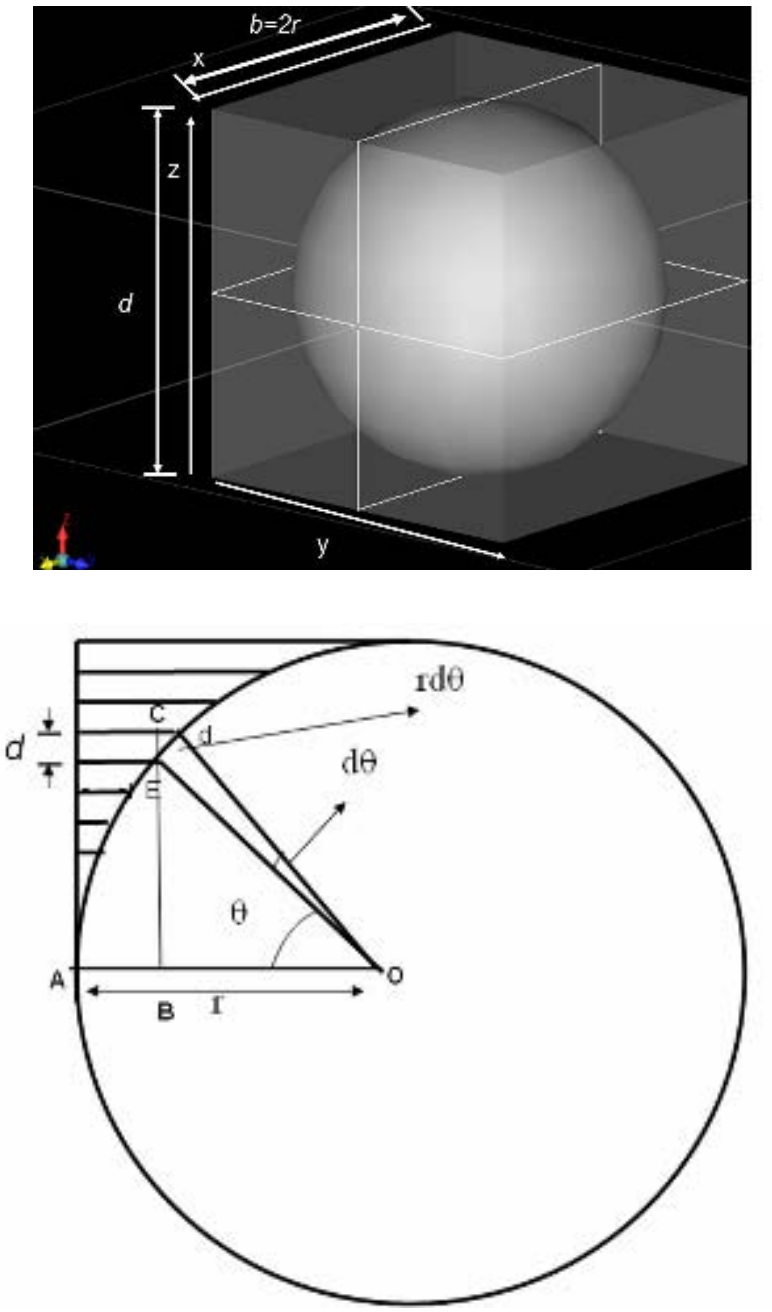

FIG. 11.Three dimensional views of the corner capacitor element and vertically cut section of inclusion sphere and corners detailing the discretization process for calculating corner capacitance value.

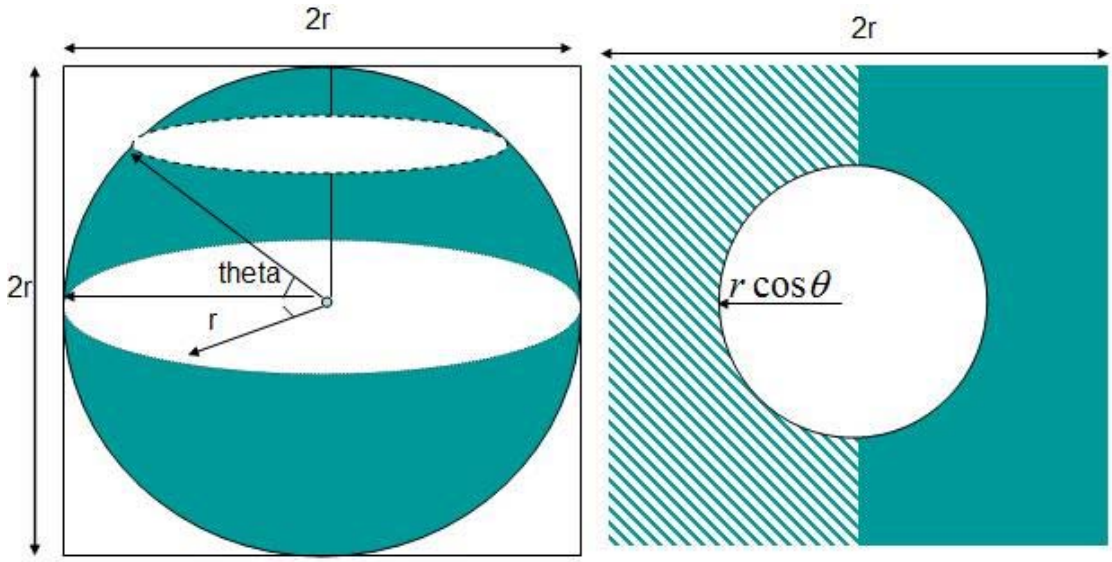

FIG. 12. Sectional front and top view of the inclusion sphere and corner elements to explain mathematics of discretization process.

The incremental capacitance of every corner plate is calculated as follows:

$$dC_i = \frac{\varepsilon_o \cdot \varepsilon_h \cdot (2r^2 - \frac{\pi \cdot r^2 \cos^2\theta}{2})}{r\cos\theta d\theta}. \tag{A5}$$

All the discretized corner capacitors are arranged in series and therefore the equivalent capacitance of the corner elements is given by the following expression

$$\frac{1}{C_d} = \frac{1}{C_1} + \frac{1}{C_2} + - - - + \frac{1}{C_n} = \frac{1}{\sum_{i=1}^{n} \frac{1}{C_i}} = \frac{1}{\int_0^{\frac{\pi}{2}} \frac{1}{dC_i}}, \tag{A6}$$

Therefore, the corner capacitance is calculated by the expression shown in (A6)

$$C_d = \frac{1}{\int \frac{1}{dC_i}} = \frac{1}{2\int_0^{\frac{\pi}{2}} \frac{d\sin\theta}{(4-\pi)\varepsilon_o\varepsilon_h r + \pi\varepsilon_o\varepsilon_h r\sin^2\theta}}, \tag{A7}$$

By substituting $\sqrt{\pi\varepsilon_o\varepsilon_h r}\cdot\sin\theta = X$ and $A^2 = \frac{\varepsilon_o\varepsilon_h r(4-\pi)}{\sqrt{\pi\varepsilon_o\varepsilon_h r}}$ which results in the expression A8 as below

$$C_d = \frac{1}{2\int_0^{\frac{\pi}{2}} \frac{dX}{A^2+X^2}} = \frac{\varepsilon_o\varepsilon_h r\pi}{2}\cdot\frac{1}{\frac{1}{\sqrt{\frac{4}{\pi}-1}}\arctan\left[\frac{1}{\sqrt{\frac{4}{\pi}-1}}\right]}, \tag{A8}$$

APPENDIX B

Calculation of the Capacitance of Dielectric Sphere

A dielectric sphere inside a parallel-plate capacitor with voltage applied to its top and bottom plates is discretized by horizontal slices of the sphere, as shown in Fig. 13. Let us consider just a quarter of the sphere shown in Fig. 13.

The distance AC, which is the radius of the slice, is labeled as q_i, and the incremental distance is:

$$\Delta q_i = q_{i+1} - q_i . \tag{B1}$$

Angle $\angle$ AOF $= \theta$, and the increment of the angle $\angle AOB = d\theta$. From ΔAOB, it is seen that:

$$\sin d\theta = \frac{l(AB)}{l(AO)} . \tag{B2}$$

Since $\angle AOB = d\theta$ is very small,

$$l(AB) = r \cdot \sin(d\theta) \approx r \cdot d\theta . \tag{B3}$$

$\angle AOF$ and $\angle CAO$ are equal, as they are internal alternate angles, and

$$\angle CAO + \angle OAE = 90^0 \Rightarrow \angle OAE = (90^0 - \theta) \tag{B4}$$

Then, since

$$\angle CAO + \angle EAB = 90^0 . \tag{B5}$$

By substituting $\angle OAE$ (B4) into (B5), one can get

$$\angle EAB = \theta . \tag{B6}$$

From ΔAEB, one can find the thickness of the individual discretized plate d,

$$\cos\theta = \frac{l(AE)}{l(AB)}. \tag{B7}$$

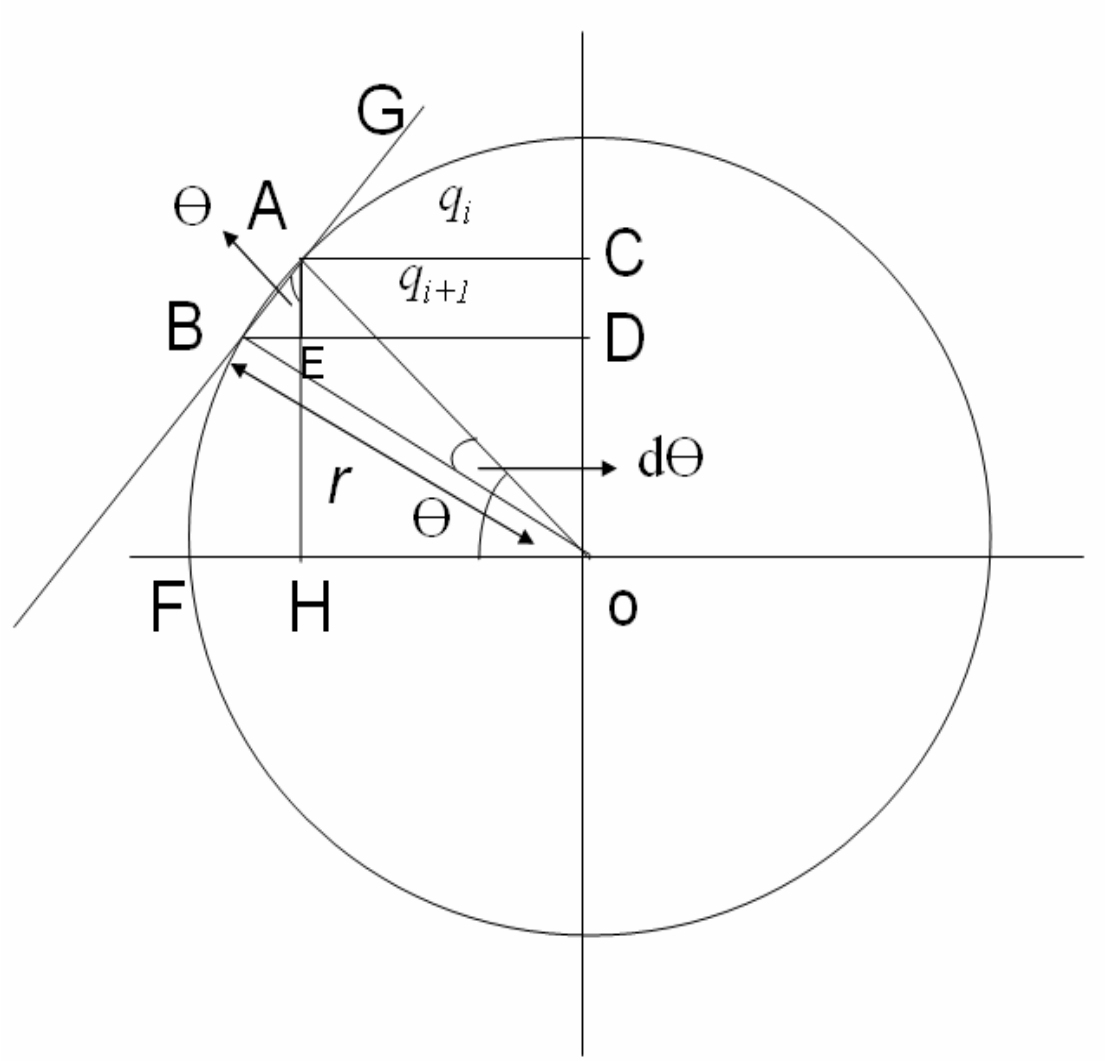

FIG 13. Vertically cut section of inclusion sphere detailing the discretization process for calculating capacitance value of inclusion dielectric sphere.

Therefore, the thickness of the discretized capacitor is given by:

$$d = r\cos\theta \cdot d\theta. \tag{B8}$$

Lengths OH and AC are:

$$l(AC) = l(OH) = q_i . \tag{B9}$$

From the triangle ΔOEH , it may be determined that

$$q_i = l(OH) = r \cdot \cos\theta . \tag{B10}$$

Only half area of the discretized plate is taken into account as the sphere is divided into 4 quarters. The area of the discretized capacitor plates is given by:

$$Area = \pi \cdot (r \cdot \cos\theta)^2 . \tag{B11}$$

The capacitance of the discretized plates can be calculated as:

$$C_i = \frac{\varepsilon_o \cdot \varepsilon_i \cdot \pi \cdot (r \cdot \cos\theta)^2}{2 \cdot R \cdot d\theta \cdot \cos\theta} . \tag{B12}$$

The inverse value is:

$$\frac{1}{C_i} = \frac{2d\theta}{\varepsilon_o \cdot \varepsilon_i \cdot \pi \cdot r \cdot \cos\theta} . \tag{B13}$$

The total capacitance of the quarter of the sphere is calculated as a series capacitance, so:

$$\frac{1}{C_{1/4}} = \frac{2}{\pi \cdot r \cdot \varepsilon_o \cdot \varepsilon_i} \int_0^{\pi/2} \frac{d\theta}{\cos\theta} . \tag{B14}$$

Finally,

$$C_{1/4} = \frac{\pi \cdot r \cdot \varepsilon_o \cdot \varepsilon_i}{2 \int_0^{\pi/2} \frac{d\theta}{\cos\theta}} . \tag{B15}$$

This capacitance $C_{1/4}$ is the capacitance of the quarter of the sphere, but it is also a total capacitance of the whole dielectric sphere, since two left hand capacitances are in series, two right-hand capacitances are also in series, and they are connected together in parallel.

$$C_5 = C_{1/4} . \tag{B16}$$

2. PREDICTION OF EFFECTIVE PERMITTIVITY OF DIPHASIC DIELECTRIC AS A FUNCTION OF FREQUENCY

Sandeep K. Patil, Marina Y. Koledintseva, Senior Member, IEEE, Wayne Huebner, Robert W. Schwartz, and **Konstantin N. Rozanov**

ABSTRACT

An analytical model based on an equivalent impedance circuit for expressing an effective permittivity of a composite dielectric as a function of frequency with complex-shaped inclusions is presented. The geometry of the capacitor containing this composite dielectric is discretized into partial impedance elements, the total equivalent impedance is calculated, and the effective permittivity of the composite dielectric is obtained from this equivalent impedance. An example application using this method is given for an individual cell of a diphasic dielectric consisting of a high-permittivity spherical inclusion enclosed in a low-permittivity parallelepiped. The capacitance and resistance for individual discretized elements in the composite cell are modeled as a function of an inclusion radius. The proposed approach is then extended to a periodic three-dimensional structure comprised of multiple individual cells. The equivalent impedance model is valid for both static and alternating applied electric fields, over the entire range of volume fraction of inclusions. The equivalent impedance model has a few advantages over existing effective medium theories, including no limitations on the shape of inclusions or their separation distance. .

Index Terms- Dielectric composites, electric field distribution, energy storage, equivalent capacitance

1 INTRODUCTION

Theoretical efforts to predict the dielectric behavior of multiphase composites have been investigated for more than 100 years [1-5], and have resulted in a number of effective medium theories. The fundamental approach is to focus on one particular inclusion and then replace all of the rest by an effective homogenous medium. Any effective medium theory then is invariant to which particular inclusion is taken as a focus [6-9], since each inclusion must be surrounded by the same effective medium. One of the most widely-used formulations for calculating the effective permittivity of mixtures is the Maxwell Garnett (MG) theory [9-12]. MG theory is satisfactory when exact interparticle interactions are not significant, *i.e.*, for small concentrations (*inclusion volume fraction*< *0.1*) of inclusions in a dielectric host [13]. The MG theory is applicable for inclusions of any arbitrary ellipsoidal shape, including spheres, spheroids, cylinders, and disks, through introducing depolarization factors [14]. Complex inclusion shapes can only be approximated by assuming a closest shape [15], which limits the overall applicability. The empirically derived logarithmic mixing rule is also widely applied for fitting experimental data [3]. However, the experimental fit of logarithmic mixing rule in some cases might be fortuitous, as was pointed out by Payne [16].

Properties of composite media have been intensively studied in the last two decades using various numerical techniques. The most prominent among these have been Monte Carlo simulations (MC) [17], the finite element method (FEM) [18, 19], the finite difference method [20] and the boundary integration method [21, 22]. It is noteworthy to consider the contribution of Sareni *et al.* who through use of numerical analysis techniques calculated the effective dielectric constant of periodic composites [21],

random composites [23], and then also analyzed the complex effective permittivity of a lossy composite material [24]. Myroshnychenko *et al.* [6] have developed an algorithm for predicting the complex permittivity of two-dimensional diphasic statistically isotropic heterostructures, and compared their results with different effective medium approaches.

Through numerical approaches it is possible in principle to study a system of any complexity, however numerical analysis requires enormous computational resources that are costly and might not be always available.

The objective of this work was to obtain a simple closed-form analytical model that would allow for predicting the effective complex permittivities of diphasic composites. This model should be free from limitations on inclusion size and shape, as well as distances between inclusions. The model presented herein is based on discretization of a dielectric body into partial impedances, specifically, R-C elements, equivalent to "lossy capacitors." This can be applied to any inclusion shape. The effective permittivity is then calculated from the resultant impedance of the appropriate equivalent circuit. It should be mentioned that the analogous electric circuit approach was used by Pan *et al.* [25] to predict the properties of a multilayer dielectric, with each single-phase layer having various grain sizes.The approach presented herein has been applied to a high-permittivity inclusion in a low-permittivity host dielectric. As an example, the host dielectric is a parallelepiped (in particular, a cube). An inclusion in this example is a sphere, which is the simplest geometry to be compared with the MG theory and logarithmic mixing rule. This structure is referred to as "an individual cell" (or just "a cell"). The impedance of the cell is modeled as a function of an inclusion radius, or a volume fraction of an inclusion. The model is then extended to a composite three-

dimensional (3D) structure comprised of periodically placed individual cells. Such a structure is found experimentally in such systems as epoxy/$BaTiO_3$ [26-30].

2 MODEL DESCRIPTION

2.1 ONE INDIVIDUAL IMPEDANCE CELL

A general diphasic slab with a three-dimensional periodic structure of inclusions A general diphasic slab with a three-dimensional periodic structure of inclusions is subdivided into individual cells (cubes), each containing one high-permittivity inclusion surrounded by a lower permittivity host material. Figure 1 shows the basic building block of the composite and its three-dimensional translation.

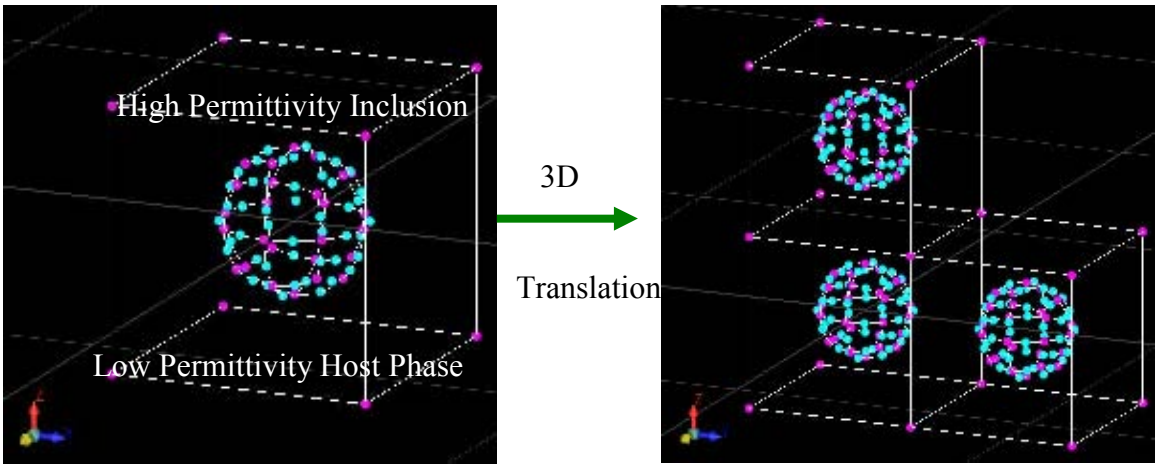

Figure 1. Basic building block of composite sphere enclosed in a cube and its 3-D translation in x, y, z directions

First consider an individual cell with an inclusion of an isotropic shape, *i.e.*, a sphere, placed at the center of a cube. The inclusion and the host are assumed to be linear isotropic and homogeneous dielectric materials, with an alternating electric field applied

along the vertical dimension of the cell. In this case, any cell is simply an individual capacitor with an inhomogeneous dielectric inside, and can be discretized into parallel and series parallel-plate partial impedances, each containing a homogeneous dielectric. Figure 2(a) shows, how this structure is discretized into partial elements. Each element has its own impedance, in which a partial capacitor is parallel to the corresponding partial resistor, responsible for loss. The equivalent circuit corresponding to an individual cell is shown in Figure 2 (b). The total equivalent reactance, X_{eq}, and impedance, Z_{eq}, of the individual cell are

$$X_{eq} = \frac{1}{j\omega C_{eq}} \tag{1}$$

$$Z_{eq} = \frac{R_{eq} \cdot X_{eq}}{(R_{eq} + X_{eq})}. \tag{2}$$

In (1) and (2), R_{eq} and C_{eq} are the equivalent resistance and capacitance of the structure. The equivalent capacitance parallel-plate capacitor filled by effective dielectric medium is,

$$C_{eq} = \frac{Z''_{eq}}{\omega(Z'_{eq} + Z''_{eq})}, \tag{3}$$

Where ω is frequency of alternating electric field and Z'_{eq} and Z''_{eq} are real and imaginary parts of impedance, respectively.

Figure 3 shows the planar projection of the 3D view presented in Figure 2(a). Z_1 and Z_2 are the impedances that are present on left and right hand side of the inclusion.

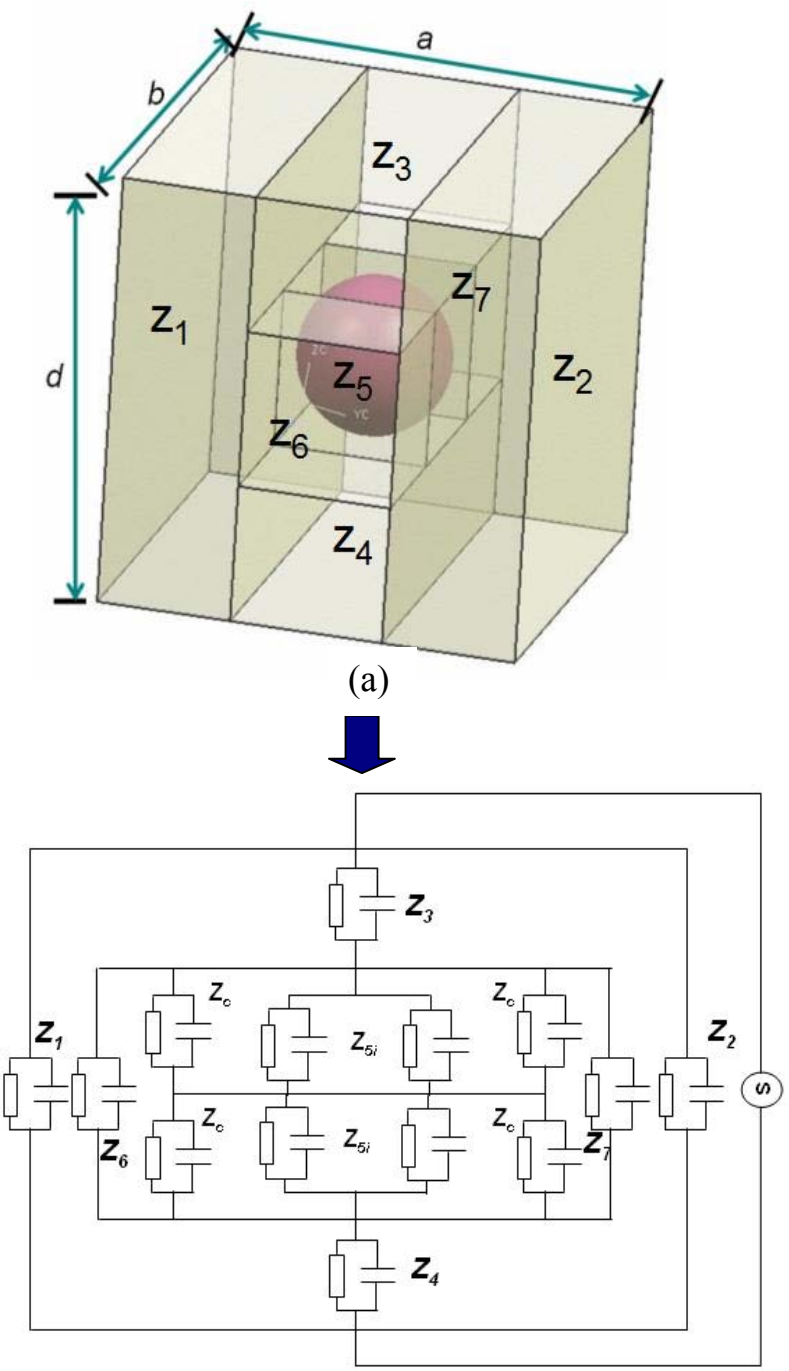

Figure 2. 3-D view of the discretized diphasic dielectric body and its corresponding equivalent circuit.

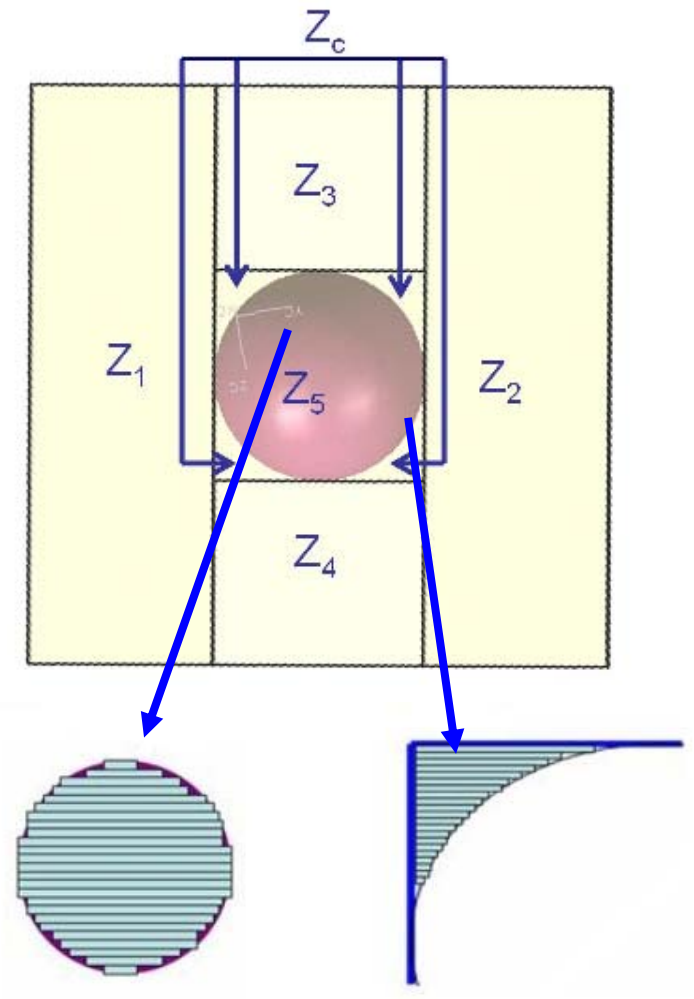

Figure 3. 2-D view of the discretized diphasic dielectric body and discretization pathway of corner shape and inclusion sphere.

sphere. Assuming the structure is symmetrical, the capacitances C_1 and C_2 are equal, and given by

$$C_1 = C_2 = \frac{\varepsilon_0 \varepsilon_h (a_c / 2 - r) b_c}{d_c}, \tag{4}$$

where ε_h is the relative permittivity of the host material. These capacitances linearly decrease as the radius of the inclusion increases. The corresponding reactance for any α-th element is $X_\alpha = \frac{1}{j\omega C_\alpha}$. If the loss tangent is taken into account, then the resistances of each element are

$$R_1 = R_2 = \frac{2d_c}{\sigma_h (a_c - 2r) b_c}, \tag{5}$$

where σ_h is the conductivity of the host; a_c, b_c, and d_c are the dimensions of the individual cell (in a particular case of a cube, $a_c = b_c = d_c$), and r is the radius of the inclusion.

The partial capacitances C_3 and C_4 and partial resistances R_3 and R_4 are the elements located on the top and the bottom of the inclusion, respectively, and are calculated as

$$C_3 = C_4 = \frac{4\varepsilon_0 \varepsilon_h b_c r}{d_c - 2r} \tag{6}$$

$$R_3 = R_4 = \frac{(d_c - 2r)}{4 \cdot r \cdot \sigma_h b_c}. \tag{7}$$

The partial capacitances C_6 and C_7 and partial resistances R_6 and R_7, located in front of and behind the sphere (see Figure 2(a)), are calculated as

$$C_6 = C_7 = \frac{\varepsilon_0 \varepsilon_h (b_c - 2r)}{2} \tag{8}$$

$$R_6 = R_7 = \frac{2}{\sigma_h (b_c - 2r)}. \tag{9}$$

Figure 3 shows the discretization pathway for the corner shape and inclusion sphere. The same discretization is adopted for calculating both partial capacitances and resistances. The resistance and capacitance of the corner elements are calculated using smaller discretization into elemental slices parallel to the electrode planes of the cell. They are connected in series, and the integration over the corner space is accomplished. The calculation of capacitance of corner capacitor elements and the inclusion sphere have been presented by Patil *et al.* [31]. The detailed calculation of the resistance of the corner element is presented in the attached *Appendix A*. The total resistance and capacitance for all four corner elements- two bottom and two top $(i = 1...4)$ are

$$C_c = C_{c_i} = 2.76\varepsilon_0\varepsilon_h r \tag{10}$$

$$R_c = R_{c_i} = \frac{1.326}{\sigma_h r} \tag{11}$$

To calculate the capacitance of the high-permittivity sphere, it is convenient to cut it into thin parallel slices, and consider series connection of the elements. The integration procedure yields the capacitance of the quarters of the dielectric sphere C_{5_i}, $(i = 1...4)$ which is the same as of the total sphere

$$C_5 = C_{5_i} = \frac{\varepsilon_0\varepsilon_i\pi \cdot r}{2\int_0^{\pi/2} \frac{d\theta}{\cos(\theta)}}. \tag{12}$$

To assure convergence of the integral in the denominator, zero in the integration was substituted by 10^{-7}. The resistance of the inclusion sphere is calculated by first calculating the conductance of the sphere as shown below.

$$G_{5_i} = \frac{C_{5_i} \cdot 2 \cdot \pi \cdot f \cdot \varepsilon''}{\varepsilon'} \Rightarrow R_5 = R_{5_i} = \frac{1}{G_{5_i}} \tag{13}$$

The real and imaginary parts of the inclusion phase permittivity are calculated using the Debye expression

$$\varepsilon_i(\omega) = \varepsilon_{\infty i} + \frac{\varepsilon_{si} - \varepsilon_{\infty i}}{1 + j\omega\tau_i} \ . \tag{14}$$

The impedance of any partial element with an index α is calculated as an impedance of parallel resistive element R_α and the reactive element X_α, connected in parallel

$$Z_\alpha = \frac{X_\alpha \cdot R_\alpha}{X_\alpha + R_\alpha} . \tag{15}$$

The impedance of the central part of the equivalent circuit is

$$Z_{central} = Z_3 + Z_4 + \frac{1}{\frac{1}{Z_6} + \frac{1}{Z_7} + \frac{1}{\frac{Z_c Z_5}{Z_c + Z_5}}} . \tag{16}$$

Finally, the equivalent impedance of the cell can be found as

$$Z_{eq} = \frac{1}{\frac{1}{Z_1} + \frac{1}{Z_2} + \frac{1}{Z_{central}}} . \tag{17}$$

Since this equivalent impedance is comprised of equivalent capacitance and equivalent resistance elements connected in parallel, the values R_{eq} and C_{eq} can be obtained from the real and imaginary parts of $Z_{eq} = Z'_{eq} - jZ''_{eq}$. The equivalent capacitance of the individual cell is

$$C_{eq} = \frac{Z''_{eq}}{\omega \cdot (Z'^{\,2}_{eq} + Z''^{\,2}_{eq})}. \tag{18}$$

Then, assuming that the homogeneous dielectric with permittivity ε'_{eff} fills the space between the cell capacitor plates, the real part of the effective permittivity is

$$\varepsilon'_{eff} = \frac{C_{eq} d_c}{\varepsilon_o a_c b_c}. \tag{19}$$

By utilizing the equivalent impedance approach, ε'_{eff} and ε''_{eff} can be found as shown below. The effective permittivity (ε'_{eff}) captures the shape of the inclusion, and there are no restrictions on the inclusion size. Thus from the equivalent capacitance, the effective static permittivity can be found.

The equivalent resistance of the individual cell is

$$R_{eq} = \frac{Z'^{\,2}_{eq} + Z''^{\,2}_{eq}}{Z'_{eq}}. \tag{20}$$

The equivalent conductance of the individual cell is simply the inverse of the equivalent resistance,

$$G_{eq} = \frac{1}{R_{eq}}. \tag{21}$$

The imaginary part of the effective permittivity can be calculated from the equivalent conductance.

$$\varepsilon''_{eff} = \frac{\varepsilon'_{eff} \cdot G_{eq}}{2 \cdot \pi \cdot f \cdot C_{eq}} \tag{22}$$

2.2 N^3 INDIVIDUAL IMPEDANCE CELLS

Let us consider a case with N inclusions in the form of spheres along each of the three dimensions of the total capacitor, resulting in N^3 individual cells. If the dimensions of the total capacitor are $a, b, \text{and } d$, then the dimensions of an individual cell are

$$a_c = a/N, b_c = b/N, \text{and } d_c = d/N, \tag{23}$$

respectively.

The equivalent circuit of the total impedances contains individual cells in vertical branches connected in series, while all the branches are connected in parallel, as is shown in Figure 4. This means that the total equivalent impedance of all the branches is

$$Z_{eq} = \frac{Z_{branch}}{N^2} = \frac{Z_{cell}}{N}. \tag{24}$$

Then the effective permittivity of an inhomogeneous dielectric inside the total capacitor can be calculated using (17) and (24) for ε'_{eff} and ε''_{eff}, respectively.

The effective permittivity of an inhomogeneous dielectric obtained using the method presented above is compared later on with the well-known homogenization technique based on the Maxwell Garnett (MG) mixing rule [9-12, 14] and logarithmic mixing rule [15]. For a mixture of a host material with relative permittivity ε_h and spherical inclusions with relative permittivity ε_i, the Maxwell Garnett mixing rule is

$$\varepsilon_{eff\ MG} \cong \varepsilon_h + \frac{3 f_i \varepsilon_h (\varepsilon_i - \varepsilon_h)/(\varepsilon_i + 2\varepsilon_h)}{1 - f_i (\varepsilon_i - \varepsilon_h)/(\varepsilon_i + 2\varepsilon_h)}, \tag{25}$$

where $f_i = \frac{V_i}{V_\Sigma}$ is the volume fraction of spherical inclusions in the total mixture. Here V_i represents volume of inclusion and V_Σ represents volume of composite.

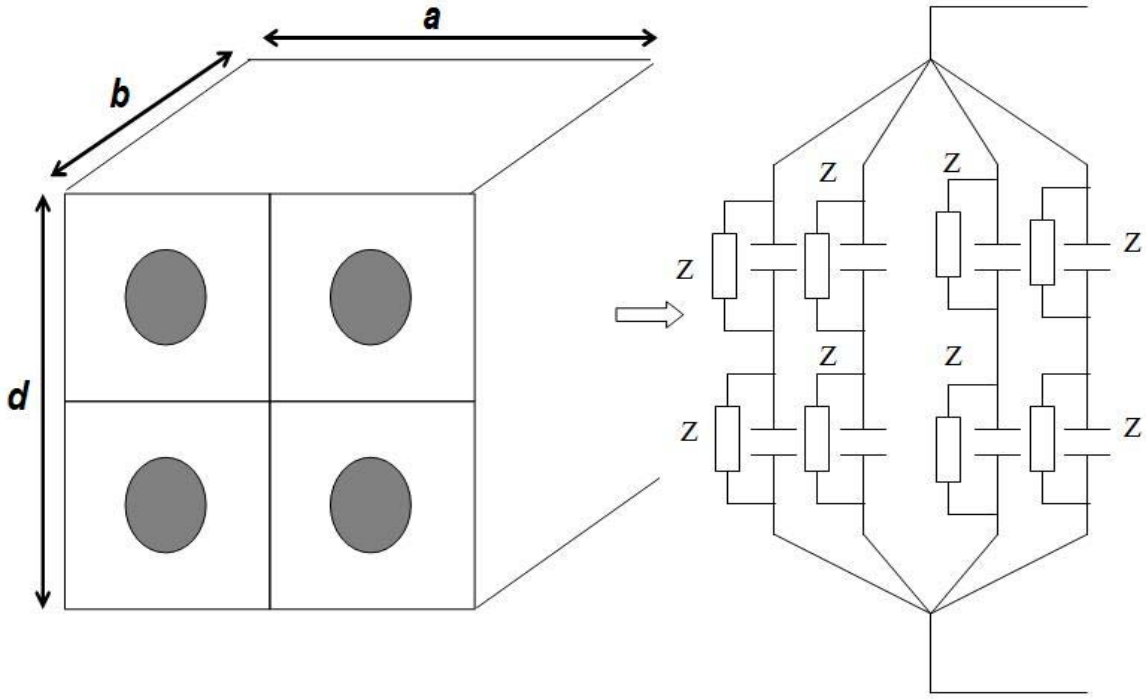

Figure 4. Discretization pathway for N^3 impedances.

The formulation for logarithmic mixing rule is given by

$$\varepsilon_{eff\ Logarithmic} \cong V_h \cdot \log \varepsilon_h + V_i \log \varepsilon_i , \tag{26}$$

Herein, V_h and ε_h is the volume fraction and permittivity of the host phase respectively. Also, V_i and ε_i is volume fraction and permittivity of the inclusion phase respectively.

3 RESULTS AND DISCUSSION

Computations of the complex effective permittivity of a composite based on the equivalent RC circuit model are presented herein. The 3D model is set up to mimic the real world system of a high permittivity phase inclusion in a polymeric host (ceramic - polymer composite) with 0-3 connectivity. Two cases have been investigated: the first

with just one inclusion in the host matrix, and the second with 1000 inclusions inside the cube.

The experimental data for computations is taken from the paper of M.P. McNeal et al. [32] which presented the microwave behavior of $BaTiO_3$, which can be approximated using the Debye frequency dependence [33],

$$\varepsilon_i(\omega) = \varepsilon_{\infty i} + \frac{\varepsilon_{si} - \varepsilon_{\infty i}}{1 + j\omega\tau_i} \ . \tag{27}$$

In McNeal et al. [32], the static permittivity for a coarse-grain $BaTiO_3$ ceramic is reported to be ε_{si}=1900, the "optical limit" permittivity is $\varepsilon_{\infty i}$=280, and the Debye constant is τ_i = 2.06 ns, which corresponds to a relaxation frequency $f_{ri} = \frac{\omega_{ri}}{2\pi}$ = 771 MHz. The polymeric host is a low-loss material, with frequency independent relative permittivity ε_h = 4, and an equivalent ohmic conductivity of $\sigma_h = 3.79 \cdot 10^{-7}$ S/m, which corresponds to a $\tan\delta$ on the order of $10^{-7}...10^{-4}$ in the microwave range of interest. The polymeric cube surrounding one ceramic sphere (or multiple spheres) has the following dimensions: $a_c = b_c = d_c = 1.1$ μm. The radius of the sphere is a varying parameter, and, hence, the volume fraction of the inclusion or inclusions is also varying.

Figure 5 (a) depicts the equivalent capacitance of the dielectric composite as a function of frequency and inclusion volume fraction. The inclusion volume fractions chosen were 2.5 %, 8.4%, 20.1%, 39.3% and 46.8% respectively. The equivalent capacitance as a function of inclusion volume fraction is dominated by the capacitor elements C_5, C_3, and C_4. As the volume fraction of the inclusion phase increases from

2.5% to 46%, the contribution of capacitor elements C_5, C_3, and C_4 increase due to the concurrent increase in area of the capacitor elements and decrease in the thickness of the host.

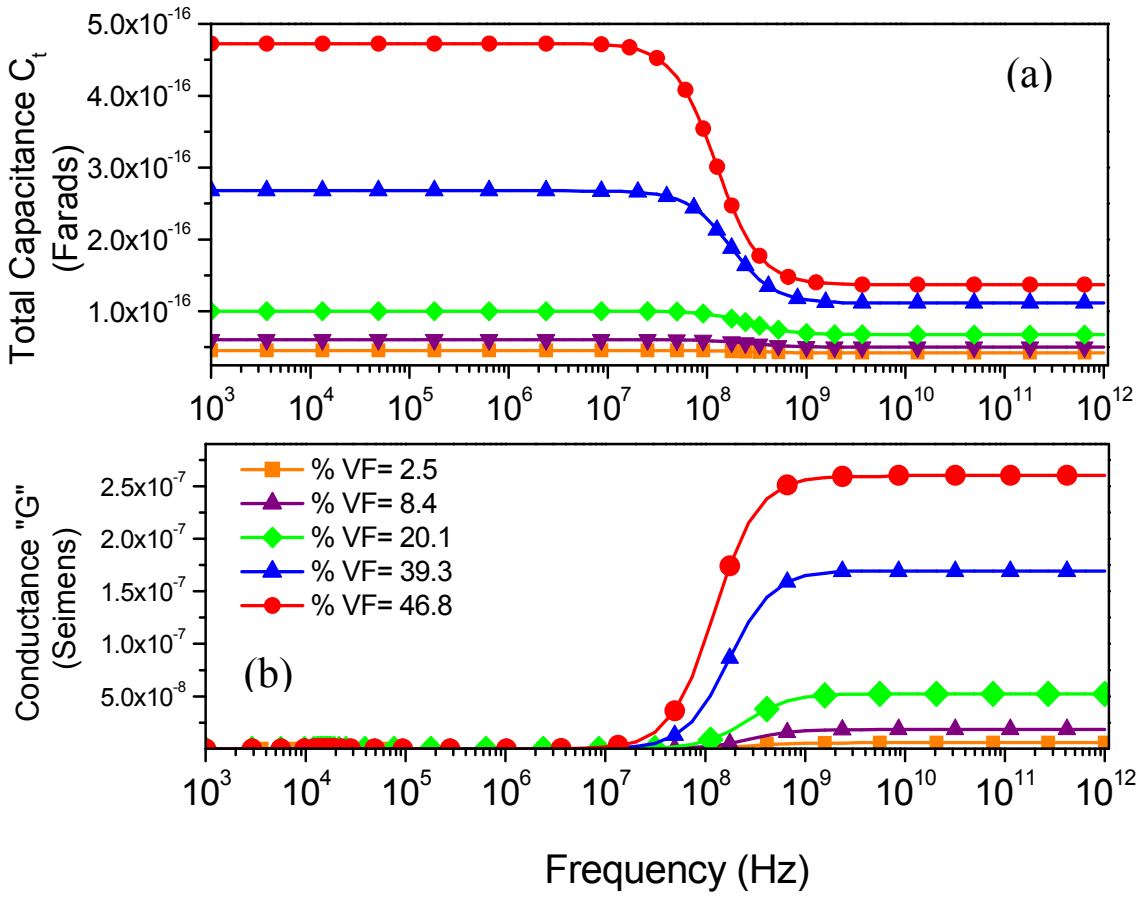

Figure 5. Magnitude of the equivalent capacitance and equivalent conductance of composite as a function of frequency and inclusion volume fraction.

It is a well known fact that at lower frequencies all the polarization mechanisms, space charge, dipolar, electronic and ionic polarization, are active. As the frequency increases

and goes beyond the relaxation frequency, only ionic and electronic polarization mechanisms are active. The decrease of dipolar and space charge polarization results in the decrease in charge that is formed on capacitor plates, and this leads to the reduction in the equivalent capacitance. Figure 5 (a) demonstrates this effect.

In Figure 5 (b), the equivalent conductance of the dielectric composite is plotted as a function of frequency. To understand the results generated by the analytical model, it is imperative to understand the physical response of a dielectric to an applied field as a function of frequency. As capacitors "conduct" current in proportion to the rate of voltage change, they will pass more current for faster-changing voltages (as they charge and discharge to the same voltage peaks in shorter time interval), and less current for slower-changing voltages. Therefore there would be an increase in the effective conductivity of the dielectric for frequencies above the relaxation frequency for all inclusion volume fractions. It is also seen from Figure 5 (b) that with the increase in the volume fraction of the high-permittivity inclusion phase, the equivalent resistance decreases, and the equivalent conductance of the composite dielectric increases.

Figure 6 depicts the response of effective permittivity ($\varepsilon_{eff}^{'}$) of the dielectric composite as a function of frequency. Figure 6 shows very clearly relaxation in dielectric properties. The real part of permittivity predicted by the equivalent impedance model at 10^3 Hz is $\varepsilon'_{eff} \approx$ 47, and it decreases to ~11 at 10^{12} Hz, so that the difference $\Delta\varepsilon_{eff} = \varepsilon'_{eff\,s} - \varepsilon'_{eff\,\infty}$ (dielectric relaxation strength) is about 35. The $\varepsilon_{eff}^{'}$ remains essentially flat up to ~ 10^7 Hz, and above this frequency it decreases and follows the Debye frequency dependence. This prediction is for the highest inclusion volume fraction of 46.8 %. With the reduction of inclusion volume fraction to 39.3%, the effective

permittivity ε'_{eff} of the composite reduced to 27 at 10^3 Hz and saturated to around 10^{12} Hz and yielding $\Delta\varepsilon_{eff} \approx 17$. $\Delta\varepsilon_{eff}$ continues to decrease with the inclusion volume fraction decrease, and this is an expected result as dispersive phase's volume fraction decreases in the non-dispersive host phase. All these predictions of permittivity were for a single inclusion in the host phase.

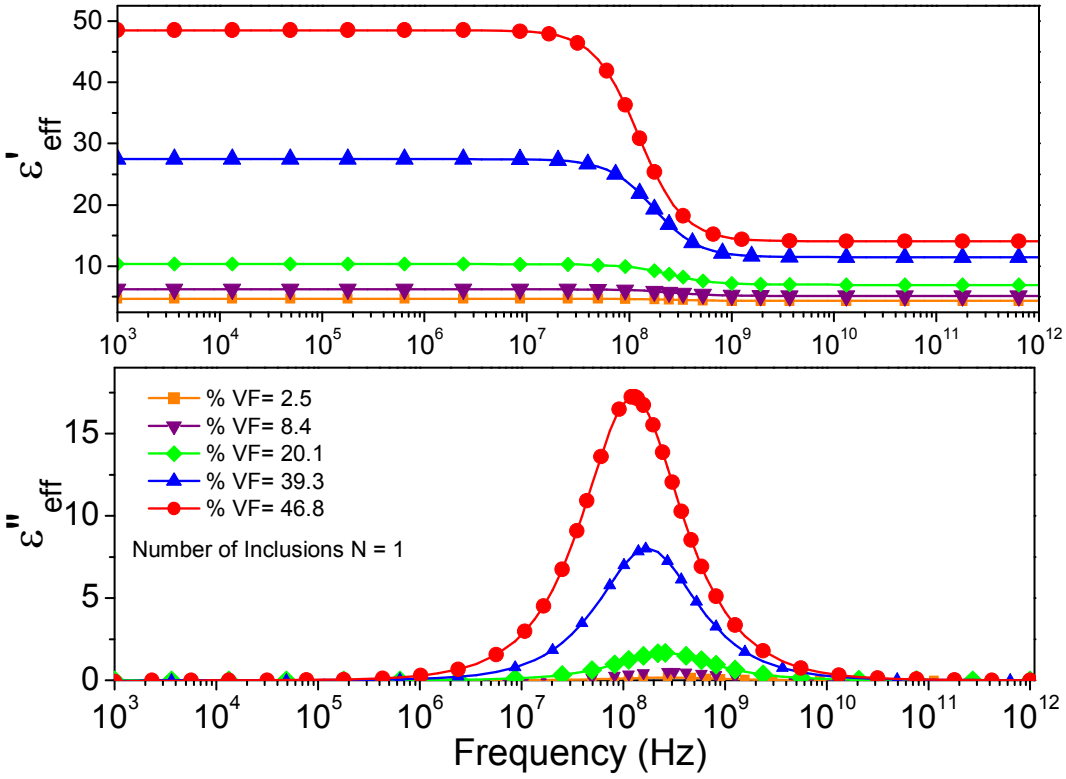

Figure 6. Prediction of effective permittivity of diphasic composite by equivalent impedance model for various inclusion volume fractions as a function of frequency.

The dielectric relaxation in $BaTiO_3$ takes place at 771 MHz [32]. The frequency dependence of ferroelectricity including apparent disappearance of ferroelectric response in the microwave regions has been explained by von Hippel [34]. For a ferroelectric material like $BaTiO_3$, there are permanent electric dipoles which are firmly anchored into position and not available for free rotation. They are unable to follow the applied field at frequencies above the relaxation frequency, and this causes the decrease in the permittivity, as the contribution of dipolar polarization is no longer there.

Another interesting observation can be made on examination of Figure 6. The characteristic peak of the imaginary part of the composite (ε''_{eff}) shifts to lower frequency with increase in inclusion volume fraction. This shift in the frequency of the ε''_{eff} peak to the lower frequencies for the bigger inclusions ($r > 0.3\ \mu m$) might be explained as follows. The dipole moments of the bigger and "heavier" inclusions start opposing the high-frequency variations at the lower frequencies than the inclusions of smaller sizes. At the same time, the peak value for ε''_{eff} increases as the size of the inclusion increases, and this is related to the enhanced total loss within the bigger inclusion. Also, there is a factor of conductivity contrast between the inclusion and the host phase. The effective conductivity of a BT inclusion with the Debye dependence under consideration, σ_i, is on the order of a few S/m in the frequency range of interest, as opposed to the conductivity of the host, σ_h, which is frequency-independent and on the order of 10^{-7} S/m. Therefore, there is not much influence of the loss in the host phase upon the maximum loss frequency of the composite. However, if $\sigma_h / \sigma_i > 10^{-3}$, there is a substantial shift of the maximum loss peak to the lower frequencies.

Figure 7 shows frequency dependencies of real and imaginary parts of permittivity for the same system with one inclusion in the host phase, modeled using Maxwell Garnett formulation.

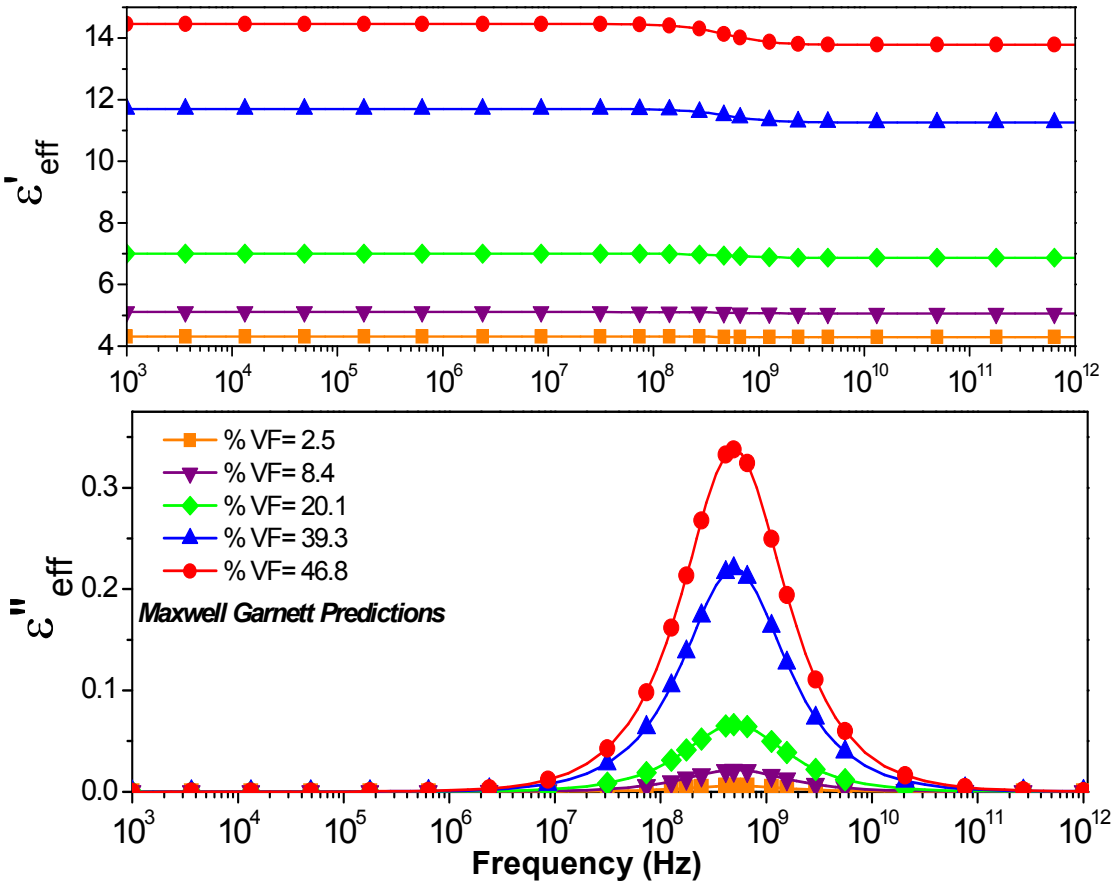

Figure 7. Prediction of the effective permittivity of a diphasic composite by Maxwell Garnett model for various inclusion volume fractions as a function of frequency.

It is seen that for the inclusion volume fraction of 46.8%, $\varepsilon'_{eff} \approx 14$ at 10^3 Hz, and it decreases to $\varepsilon'_{eff} \approx 13$ at $f = 10^{12}$ Hz, yielding a dielectric constant difference $\Delta\varepsilon_{eff} \approx 1$. This shows that the MG model is unable to accurately predict the frequency dependence of dielectric properties in mixtures with higher inclusion volume fractions. The MG model predictions also considerably underestimate the effective permittivity of the composite.

The results of simulations, shown in Figure 6 and 7, can be compared with the simulations based on the well-known logarithmic mixing rule (Figure 8). As is seen from Figure 8, the real part of permittivity predicted by the equivalent impedance model at 10^3 Hz is $\varepsilon'_{eff} \approx 71$, and decreases to ~29 at 10^{12} Hz, so that the difference $\Delta\varepsilon_{eff} = \varepsilon'_{eff\,s} - \varepsilon'_{eff\,\infty}$ is about 42. The logarithmic mixing rule gives the static real permittivity value of approximately 1.5 times greater than that predicted by the equivalent impedance model for the inclusion volume fraction of 46.8%. The "optical" limit permittivity predicted by the logarithmic rule is about 2.5 times higher than in the equivalent impedance model for the same inclusion volume fraction. The discrepancy between the logarithmic mixing rule and the equivalent impedance model decreases as the inclusion volume fraction reduces.

The results of computations based on both models almost coincide, when the inclusion volume fraction is less than 20%. At the same time, the Maxwell Garnett model agrees well with our model for the volume fraction of inclusions less than 10%. The logarithmic rule and Maxwell Garnett formulation and does not take into account shapes of inclusions, and multiple inclusions in three dimensions.

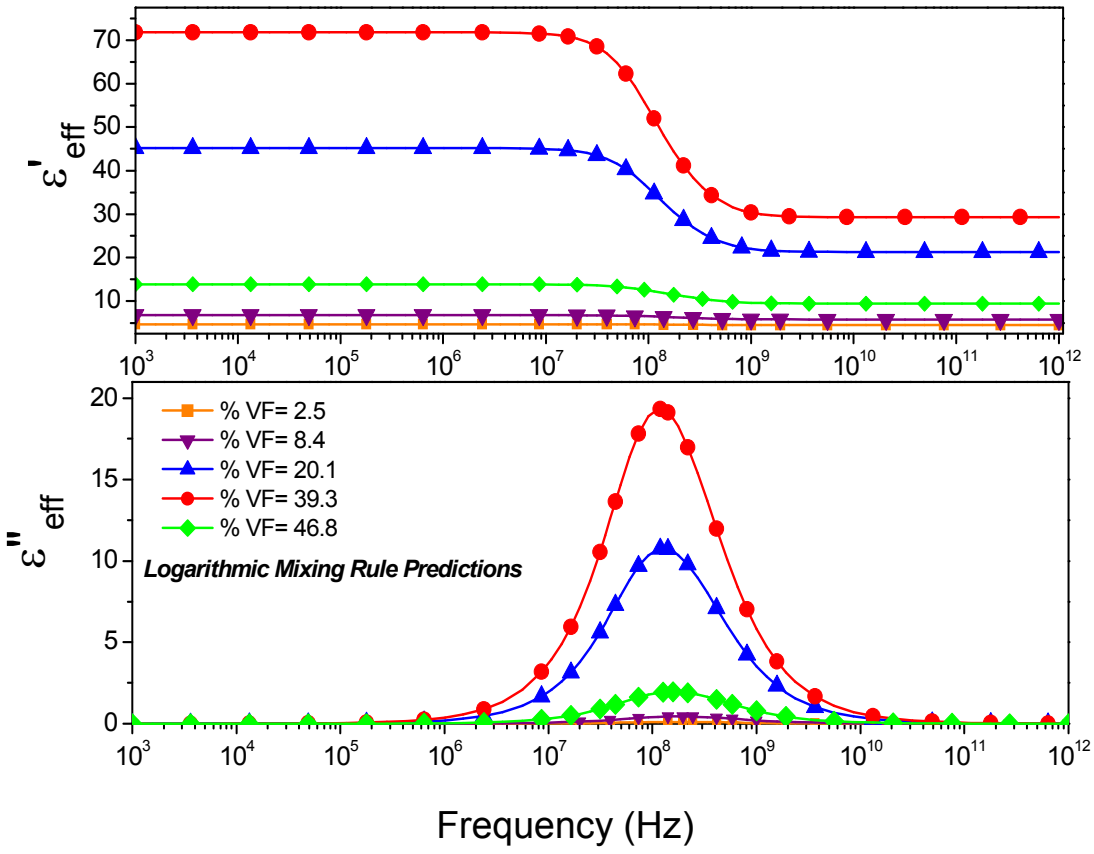

Figure 8. Prediction of effective permittivity of diphasic composite by Logarithmic mixing model for various inclusion volume fractions as a function of frequency.

The consistency of the equivalent impedance model for multiple inclusions in three dimensions has been tested by studying a diphasic dielectric but with 1000 high permittivity inclusions instead of a single inclusion. The inclusion volume fraction was held constant in both cases. The maximum radius of each inclusion is 10 times smaller than in the previous example. In this particular case the inclusion size reduces and is

varied from 10 nm to maximum 54.9 nm as opposed to the earlier case when single inclusion size was varied from 0.1 μm to a maximum of 0.549 μm. It has been verified that the predictions that the equivalent capacitance model for multiple inclusions remains the same as that for single inclusion predictions.

4 CONCLUSIONS

The equivalent impedance circuit model for estimating the effective permittivity of a composite mixture as function of frequency was presented in this paper. This model is based on discretizing a dielectric body into partial impedance elements. The discretization process uniquely takes into account any inclusion size and shape. An RC Circuit analogy was used to account for loss in this model by assigning partial resistances along with the partial capacitances.

The model system addressed in this paper was for a periodic system consisting of high-permittivity spherical inclusion(s) enclosed in a cube with a lower permittivity phase. The complex permittivity prediction of the equivalent impedance model showed characteristic Debye relaxation behavior. The equivalent impedance model was compared to Maxwell Garnett mixing theory and Logarithmic mixing rule. The equivalent impedance model is simple solution to a complex problem and is able to take into account any inclusion shape and can predict dielectric permittivity and dielectric loss as a function of frequency.

5 ACKNOWLEDGMENTS

6

Authors would like to kindly acknowledge the help of Dr. Wei Li in going through some of the details of the mathematical foundation of the work. This work was

supported through a MURI program sponsored by the Office of Naval Research under Grant No. N000-14-05-1-0541

6 REFERENCES

[1] J.C. Maxwell, *Electricity and Magnetism*, vol. 1, Clarendon Press, Oxford, 1892.

[2] L.K.H. van Beck, "Dielectric behavior of heterogeneous systems," Ch. 3 in *Progress in Dielectrics*, vol. 7, J.B. Birks, Ed., London: Heywood Books, 1967.

[3] K. Lichtenecker,"Der elektrische Leitungswiderstand kiinstlicher und natfirlicher Aggregate," *Phys. Z.*, **10**, 1005, 1909.

[4] S. P. Mitoff, in "Advances in Materials Research", edited by H. Herman (Wiley-Interscience, New York, 1968), Vol. 3, pp. 305–329.

[5] A. H. Sivhola, "How strict are theoretical bounds for dielectric properties of mixtures?" *IEEE Trans. Geosci. Rem. Sens*., **40** [4], 880 2002.

[6] V. Myroshnychenko and C. Brosseau, "Finite-element modeling method for the prediction of the complex effective permittivity of two-phase random statistically isotropic heterostructures," *J. Appl. Phys*, vol. 97, 044101-14 2005.

[7] T.C. Choy, *Effective Medium Theory, Principles and Applications* (Oxford University Press, Oxford, 1999.

[8] G.W. Milton, *Theory of Composites,* (Cambridge University Press), Cambridge, 2002.

[9] A.H. Sihvola, *Electromagnetic Mixing Formulas and Applications,* (IEEE Publishing, London, 1999.

[10] J.C. Maxwell Garnett, in "Colors in Metal Glasses and in Metallic Films,**"** *Trans. of the Royal Society,* London, Vol. CCIII, pp. 385-420, 1904.

[11] R. Landauer, in *Electrical Transport and Optical Properties of Inhomogeneous Media, AIP Conf. Proc*., edited by J. C. Garland and D.B. Tanner, New York, Vol. 40, pp. 2, 1978.

[12] D. J. Bergman and D. Stroud, "Physical properties of macroscopically inhomogeneous media," *Solid State Phys*., **46,** 147 1992.

[13] A. Spanoudaki, R. Pelster, "Effective dielectric properties of composite: The dependence on the particle size distribution," *Phys. Rev. B*: **64,** 064205 2001.

[14] M. Y. Koledintseva, J. Wu, J. Zhang, J. L. Drewniak, and K. N. Rozanov, "Representation of permittivity for multi-phase dielectric mixtures in FDTD modeling," in *Proc. IEEE Symp. Electromag. Compat.* Santa Clara, CA, Vol. 1, pp.309-314, 2004.

[15] J. Avelin and A. Sihvola, "Polarizability of polyhedral dielectric scatterers," Micro. Opt. Technol. Lett., **32** [1], 60-64, 2002.

[16] D. Payne, "The Role of Internal Boundaries upon the Dielectric properties of Polycrystalline Ferroelectric Materials," Ph.D. Thesis: The Pennsylvania State University (1973).

[17] K. Wakino, T. Okada, N. Yoshida, and K. Tomono, "A New Equation for Predicting the Dielectric Constant of a Mixture," *J. Am. Ceram. Soc.***, 76,** 2588 1993.

[18] C. Brosseau and A. Beroual**, "**Computational electromagnetics and the rational design of new dielectric heterostructures," *Prog. Mater. Sci.,* 48, 373 2003.

[19] C. Ang, Z. Yu, R. Guo, and A. Bhalla, "Calculation of dielectric constant and loss of two-phase composites,**"** *J. Appl. Phys.***, 93**, 3475 2003.

[20] A. H. Sihvola, and K.I. Nikoskinen, "Effective permittivity of mixtures: numerical validation by the FDTD method" *IEEE Trans. Geosco. Remote Sens.,* **38**, 1303 2000.

[21] B. Sareni, L. Krähenbühl, A. Beroual, and C. Brosseau, "Effective dielectric constant of periodic composite materials," *J. Appl. Phys.,* **80**, 1688 1996.

[22] S.K. Patil and R. W. Schwartz and, "Modeling Field Distribution and Energy Storage in Diphasic Dielectrics," 12th US-Japan Seminar on Dielectric & Piezoelectric Ceramics, 397 - 400 (Nov. 2005, Annapolis, MD).

[23] B. Sareni, L. Krähenbühl, A. Beroual, and C. Brosseau, "Effective dielectric constant of random composite materials," *J. Appl. Phys.***, 81**, 2375 1997.

[24] B. Sareni, L. Krähenbühl, A. Beroual, and C. Brosseau, "Complex effective permittivity of a lossy composite material," *J. Appl. Phys.,* **80**, 4560 1996.

[25] M.-J. Pan, B.A. Bender, and E.P. Gorzkowski, "Complex Permittivity Model of Barrier Layer Capacitor with Bimodal Grain Size Distribution," Proc. 12th US-Japan Seminar on Dielectric and Piezoelectric Ceramics, Nov. 6-9, Annapolis, MA, USA, pp. 321-324, 2005.

[26] Y. Bai, Z. Y. Cheng, V. Bharti, H. S. Xu, and Q. M. Zhang, "High-dielectric-constant ceramic-powder polymer composites," *Appl. Phys. Lett.*, **76**, 3804 2000.

[27] M. Dang, Y. Shen, and C. W. Nan, "Dielectric behavior of three-phase percolative Ni–$BaTiO_3$/polyvinylidene fluoride composites," *Appl. Phys. Lett.,* **81**, 4814 2002.

[28] Y. Rao, J. M. Qu, T. Marinis, and C. P. Wong, "A precise numerical prediction of effective dielectric constant for polymer-ceramic composite based on effective-medium theory,**"** *IEEE Trans. Compon. Packag. Technol.***, 23**, 680 2000.

[29] Y. Rao, A. Takahashi, and C. P. Wong, "Di-block copolymer surfactant study to optimize filler dispersion in high dielectric constant polymer-ceramic composite," *Composites, Part A*, **34**, 1113 2003.

[30] C. J. Dias and D. K. Das-Gupta, "Inorganic ceramic/polymer ferroelectric composite electrets**"** *IEEE Trans. Dielectr. Electr. Insul*. **3**, 706–734 (1996)

[31] S.K. Patil, M.Y.Koledintseva, K. Rozanov, W. Huebner, R. W. Schwartz, "Prediction of Effective Permittivity of Diphasic Dielectrics Using an Equivalent Capacitance Model" Manuscript to be sent to JAP.

[32] M. P. McNeal, S. J. Jang, and R. Newnham, "The effect of grain and particle size on the microwave properties of barium Titanate," *J. Appl. Phys.,* **83**, 3288, 1998.

[33] A. J. Moulson & J. M. Herbert, 2nd Edition *Electroceramics: Materials, Properties, Applications* (John Wiley & Sons) 2003.

[34] A. von Hippel," Piezoelectricity, ferroelectricity and crystal structure" Z. Phys.133, 1952.

APPENDIX

Calculation of the Corner Resistance

Consider the corner resistor elements, as shown in Figure 9. The area of the discretized corner plate for calculating corner resistances can be calculated from the Figure 10 as

$$S = 2r^2 - \frac{\pi \cdot r^2 \cos^2 \theta}{2} \tag{B1}$$

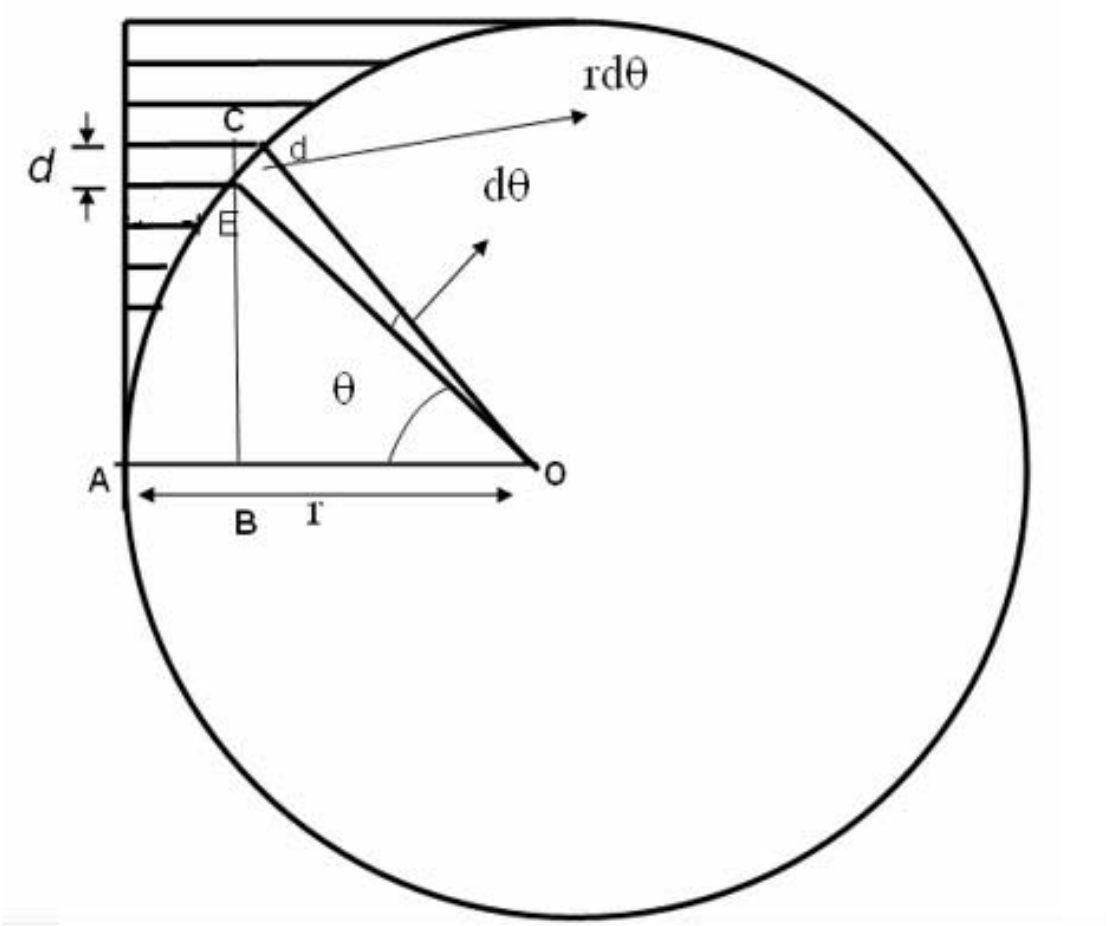

Figure 9. Vertically cut section of the inclusion sphere and corners detailing the discretization process for calculating the corner capacitance value.

From the triangle Δ EDO, the length ED is

$$l(ED) = r \cdot \sin(d\theta), \tag{B2}$$

As the angle $d\theta$ is very small,

$$l(ED) \approx rd\theta, \tag{B3}$$

From the triangle Δ ECD, the thickness d of any discretized plate can be found as

$$d = l(EC) = r\cos\theta \cdot d\theta, \tag{B4}$$

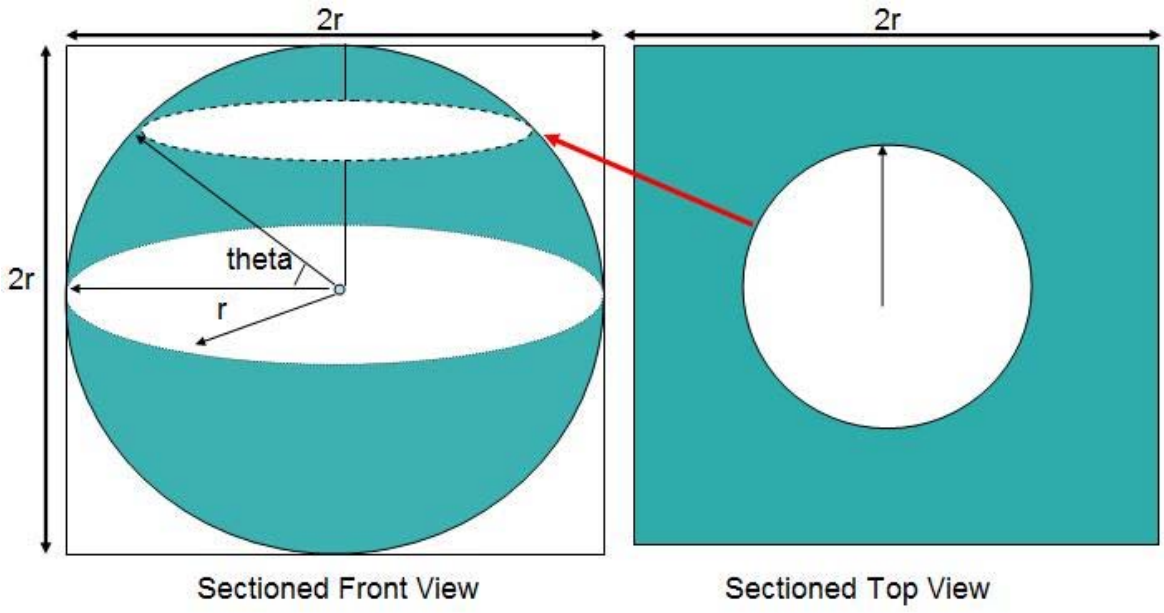

Figure 10. Sectional front and top view of the inclusion sphere and corner elements to illustrate the mathematics of the discretization process.

The resistance is derived as follows.

$$dR_i = \frac{r\cos\theta \cdot d\theta}{\sigma_h\left[2r^2 - \frac{\pi \cdot r^2\cos^2\theta}{2}\right]}, \tag{B5}$$

or

$$dR_i = \frac{2d(\sin\theta)}{r^2\sigma_h\left[(4-\pi)+\pi\sin^2\theta\right]}. \tag{B6}$$

Substituting $x = \sin\theta$ into equation (B6), one can get

$$R_{ci} = \frac{2}{r\sigma_h\pi}\int_0^1 \frac{dx}{\frac{(4-\pi)}{\pi}+x^2}. \tag{B7}$$

After integrating, the final expression for the corner resistance is obtained,

$$R_{ci} = \frac{2}{r\sigma_h\pi}\cdot\frac{1}{\sqrt{(\frac{4}{\pi}-1)}}\arctan\left[\frac{1}{\sqrt{(\frac{4}{\pi}-1)}}\right], \tag{B8}$$

or

$$R_{ci} = \frac{1.326}{r\sigma_h} \tag{B9}$$

3. MODELING OF FIELD DISTRIBUTION AND ENERGY STORAGE IN DIPHASIC DIELECTRICS

S. K. Patil, M. Y. Koledintseva, R. W. Schwartz, and W. Huebner
Missouri University of Science and Technology, Rolla, MO, 65409, USA

ABSTRACT: Modeling of electrostatic field distribution and energy storage in diphasic dielectrics containing high-permittivity $BaTiO_3$ in a polymeric or glass host has been carried out analytically and numerically. The analytical formulation employs the Maxwell Garnett (MG) mixing rule, while numerical simulation uses software based on the boundary element method (BEM). The field distribution was studied as a function of dielectric contrast and volume fraction of phases. For a high-permittivity sphere enclosed in a low-permittivity polymer or glass cube, it was found that a dielectric contrast of 75 and volume fraction of ~ 47% led to increased energy storage density. For composites with lower volume fractions (2.51%) of high-permittivity inclusions, a field enhancement factor of 2.6 was observed, whereas for higher volume-fraction composites (47%), field enhancements as high as 10 were observed. The higher field enhancement factors are expected to lead to dielectric breakdown at lower applied fields, limiting energy storage density. The upper limit of applicability of the MG formulation in terms of inclusion volume fraction was also established, and was found to be a function of the dielectric contrast. The host material permittivity results in a substantial variation in the applicability limit of the MG mixing rule, while the permittivity of inclusion phase does not affect the limit.

Keywords: Dielectric composites, electric field distribution, energy storage

1. INTRODUCTION

The properties of dielectric mixtures have been investigated for more than 100 years.[1-5] One of the more recent objectives of research in this area has been to develop dielectric bodies with enhanced energy storage capabilities, for example, crystallization of a phase with higher permittivity, like $BaTiO_3$, in a glass matrix.[6] The general goal of such approaches is to take advantages of both the high energy storage capacity of the $BaTiO_3$ inclusions and the high breakdown strength of the glass phase. This approach may eliminate porosity that causes field concentration (enhancement), adversely impacting breakdown.[7]

Other ways of solving this problem are based on dispersing materials with high permittivities, such as $BaTiO_3$, into polymeric hosts to assure high energy density and breakdown strength, low dielectric loss, fast charge and discharge rates, low cost, and graceful failure leading to higher reliability.[8-9] Recent studies of such composites have resulted in effective permittivities between 20 and 115,[10-11] depending on the volume fraction of the filler phase and various characteristics of the synthesis process.

The dielectric response of filled composites, such as those described above, has been modeled using a variety of effective medium theories.[12-16] Dielectric behavior is typically described based on formulations that include the dielectric properties of constituent phases and their volume fractions. The geometry of the inclusions is also important, and typically, ellipsoidal inclusions are considered.[17-18] The effective permittivity of the composite is usually determined using a quasistatic approximation; i.e., the size of the inclusions is much smaller than the wavelength in the medium. Another common assumption in this analysis is that the phases behave in a linear manner.

Employing these assumptions, the estimated effective permittivity and defining the applied field allow for estimation of the energy storage characteristics of the composite.

It is known that the Maxwell Garnett (MG) formulation for diphasic dielectrics can be applied for comparatively dilute mixtures.[19] Most mixing rules assume that the lines of electric flux are *not distorted* by the particles, and hence, there are inherent limitations in accurately predicting the energy storage capabilities of composites.[20] For heterogeneous composites, the electric flux lines tend to distribute according to the permittivity ratios of the host and inclusion phases.[21] Local inhomogeneities in electric field distribution, i.e., field enhancement in the low permittivity phase and field penetration in the high permittivity phase, are not taken into account by classical mixing theories.

Numerical simulation results have illustrated that the electric field distribution in composites may be of three different types. The first type is field enhancement in the low-permittivity phase at the boundary separating the two phases in the direction of the applied field. The second distribution type is field penetration into the high-permittivity phase. Typically, this is a low-intensity field. The third type of field distribution is field of intermediate intensity in the low permittivity phase. The first two types of field distribution are important from standpoint of breakdown strength of composite and the third type of distribution is significant from standpoint of energy density of composites. An insightful study to understand field distribution in such composites has been carried out, but it is limited to only two-dimensional cases.[22]

The present study is aimed at a comprehensive analysis of the impact of the field distribution on the energy storage and breakdown strength of diphasic composites. To complete this analysis, and to suggest composite designs that are attractive for high energy densities, it is necessary to quantify the electric field distribution and gain a thorough understanding of the parameters that determine this distribution. To solve this problem, the dielectric properties of the constituent phases and their volume fractions should be known. This specifically involves identifying the *dielectric contrast* between the phases that would lead to increased energy storage. The dielectric contrast is defined herein as the ratio of the permittivity of the inclusion phase to the permittivity of the host phase:

$$c = \frac{\varepsilon_{incl}}{\varepsilon_{host}}. \qquad (1)$$

The three-dimensional (3D) numerical simulation software *Coulomb* is used in the present study to comprehensively analyze the impact of field distribution on the energy storage and breakdown strength of diphasic composites. This software is based on the solution of Laplace's electrostatic equation, and enables study of local field inhomogeneities. The results of simulations are interpreted from the perspectives of field enhancement in the host phase and field penetration into the high permittivity inclusion phase.

Another goal of this work is to determine the limits of applicability of the Maxwell Garnett formulation in terms of the inclusion volume fraction. Maxwell Garnett theory has been accepted as a satisfactory approximation, when inter-particle interactions are not significant; *i.e.*, when the composites are dilute mixtures (*inclusion volume*

fraction <0.1).[23] Though the scientific community has been cognizant of this limitation, the minimum limit on the inclusion volume fraction (or inter-inclusion separation distance) has not been established yet.

Herein, the results for diphasic dielectric bodies with different permittivities and volume fractions are reported. A three-dimensional model of a composite is developed from a sphere enclosed in a cube (SEC) geometry, with the cube representing a low-permittivity (e.g., glass or polymer) phase, and the spherical inclusion representing a high-permittivity (e.g., barium titanate) phase. It should be noted that the assumption of a sphere enclosed in a cube matrix is a special "non-random" case. Myroshnychenko et al.[24] have rightfully acknowledged the fact that, in spite of significant computational advances and the ability to model random composites, as well as non-random structures, it has been difficult to find experimental systems that bear close resemblance to the idealized models. In the reported work[24], an algorithm for the 2D case with random inclusions has been developed, and two cases of surface fractions, percolating and non-percolating systems, have been considered and compared with other EMT theories. However, local electric field distribution as a function of inclusion volume fraction and dielectric contrast has not been explored. In the present study, local electric field enhancements have been quantified as a function of the properties of the inclusion and the host phase for ordered systems. The MG formulation was also applied to calculate the effective permittivity of the systems investigated, and the results of the two approaches are compared.

2. SIMULATIONS

2.1. METHOD AND SOFTWARE FOR NUMERICAL SIMULATIONS

Simulations were carried out using the commercially available software *Coulomb* from Integrated Engineering Software (Winnipeg, Manitoba, Canada). *Coulomb* is a 3D code that uses a boundary element method to solve Laplace's equation for electrostatic potential inside the geometry of interest.[26, 27] The Laplace equation,

$$\nabla^2 V = 0 , \qquad (2)$$

is a specific case of the Poisson's equation:

$$\nabla^2 V = -\frac{q_{vol}}{\varepsilon} , \qquad (3)$$

where q_{vol} is the free charge volume density, V is the electric potential, and $\varepsilon = \varepsilon_0 \varepsilon_r$ is the permittivity of the medium, where ε_o is the permittivity of free space and ε_r is the relative permittivity of the dielectric.

Compared to finite element methods (FEM) and finite difference methods (FDM), the boundary element method (BEM) reduces the number of calculations that must be performed for problems formulated in terms of electrostatic potentials.

Simulations using *Coulomb* were carried out to understand local field distribution as a function of inclusion volume fraction and its impact on the energy stored in the composite.

Coulomb allows for the construction of 3D structures containing periodically repeated cells with identical properties to represent a uniform diphasic dielectric. It should be noted that the dielectric behavior of a composite can also be obtained through

studying a single cell. Fig. 1 shows a cell with a "sphere enclosed in a cube" (SEC) geometry and its 3D translation in *x*, *y*, and *z* directions.

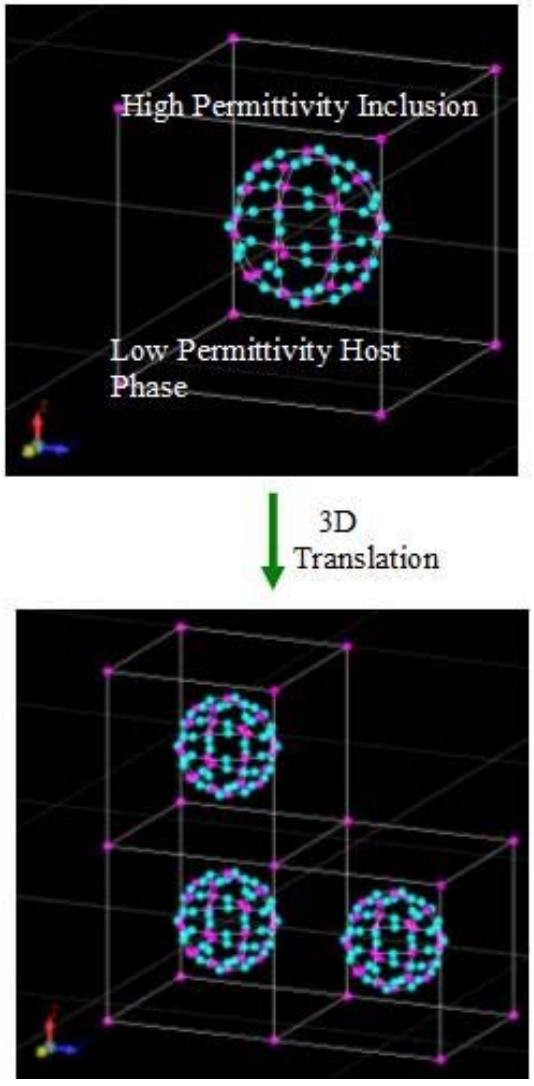

FIG. 1. Basic building block of composite sphere enclosed in cube and 3-D translation in *x, y, z* directions.

In the present simulations, the applied electric field was E_{appl} = 50 kV/cm; the host phase was assigned a permittivity $\varepsilon_{r\,\mathrm{host}}$ ranging from 4 to 36, and the inclusion

'high-permittivity' phase was assigned a permittivity $\varepsilon_{r\,incl}$ of 600 or 1200. The simulated dielectric body was a $9\times9\times9$ matrix of cubes (1.1 μm edge length/cube) and included 729 inclusion spheres. The linear periodic simulation function of the *Coulomb* code was used to create the dielectric body. The inclusion volume fraction was varied from approximately 1 to 50 % by varying the radius of the spherical inclusions from 0.2 μm to 0.53 μm. This results in a concomitant variation in interparticle separation, which may be equally important in defining local field behavior. In the present study, however, analysis of the results obtained is discussed from the context of particle size and volume fraction. Energy density predictions of *Coulomb* were compared with MG results for inclusion volume fractions up to 30%.

The *Coulomb* software was also used to simulate the impact of the permittivity of the host phase on the field enhancement within that phase. Studies in this area are of interest since field enhancement can affect breakdown strength.[28] The effects of dielectric contrast were studied by adopting two strategies: (1) varying the permittivity of the host phase, and (2) varying the permittivities of both host and inclusion phases. Simulations were also carried out to map field penetration into the high-permittivity phase, since this can result in higher energy storage densities for the composite.

2.2. MAXWELL GARNETT MIXING RULE

The Maxwell Garnett (MG) formulation has historically been the simplest and most popular mixing rule for homogenizing particulate composite media. Homogenization of a mixture is used in the quasistatic approximation, when sources and fields are slowly varying. This demands that the characteristic size of the scattering particles or correlation distance is small compared to wavelength in the effective

medium.[29] In addition, a mixture should be sparse, and inter-particle distances sufficiently long,(*Particle separation distances corresponding to 10% inclusion volume fractions in 0-3 composites)* so that multiple scattering is negligible.[17, 29]

The MG rule for a mixture of a host material with relative permittivity ε_{rhost} and spherical inclusions with relative permittivity ε_{rincl} as given by [1, 17]:

$$\varepsilon_{eff} \cong \varepsilon_{r\,\mathrm{host}} + \frac{3 f_{incl} \cdot \varepsilon_{r\,\mathrm{host}} (\varepsilon_{r\,\mathrm{incl}} - \varepsilon_{r\,\mathrm{host}}) / (\varepsilon_{r\,\mathrm{incl}} + 2\varepsilon_{r\,\mathrm{host}})}{1 - f_{incl} (\varepsilon_{r\,\mathrm{incl}} - \varepsilon_{r\,\mathrm{host}}) / (\varepsilon_{r\,\mathrm{incl}} + 2\varepsilon_{r\,\mathrm{host}})} \qquad (4)$$

Herein, inclusion volume fraction is designated as "$f_{inclusion}$". For linear dielectrics, the electric energy stored within an elemental volume (energy density) is a function of the effective permittivity ε_{eff} and the square of the applied electric field E:

$$w = \frac{1}{2} \varepsilon_0 \varepsilon_{eff} E_{appl}^2 . \qquad (5)$$

Below, the energy density calculated in this manner is compared with the energy density determined from the *Coulomb* simulations.

3. RESULTS AND DISCUSSION

3.1. FIELD BEHAVIOR IN COMPOSITES

The effect of particle size on field distribution within the composite dielectric was studied. Cross-sections of the electric field distribution for different size inclusion spheres within a single cell are shown in Fig. 2 (a, b). The inclusion particle in Fig. 2 (a) has a diameter of 0.4 μm, and the particle in Fig. 2 (b) has a diameter of 0.8 μm. The single

cells shown are translated in three directions to form the $9 \times 9 \times 9$ dielectric body. The permittivity of the inclusion phase is 1200, the host phase permittivity is 4, the applied electric field is 50 kV/cm. The field magnitude may be estimated using the color scale on the left hand side of each figure with the red color indicating maximum electric field value and dark blue indicating the lowest magnitude of electric field.

The field distribution inside a composite has three main regions. The first region is the enhanced field in the low-permittivity phase at the boundary separating two phases in the direction of the applied field. This is visible at the top and the bottom of the inclusion spheres in Fig. 2 (a, b). The second region is the low-intensity field in the high permittivity phase, namely, inside the inclusion spheres. The third region is the field of intermediate intensity in the low-permittivity phase. The enhancement of the field in the first region is an important parameter that affects the breakdown strength of the composite. Higher field penetration into the high-permittivity inclusion will lead to higher energy densities for a composite.

One important result is that the field magnitude within the high permittivity particles is greatly reduced compared to the magnitude of the applied field. The field magnitude within the particle is below 5 kV/cm. Because larger inclusions occupy a significant volume fraction of the cube, lower energy densities are expected. This suggests that, despite the high permittivity of the inclusion phase, the energy storage density of this phase is greatly reduced due to minimal field penetration into the phase. This result agrees with the prior reports of limited energy storage densities for composite materials prepared from polymers and high permittivity inclusions.[25] This suggests that, despite the high permittivity of the inclusion phase, the energy storage density of this

phase is greatly reduced due to minimal field penetration into the phase. This result agrees with the prior reports of limited energy storage densities for composite materials prepared from polymers and high permittivity inclusions.[25]

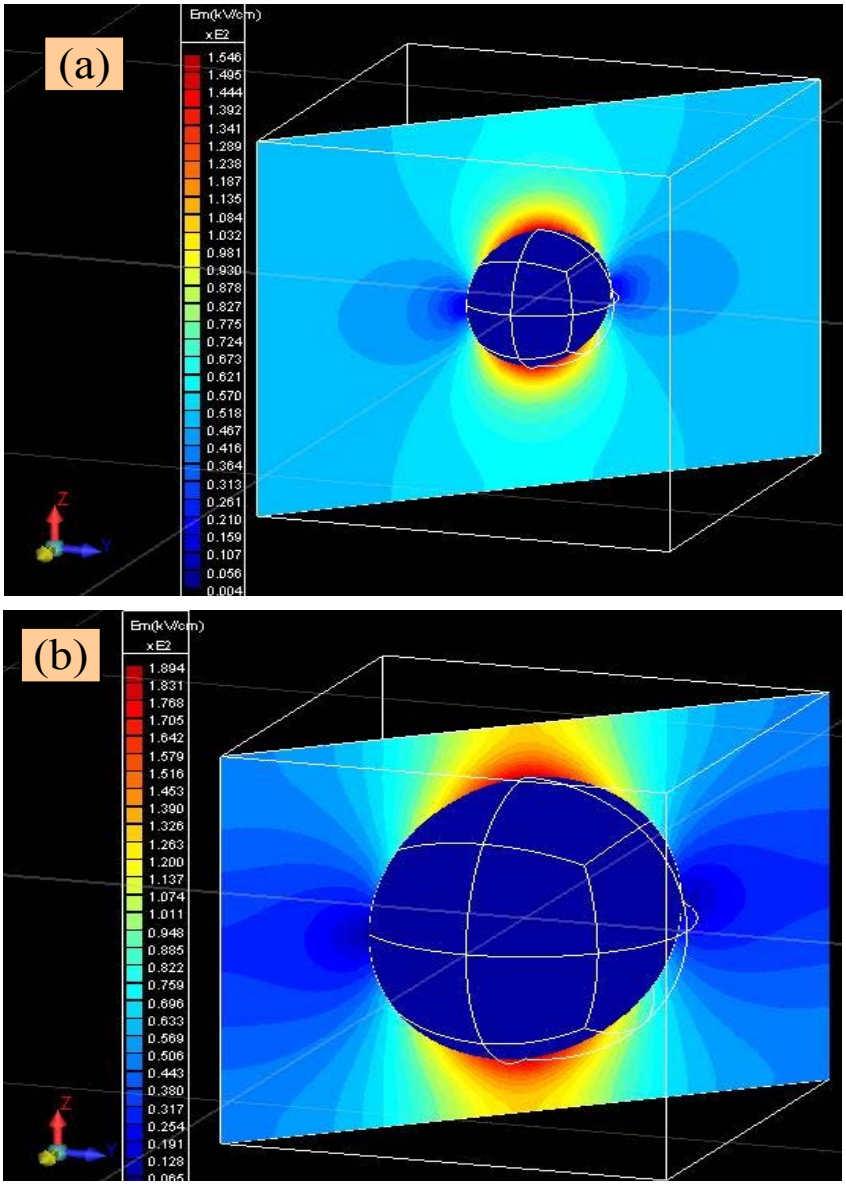

FIG. 2. Electric field distribution in the composite with low volume fraction of the inclusion (2.5 %) and high volume fraction of the inclusion (20.1 %).

Other characteristics of field distribution for both composites, as seen in Fig. 2 (a) and (b), are similar, though the magnitude and extent of the field enhancement in the host phase depends on the particle size of the high-permittivity inclusion. Composites containing smaller size (<0.4 μm) inclusions exhibit a lower field enhancement compared to the particles of larger diameter. Smaller inclusion size and the proximity of the high-permittivity inclusions to each other can have a significant impact on the *field enhancement factor*. The field enhancement factor is defined as the ratio of the maximum field present in the composite to the magnitude of the applied field.

$$F_e = \frac{E_{\max}}{E_{appl}}. \qquad (6)$$

The field enhancement for the 0.4μm particle composite is approximately $F_e = 3.1$, while the field enhancement factor for the 0.8μm particle composite is approximately $F_e = 3.8$. Other notable differences are that for the 0.4μm particle composite, a field slightly greater than the applied field exists at most locations within the matrix phase, as indicated by the light blue color representing a field of $E \sim 60$ kV/cm. Other locations in the matrix exhibit a field of magnitude that is approximately equal to the applied field (next field gradation of blue, $E \sim 49.8$ kV/cm). A similar result is observed for the composite prepared from the 0.8μm particle, though the specifics of the field distribution are noticeably different. For this composite, significant field enhancement extends to the cell border (in the field direction), albeit in a more localized fashion than for the 0.4μm particle composite.

The particular case considered above demonstrates that field penetration, enhancement, and distribution characteristics all depend on the volume fractions of phase. The examples given below will show that these field characteristics depend on dielectric contrast as well.

3.2. EFFECTS OF INCLUSION VOLUME FRACTION AND DIELECTRIC CONTRAST ON LOCAL FIELD DISTRIBUTION

This section contains quantitative results that show the effect of dielectric contrast on both field penetration into the high-permittivity inclusion and field enhancement in the low permittivity host. To the best of our knowledge, such quantitative estimates have not yet been reported.

It is critical to develop insights into field enhancement and penetration as a function of inclusion volume fraction f_{incl} and dielectric contrast c. This is important for the development of guiding principles to engineer dielectrics for high-energy density capacitors. Fig. 3 illustrates how the properties of the two phases and the volume fraction of the inclusion can impact the field enhancement within the composite. According to Fig. 3, for the smallest inclusions (0.2μm radius, f_{incl} = 2.51%), the field enhancement factor is about $F_e = 2.6$. In contrast, for larger inclusions (0.53μm radius, f_{incl} = 46.8%), field enhancement factors $F_e > 10$ are observed. Thus, in a system with inclusion permittivity $\varepsilon_{incl} = 1200$ and host permittivity $\varepsilon_{host} = 4$, the local field in the vicinity of an inclusion can vary from ~ 140 kV/cm to ~ 600 kV/cm, when the applied field is 50 kV/cm, depending on the volume fraction of the high permittivity inclusion phase.

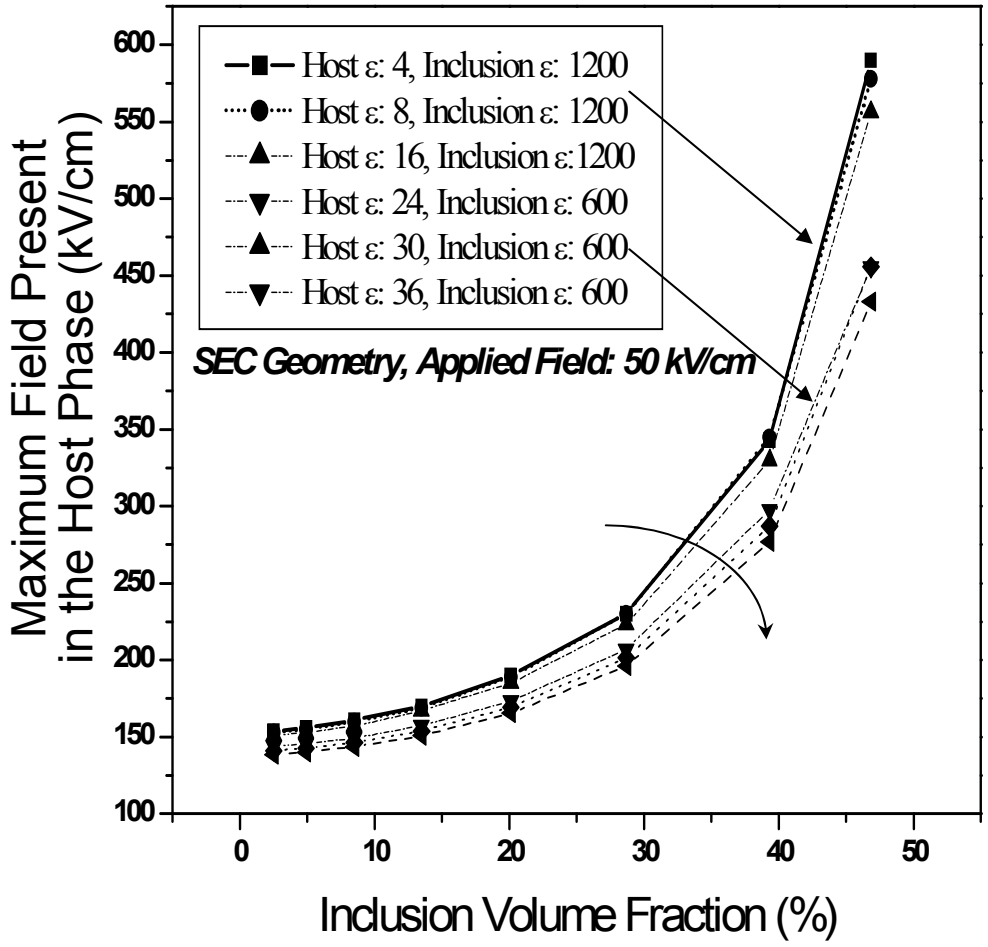

FIG. 3. Coulomb simulations of the maximum field in the host material as a function of the inclusion volume fraction (%) with applied field of 50 kV/cm.

The impact of the dielectric contrast on the field enhancement is also evident in Fig. 3. Based on the permittivities of the two phases, the dielectric contrast was varied from approximately 16 (ε_{host} = 36 and ε_{incl} = 600) to 300 (ε_{host} = 4 and ε_{incl} = 1200). If

the permittivity of the host phase increases (4 vs. 36), the field enhancement factor reduces by approximately 25%. Because there is likely a strong link between the dielectric breakdown strength and local field enhancement, this result suggests that the ability to develop host phases with higher permittivities (assuring lower dielectric contrast compared to the inclusion phase) can be beneficial to improve the breakdown characteristics of composites.

Fig. 4 shows the field penetration that takes places along the z-axis of the inclusion, when an electric field of 50 kV/cm is applied in the z-direction. It is interesting to independently consider the volume fraction and dielectric contrast effects from Fig. 4. For a dielectric contrast of 300, increasing the inclusion volume fraction from 2.5 to 46.8 %, results in a 17 fold increase in the maximum field penetration into the high-permittivity phase. However, for a dielectric contrast of 16, the same increase in volume fraction only results in an increase in field of ~3.25.

Considering dielectric contrast effects, at a constant volume fraction of 2.51% varying dielectric contrast from 300 to 16 results in an increased field penetration of nearly a factor of 13. At a constant volume fraction of 46.84%, the same change in dielectric contrast results in an increase of field penetration of 2.5 times. These results reveal important information about volume fraction and dielectric contrast effects. Significant field penetration into a high-permittivity inclusion occurs only when the dielectric contrast is reduced below approximately 75. Fig. 4 also suggests that field penetration into the inclusion may be increased when the volume fraction of the high permittivity phase increases. This effect, however, is comparatively less important than

dielectric contrast, and only becomes significant when inclusion particles are in close proximity.

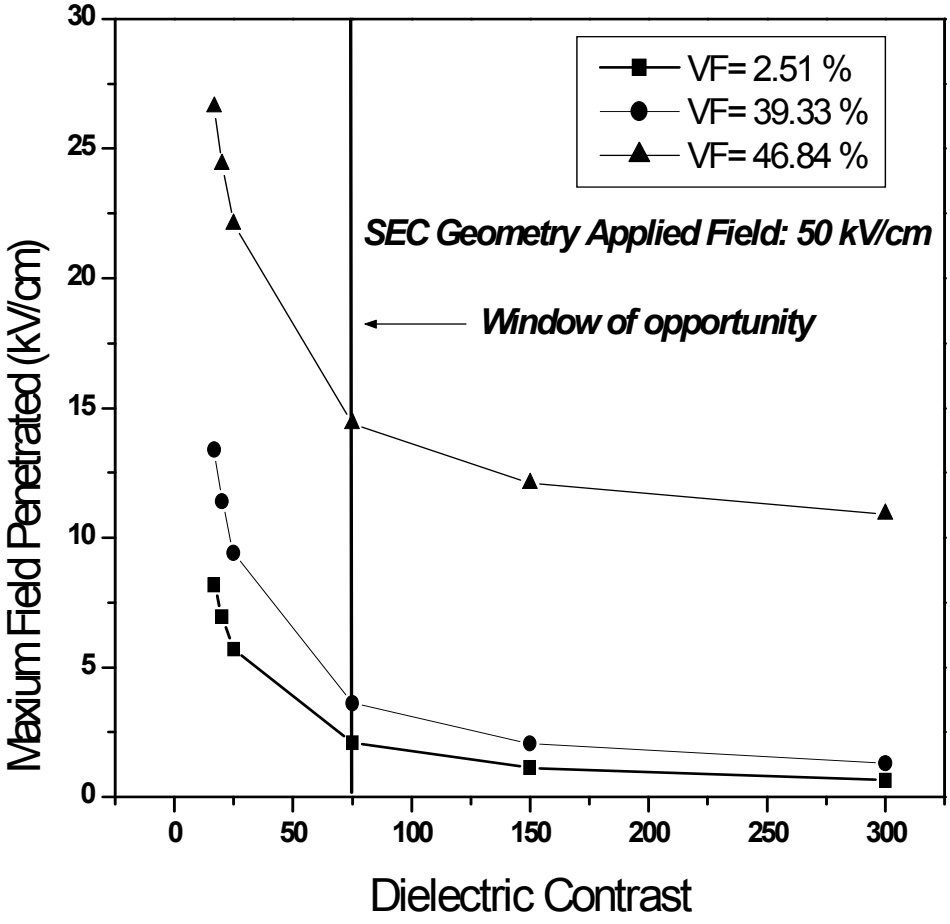

FIG. 4. ***Coulomb*** **simulations of the maximum field present in a high-permittivity spherical inclusion enclosed in the host matrix as a function of dielectric contrast for different inclusion volume fractions.**

Comparing the results in Fig. 4 for the three volume fractions, field penetration for the 39.33 and 2.51 vol% cases show a smaller variation than those for the 39.33 and 46.84 vol% cases. At 46.84%, the spherical inclusions are only separated by x μm.

The conclusion is that lower dielectric contrast and higher inclusion volume fraction of high-permittivity phase will lead to greater field penetration into the high permittivity inclusion phase.

3.3. BENCHMARKING ENERGY STORAGE CALCULATIONS

To validate energy density calculations carried out by Coulomb, computer simulation results are compared to experimental data for glass-ceramic systems studied at the Pennsylvania State University.[6] Consider a single-phase dielectric (e.g., glass $\varepsilon = 41$) cube with a side of 1.1 μm, as shown in Fig. 5 (a). The electric field applied in the vertical direction of the cube is assumed to be 81 kV/mm. This is the same value of electric field as in the experiments carried out at the Pennsylvania State University[6]. The energy storage within glass phase was calculated using *Coulomb*. The cube in this example is subdivided into 1000 tetrahedral elements to increase the accuracy of simulations. *Coulomb* predicts energy stored within the cube of $1.55 \cdot 10^{-12}$ J, which corresponds to the energy density of 1.16 J/cm^3. These results match those obtained at Penn State University[6]: the experimentally predicted energy storage for glass with permittivity of 40 was also 1.16 J/cm^3, as is shown in Fig. 5(b).

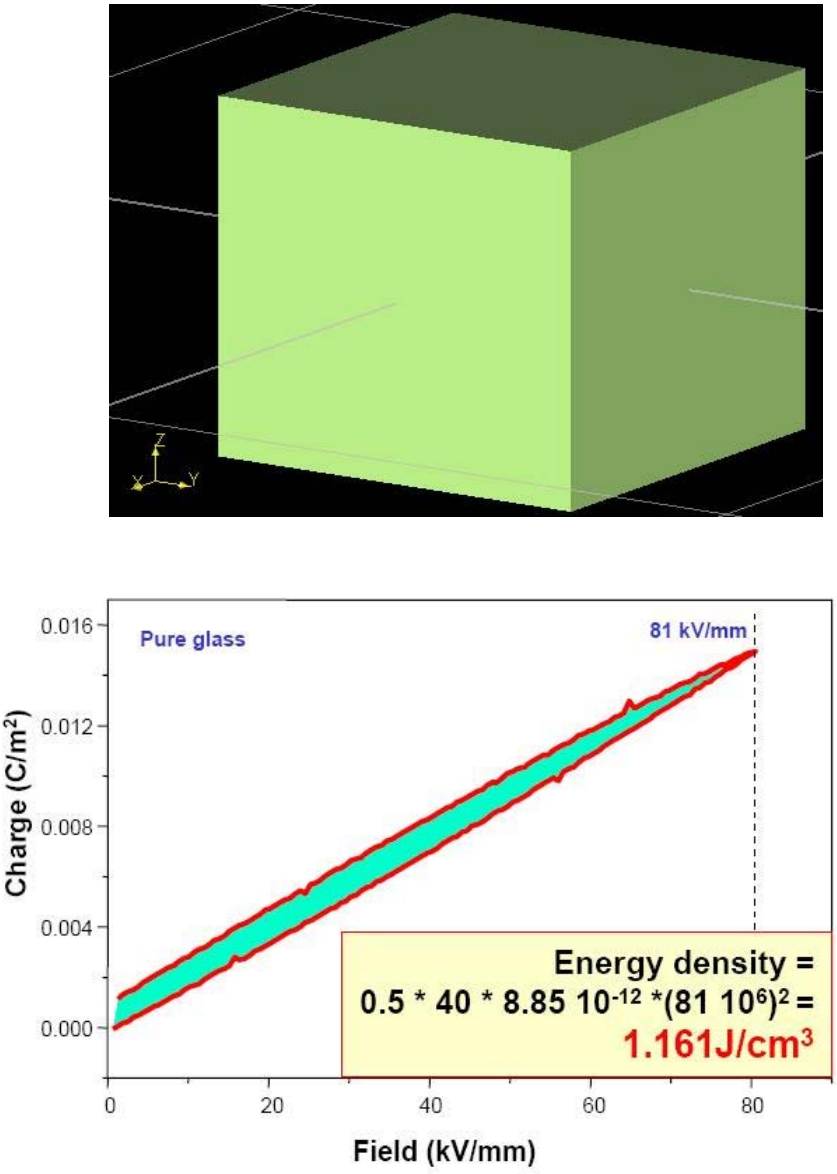

FIG. 5. 3D cube, generated in *Coulomb*, representing pure glass phase and experimentally obtained energy storage in the pure glass phase system for similar parameters.

3.4. COMPARISON OF *COULOMB* AND MAXWELL GARNETT MODELS

One of the primary limitations of mixing theories is the inability to predict energy density beyond a particular limit of inclusion volume fraction, as discussed in Section II.2. To our knowledge, a precise limit at which mixing theories incorrectly account for field enhancement and penetration has not been established. This is the topic of the present investigation.

Maxwell Garnett theory was applied to the same model systems investigated using *Coulomb* for different volume fractions of inclusions. The host matrix is assumed to possess various permittivities identical to those studied by Coulomb. The inclusions are spheres with permittivity of 1200. The effective permittivity, obtained using equation (*4*), as a function of the volume fraction at different values of the host permittivity, is plotted in Fig. 6. As expected the effective permittivity increases with increasing host permittivity. Analogous energy storage densities can be calculated using equation (5), if the effective permittivity is known. The energy densities for analogous composites are calculated using both *Coulomb* and the MG mixing rule. These calculations are done only for the volume fractions of inclusions less than 30%, because the deviation between the *Coulomb* and MG predictions starts at very low inclusion volume fractions ($f_{incl} < 1\%$). It is convenient to introduce a criterion regarding the agreement between the MG and *Coulomb* result. The formula used for this comparison is:,

$$p = \frac{\left|E_{MG} - E_{Coulomb}\right|}{E_{av}} \cdot 100\%, \qquad (7)$$

where $E_{av} = \frac{E_{MG} + E_{Coulomb}}{2}$ is the average energy stored in the composite, calculated through both the MG model and *Coulomb* software.

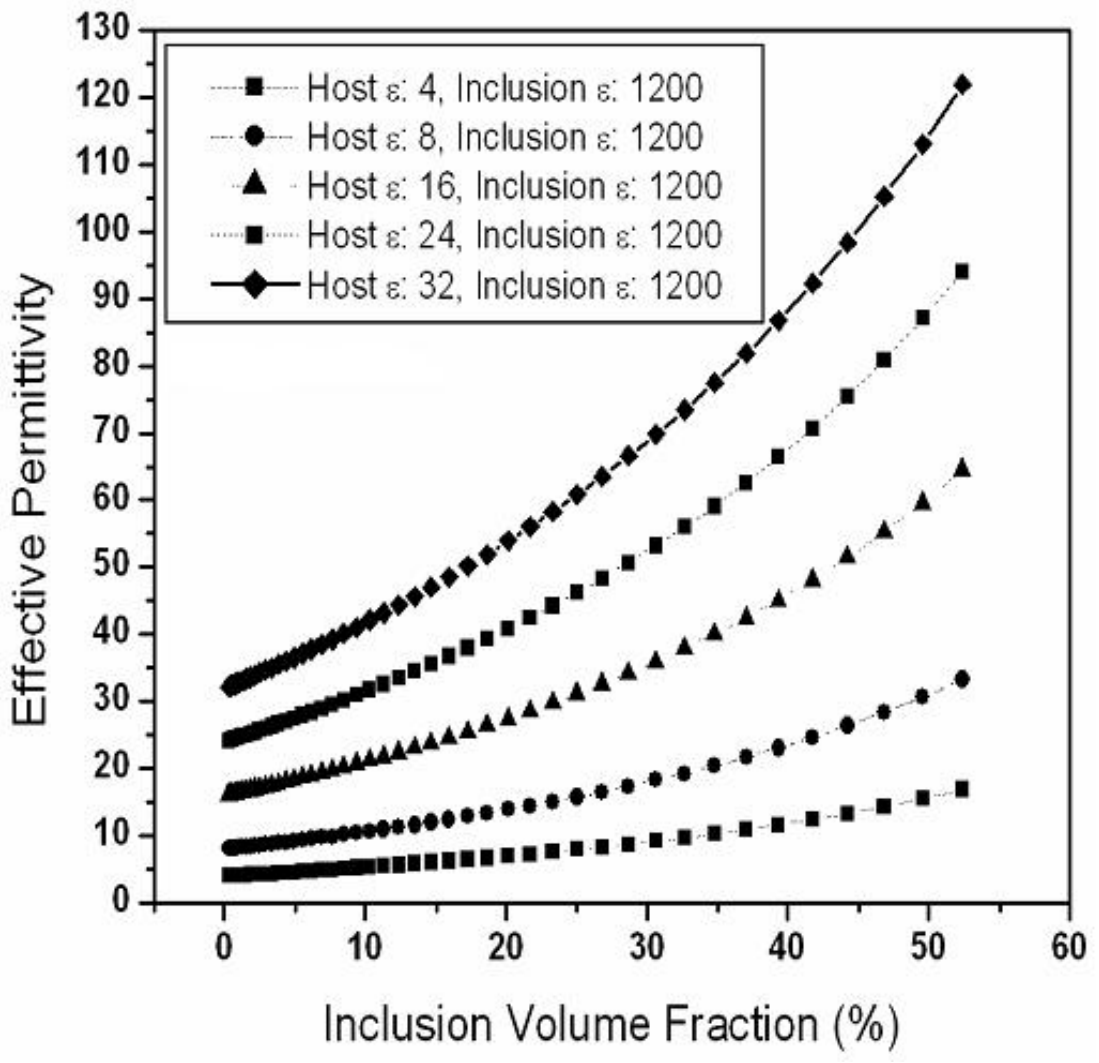

FIG. 6. MG prediction of effective permittivity for a sphere enclosed in cube as a function of volume fraction for different values of host permittivity.

It was assumed that $p > 10\%$ suggested a significant *discrepancy* from the MG mixing rule. Fig. 7 shows a plot of p (in %) between the MG mixing rule and *Coulomb* as a function of the volume fraction f_{incl} for the SEC structure. The applied field is 50 kV/cm. When the dielectric contrast is 300, a significant discrepancy between MG and *Coulomb* (more than 10 %) occurs at the volume fraction of inclusions $f_{incl} \sim 4\%$. This is

the *volume fraction limit* denoted as f_{lim}. The value f_{lim} shifts to about 5.5%, when the dielectric contrast c reduces to 16. The value f_{lim} shifts to a value of approximately 7%, when the dielectric contrast c is further decreased to 6.

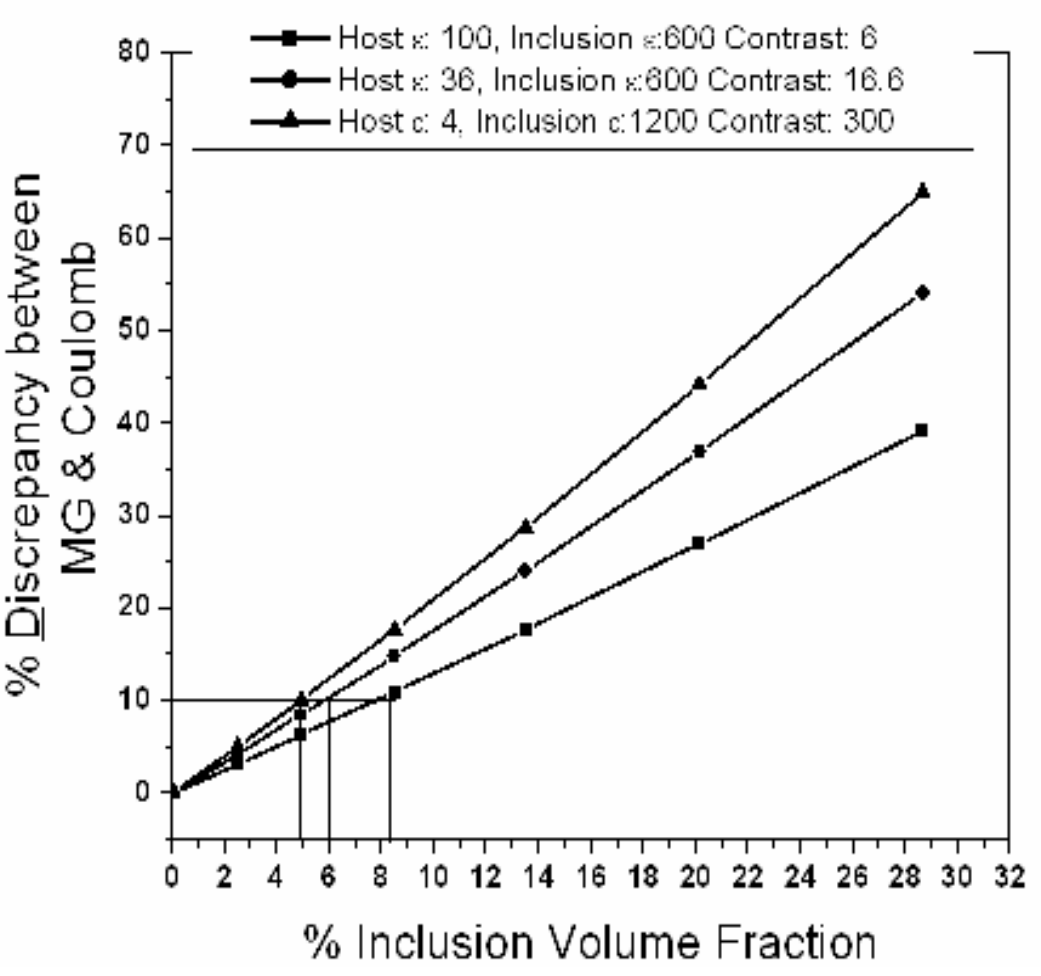

FIG. 7. Discrepancy between MG and *Coulomb* predictions as a function of inclusion volume fraction. The dielectric contrast is varied by varying both host and inclusion permittivity.

Thus, Fig. 7 demonstrates that the volume fraction limit f_{lim} increases as the dielectric contrast decreases. This result thus indicates that the lower the dielectric contrast, the higher volume fraction up to which the MG formulation can be applied.

Two sets of simulations were carried out to determine the effect of the individual permittivities of the inclusion and host phases on the inclusion volume fraction limit f_{lim} for use of MG theory. First, the permittivity of the host was varied while the inclusion permittivity remained constant. Second, the inclusion permittivity was varied while the host permittivity was kept constant. Fig. 8 shows the discrepancy between the MG model and *Coulomb* for the case of varied host permittivity. It may be seen that there is a substantial difference in the inclusion volume fraction limit when only the permittivity of the host is varied. The volume fraction limit for applicability of the MG formalism varies from approximately 5 to 8% for the range of dielectric contrasts (obtained by changing host permittivity) studied.

In contrast to this result, Fig. 9 shows that when the dielectric contrast is varied by varying inclusion permittivity, there is *minimal effect* upon the inclusion volume fraction limit f_{lim}. $f_{\lim}$ is found to be in this case to be around 5.8 % and it does not change inspite of change in the dielectric contrast. Even though from these computations it seems that the variation of dielectric contrast by variation of inclusion phase permittivity has less visible impact, the impact of permittivity of inclusion itself cannot be ruled out.

Thus, the volume fraction limit definitely depends on the dielectric contrast; however, it is the host permittivity that plays the crucial part in governing this limit. It is important to note that although the inclusion volume fraction limit has been estimated for the first time, there are ways to extend the applicability of MG theory. For example, there

is an incremental MG model proposed by A. Lahtakia,[19] in which the inclusion phase is always dilute, and it is added incrementally to the new homogenized host at every iteration cycle.

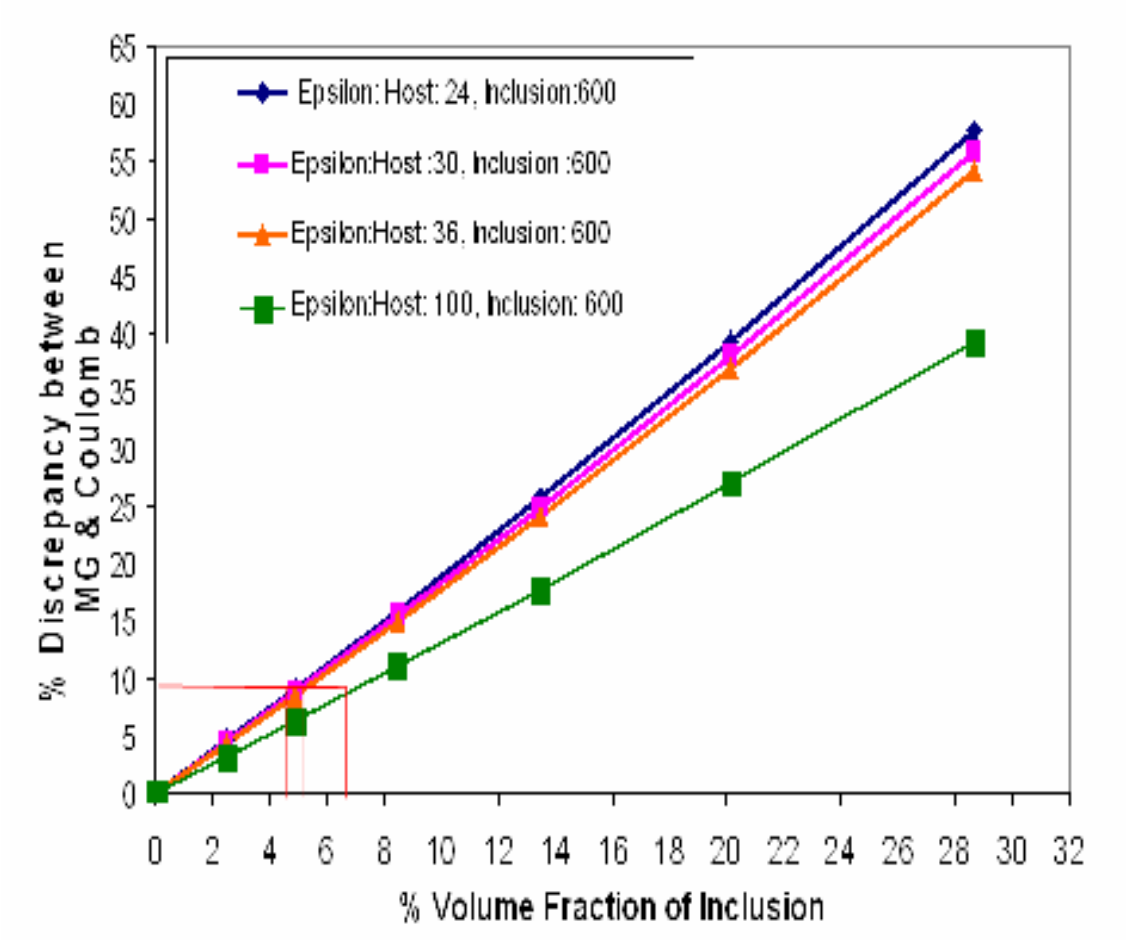

FIG. 8. Discrepancy between the MG and *Coulomb* predictions as a function of the inclusion volume fractions.

The resultant effective permittivity converged to the result predicted by the Bruggeman formula.[29] Another approach is described in Sihvola's paper,[28] where the v-parameter is introduced to take into account the interaction of polarizations of

neighboring inclusions, when calculating the dipole moment of a single scatterer. The parameter $v = 0$ corresponds to the MG formulation; $v = 2$ corresponds to the Bruggeman's formula, and $v = 3$ gives the CP ("Coherent Potential") formula.[30, 31, 32] The discrepancy between the MG ($v = 0$) and the other mixing rules ($v = 1, 2, 3$) starts to be noticeable, when the inclusion volume fraction is around 10 % [30, Fig. 3].

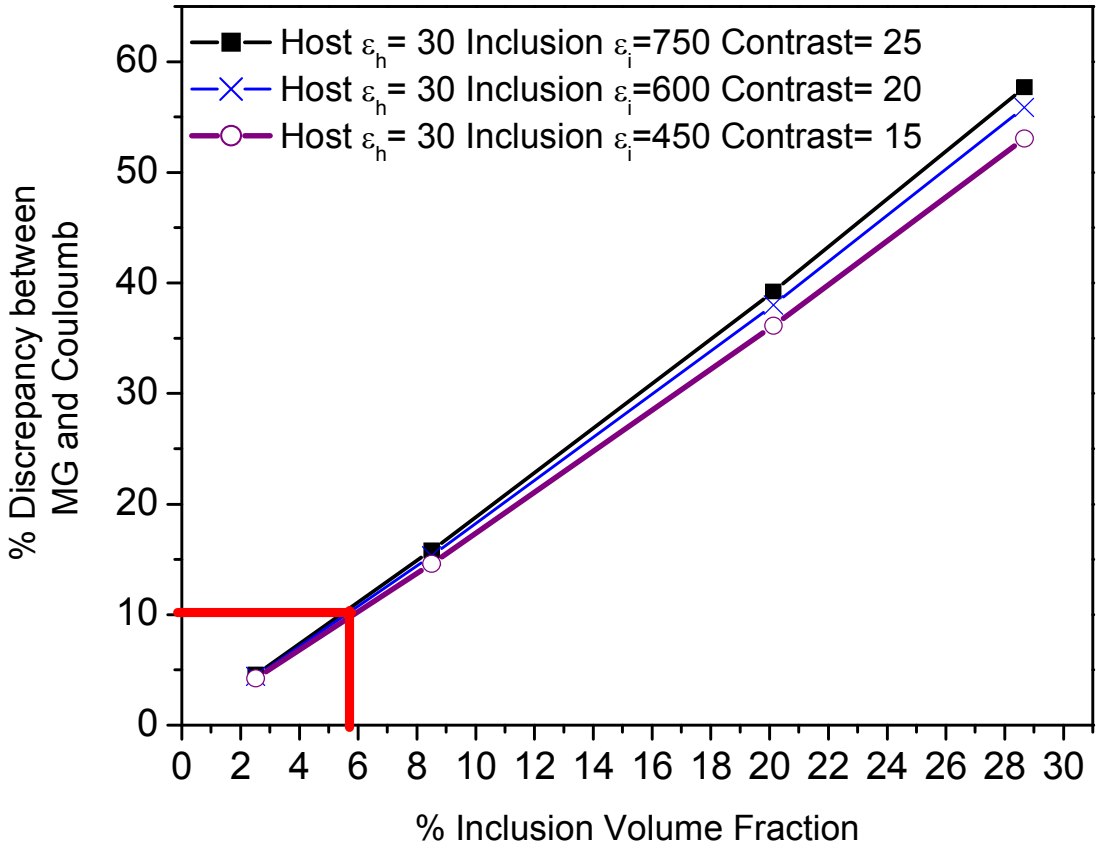

FIG. 9. Discrepancy between the MG and *Coulomb* predictions as a function of volume fraction of inclusions.

The dielectric contrast in these computations appears to be very low. Our comparison of the MG formulation with *Coulomb* numerical modeling yields the limit from 4 to 8 %, depending on the dielectric contrast ($c = 16 - 300$), which reasonably agrees with the results in papers.[30, 31]

4. CONCLUSIONS

Electrostatic field distribution and energy storage in diphasic dielectrics containing high-permittivity $BaTiO_3$ inclusions in a low-permittivity host have been studied numerically using the software *Coulomb*. The results of numerical simulations have been compared with those obtained from the Maxwell Garnett mixing rule. Based on *Coulomb* modeling, it has been possible to quantify the electric field enhancement and field penetration in the host and inclusion phases, respectively. It is observed that the electric field distribution in 0-3 composites is governed by dielectric contrast and inclusion volume fraction. This study demonstrated that both electric field enhancement in a low-permittivity host phase and electric field penetration in the high-permittivity inclusion demonstrate the following trends:

- They increase with increasing high-permittivity inclusion volume fraction, and
- Electric field enhancement increases with the increase in dielectric contrast.
- Electric field penetration decreases with the increase in dielectric contrast

Higher field enhancement factors lead to a higher probability of electric breakdown. Thus, it was found that increasing inclusion volume fraction from 2.5% to 46.8%, when the dielectric contrast was 75 ($BaTiO_3$ sphere in a low-permittivity cube), leads to an 80% increase in field penetration in the inclusion phase, and to a 25%

decrease of the field enhancement factor in the host phase. These results suggest opportunities for microstructural and compositional engineering to achieve high energy density dielectrics. Stated otherwise, increasing effective permittivity occurs at the cost of decreased breakdown strength, and field penetration into the inclusion must be balanced by minimizing field enhancement in the host.

The upper limit of applicability of the MG formulation in terms of the inclusion volume fraction was also investigated, and it appears to depend on the dielectric contrast of the diphasic composite. The discrepancy between the MG and numerical results decreases with decrease of the dielectric contrast. Variation in the host material permittivity causes a substantial effect on the upper limit of applicability of the MG mixing rule

5. ACKNOWLEDGMENTS

This work was supported through a MURI program sponsored by the Office of Naval Research under Grant No. N000-14-05-1-0541. The authors also gratefully acknowledge the valuable assistance of Mr. Dennis Owsianyk of Integrated Engineering Software.

6. REFERENCES

[1] J.C. Maxwell Garnett, *in Trans. of the Royal Society,* London, 1904, Vol. CCIII, pp. 385-420.

[2]L. K. H. Ven Beck, Prog. Diel., **7**, 71 (1967).

[3]K. Lichtenecker, Phys. Z., **10**, 1005 (1909).

[4]S. P. Mitoff, Adv. Mater. Res., **3**, 305 (1968).

[5]A. H. Sihvola, IEEE Trans. Geosci. Rem. Sens., **40** [4], 880 (2002).

[6] J.W. McCauley, R. E Newnham, and C.A. Randall, J. Am. Ceram. Soc., **81,** 979 (1998).

[7] R. Gerson and T.C. Marshall, J. Appl. Phys., **30** [11], 1650 (1959).

[8] C. Baojin, X. Zhou, K. Ren, B. Neese, M. Lin, Q. Wang, F. Bauer, Z. M, Qing, Science, **313**, 334 (2006)

[9] J. H. Tortai, N. Bonifaci and A. Denat, J. Appl. Phys. **97**, 053304 (2005).

[10]T. Kim, J. Nath, J. Wilson, S. Mick, P. D. Franzon, M. B. Steer, and A. I. Kingon, *in Mater. Res. Soc. Symp.* Proc., **833**, 201 (2005).

[11]M. Kawasaki, Y. Hara, Y. Yamashiki, N. Asahi, R. Nagase, T. Ueoka, M. Yoshioka, and T. Noaka*, in Proc. 54th Electron. Comp. Tech. Conf.*, **1**, 525 (2004).

[12] P.S. Neelakanta, Handbook of Electromagnetic Materials (CRC Press, Boca Raton, FL, 1995).

[13] E.F. Kuester and C.L. Holloway, IEEE Trans. Microw. Theory Techn., **3**, 1752-1755 (1990).

[14] P. Sheng, Phys. Rev. Letters, **45,** 60 (1980).

[15] W.T. Doyle and I.S. Jacobs, J. Appl. Phys., **71**, 3926 (1992).

[16] R.E. Diaz, W.M. Merrill, and N.G. Alexopoulos, J. Appl. Phys., **84**, 8615 (1998).

[17] A. Sihvola, *Electromagnetic Mixing Formulas and Applications* (IEE, London, UK, 1999).

[18]M. Y. Koledintseva, J. Wu, J. Zhang, J. L. Drewniak, and K. N. Rozanov, in *Proc. IEEE Symp. Electromag. Compat.*, Santa Clara, CA, 2004, Vol. 1, pp. 309-314.

[19]A. Lakhtakia, Microwave and Optical Technology Letters*.,* **17** [4], 276 (1998).

[20]G. Goodman, R. C. Buchanan, and T. G. Reynolds, III in *Ceramic Materials for Electronics*, 2nd ed. (Marcel Dekker Inc., New York, 1991), pp. 72.

[21]D. A. Payne, *in Tailoring Multiphase and Composite Ceramics,* Mat. Sci. Res. **20,** edited by R. E. Tressler et al. (Plenum Press, New York, 1986), pp. 413-431.

[22] C. Ang, Z. Yu, R. Guo, and A. S. Bhalla , J. Appl. Phys, **93**[6], 3475 (2003).

[23] A.Spanoudaki and R. Pelster, Phys. Rev. B: **64,** 064205 (2001).

[24] V. Myroshnychenko and C. Brosseau, J. Appl. Phys, **97**, 044101-14 (2005)

[25] A. L. An, S. A. Boggs and J. Calame, *IEEE Int. Symp. Elec. Insul*., 466-469 (2006)

[26] J. Lopez-Roldan, P. Ozers, T. Judge, C. Rebizant, R. Bosch, and J. Munoz, *in IEEE Int. Symp. Elec. Insul*., **2**, 685 (1998).

[27] W. Que and S. A. Sebo, *Proc. Elec./Electron. Insul. Conf.*, 441 (2001).

[28] B. Rangaranjan, B. Jones, T. Shrout, and M. Lanagan, J. Am. Ceram. Soc., xx [x] x–x (2007)

[29] A. H. Sihvola, IEEE Trans. Geosci. Rem. Sens., **40** [4], 880 (2002).

[30] D. A. G. Bruggeman, *Ann. Phys*., **24**, 636 (1935).

[31] W.E.Kohler and G.C.Papanicolaou, *in Multiple Scattering and Waves in Random Media*, edited by P.L.Chow, W.E.Kohler, and C.G. Papanicolaou (North-Holland, N.Y., 1981), pp. 199-223.

[32] A. Sihvola and F. Olyslager, *Radio Science*, **31** [6], 1399-1405 (1996).

SECTION
2. APPENDIX

This appendix is included with this dissertation to document other studies that have been completed that are not discussed in the research papers presented. This section will identify strengths of the analytical and numerical models developed, and will report the ability of the equivalent capacitance model to account for inclusion orientation. It will also highlight that results from the mode are independent on the discretization approach which confirms the requisite physical foundation. Lastly, this section includes an extension of the numerical mode for random composites, and a combinational approach of numerical modeling with a percolation model to establish the correlation between the local electric field distribution and breakdown phenomenon.

2.1. ANALYTICAL MODELING

2.1.1 Energy Storage. In this research, the impact of dielectric contrast and inclusion volume fraction on the electric field enhancement in the host phase and electric field penetration in the high permittivitiy inclusion phase were examined. Field enhancement in the low permittivity phase concentrates the electric flux lines, and is likely to be the place of origin for breakdown. Thus field enhancement significantly reduces the breakdown strength of a composite. It is imperative to connect the information generated in numerical simulations together with predicted effective permittivity values in order to predict the energy storage characteristics of the diphasic dielectrics.

For linear dielectrics, the electric energy stored within an elemental volume (w; energy density) is a function of the permittivity of free space, the effective permittivity ε_{eff} of the composite dielectric and the square of the applied electric field E_{appl}:

$$w = \frac{1}{2}\varepsilon_0 \varepsilon_{eff} E_{appl}^2 . \qquad (1)$$

The reported breakdown strength (BDS) of (single phase) glass is very high (~ 800-1200 kV/cm) and for single phase polymeric materials is even higher (*Polyimide BDS: 1450 kV/cm, Polyethylene BDS: 1250 kV/cm, Epoxy BDS: 3100 kV/cm*). The addition of a second phase of higher permittivity results in field concentration in the low permittivity phase at the interface, resulting in lower breakdown strengths. Considering this physical reality, the important question is at what inclusion volume fraction does the advantage of adding a high permittivity phase persist before field enhancement factors start to dominate energy density? A corrolary question is how is this "optimum" volume fraction influenced by dielectric contrast?

The approach used for prediction of energy storage density is outlined below. The predictions of equivalent capacitance model were used to calculate effective permittivity. These results were combined with those of numerical modeling, which was used to determine field enhancement factors. These factors were studied as a function of inclusion volume fraction and dielectric contrast between the host and inclusion phases. It was assumed that the maximum electric field that could be safely applied to the dielectric was reduced in an inverse linear relationship to the field enhancement factor. In microscopic composites, i.e., composites based on the incorporation of micron-sized inclusions, it is known that the breakdown strength of the composite is reduced. In

nanoscale composites, scattering and electron trapping processes are believed to contribute to higher breakdown strengths [54]. The current simulations are based on microcomposites and the breakdown strength of these composites is believed to be less than that of the pure host phase, with a corresponding decrease in energy density. The physics of electron trapping and scattering are not incorporated in the present model.

In Fig. 2.1 the predictions of the equivalent capacitance model are shown as a function of inclusion volume fraction and dielectric contrast.

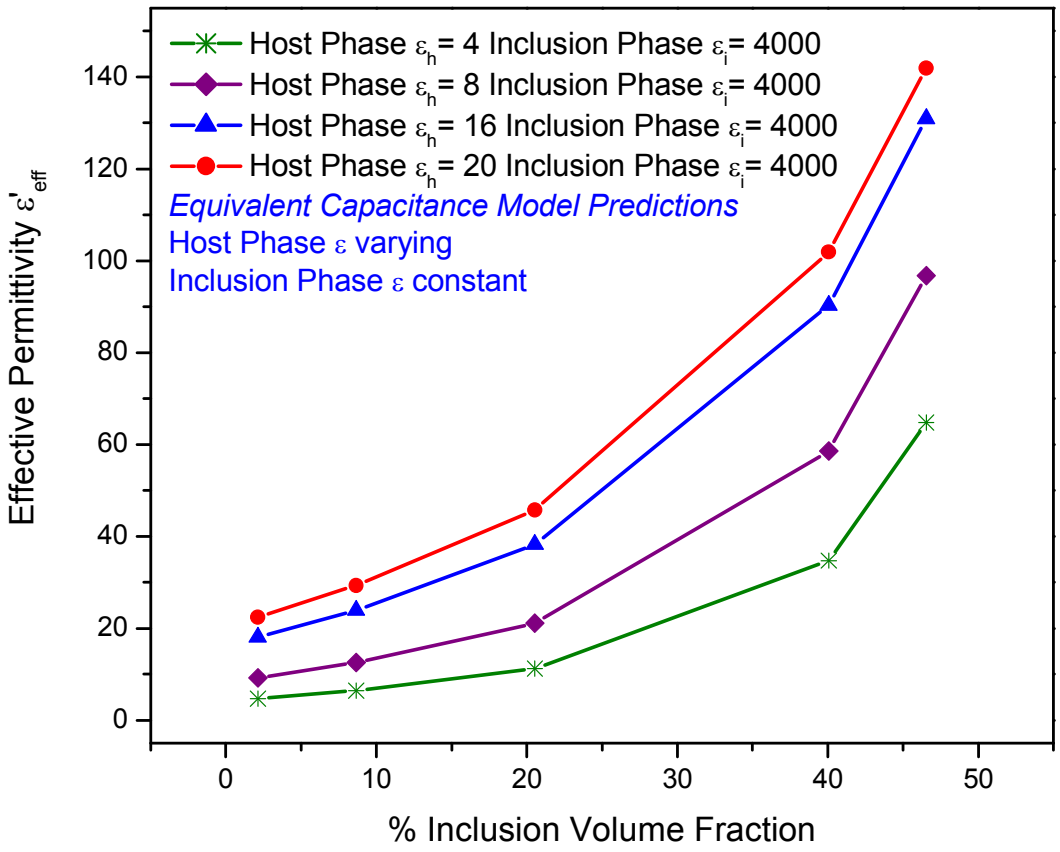

Fig. 2.1. Equivalent capacitance model predictions for effective permittivity as a function of inclusion volume fraction and dielectric contrast of the composite.

The dielectric contrast of the composite was varied from 200 to 1000, first by varying the host phase permittivity and then by varying the inclusion phase permittivity. Permittivities were chosen to approximate the permittivities of polymers and barium titanate. An ordered 0-3 composite structure was used for the simulations. Dielectric contrast is varied by variation of host phase permittivity. The maximum permittivity observed is approximately 140 at the highest inclusion volume fraction considered in this case, 46.54%, and with a dielectric contrast of 200.

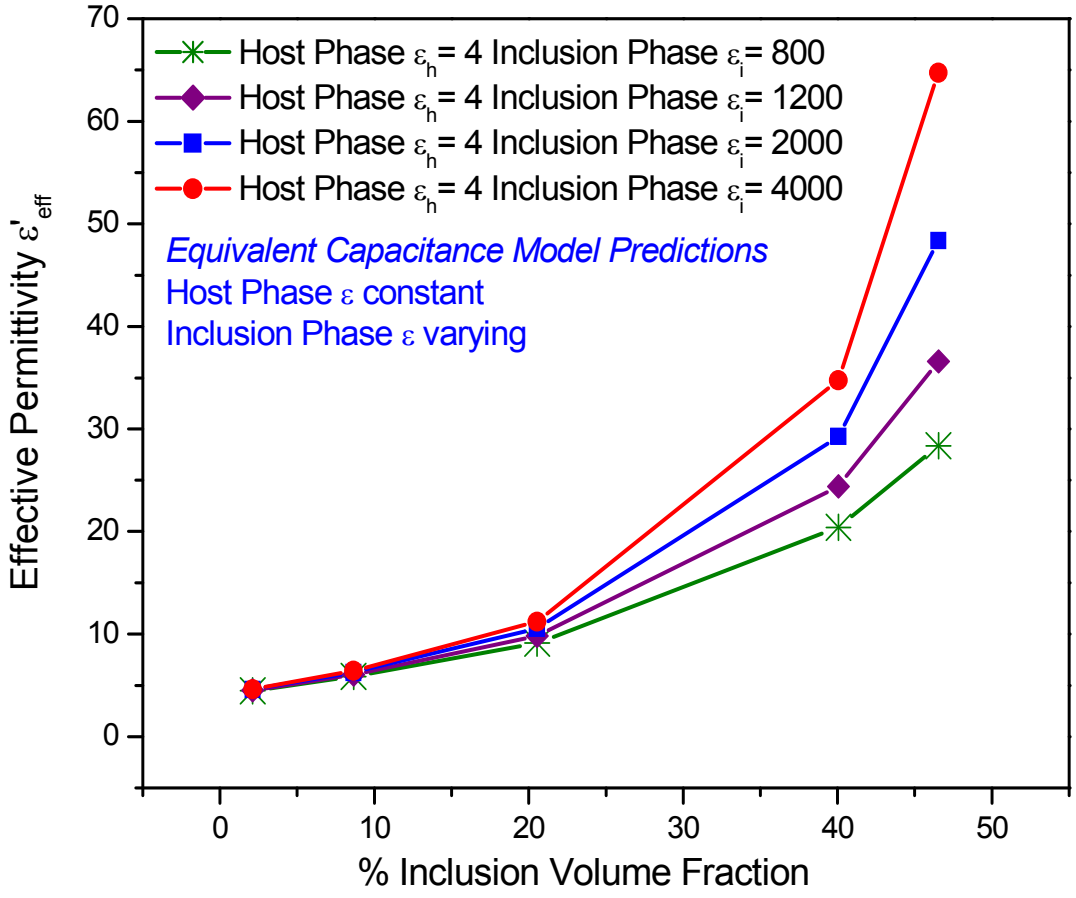

Fig. 2.2. Equivalent capacitance model predictions for effective permittivity as a function of inclusion volume fraction and dielectric contrast of the composite.

In Fig. 2.2 the predictions of the equivalent capacitance model are shown as a function of inclusion volume fraction and dielectric contrast. Compared to the previous case, dielectric contrast is varied by variation of inclusion phase permittivity. The maximum permittivity observed is around 65 at the highest inclusion volume fraction considered in this case of 46.54 % and with dielectric contrast of 1000. The results of the energy storage calculations for both cases are plotted in Fig. 2.3 and Fig. 2.4. For energy storage calculations the applied field was chosen to be 800 kV/cm for all the cases. The maximum electric field that could be safely applied to the dielectric was assumed to be reduced in an inverse linear relationship to the field enhancement factor. To give an example, in case of a composite with inclusion volume fraction of 2.12, host phase permittivity of 4 and inclusion phase permittivity of 4000, the maximum field present was 2452 kV/cm for an applied electric field of 800 kV/cm. This results in a field enhancement factor of 3.06. Thus the maximum electric field that could be safely applied to this dielectric composite was 261 kV/cm. The energy stored in the composite was then computed using equation 1 where effective permittivity was calculated using equivalent capacitance model and electric field value was calculated as explained above. It is observed from energy storage predictions that inclusion additions significantly drop the stored energy density ($\approx$ 85-90%) as compared to the pure host phase.

As noted above, this is an expected result for micro-composite. Trapping, scattering and any beneficial interfacial effects are not accounted for in the model. The interesting aspect of the figures is that as the inclusion volume fraction is increased, the highest energy storage occurs for the case where the dielectric contrast is 200 (*lowest contrast studied*) and at 20 vol% inclusion phase. It is evident that increasing the

permittivity of the host phase leads to an increase in the energy stored in the composite. This increase in host phase permittivity also leads to reduction in dielectric contrast. Reduction of dielectric contrast also leads to lowering of field enhancement factors. This increases the maximum electric field that can safely be applied to the composite , thereby leading to an increase in energy stored. The breakdown strength decrease due to increased inclusion proximity beyond 20 % inclusion volume fraction limit leads to decrease in energy storage.

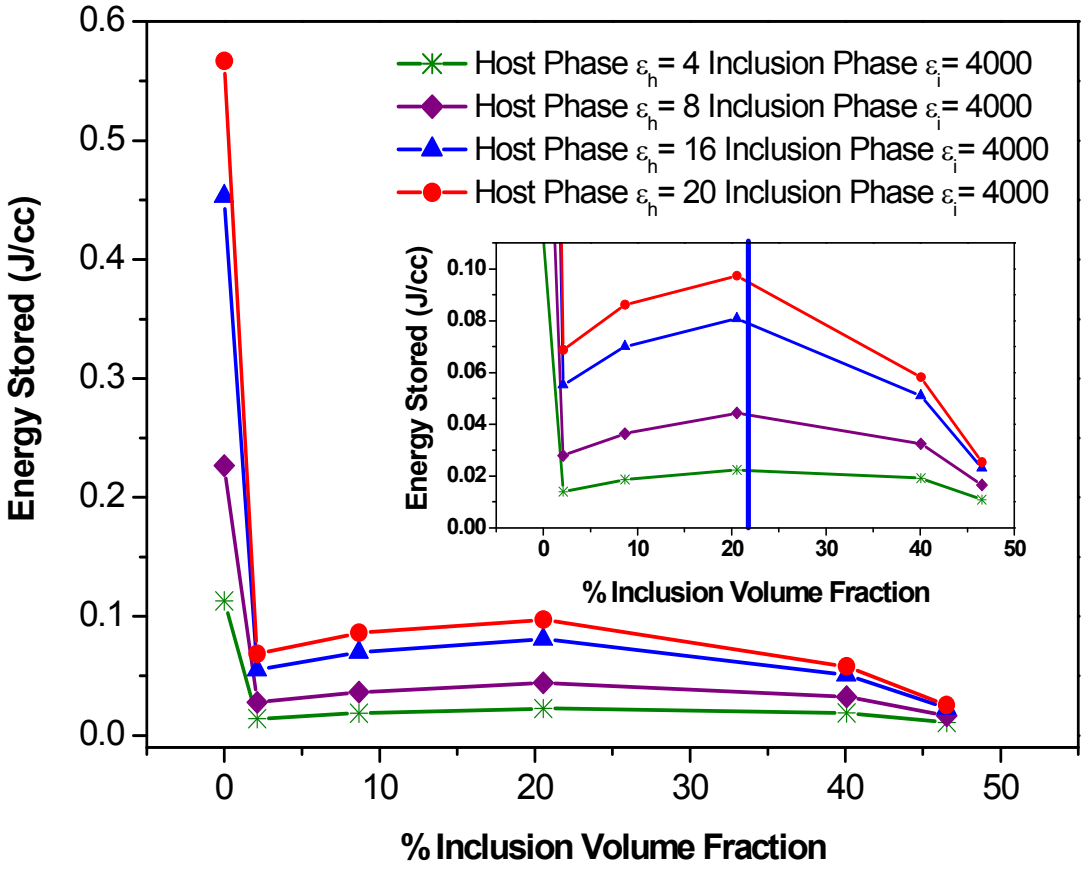

Fig. 2.3. Energy storage predictions for composite as a function of inclusion volume fraction and dielectric contrast.

The impact of dielectric contrast by variation of inclusion phase permittivity was also examined. It was found that decreasing the dielectric contrast leads to a decreased energy storage. Even if lowering the dielectric contrast leads to lower field enhancement factors and thus a high breakdown strength, the effective permittivity of the composite assumes significance in this case. It is the effective permittivity that is reduced with the decrease in contrast and which has an effect on energy storage. The inclusion volume fraction limit of 20 % seen in earlier case is also seen in this case as well.

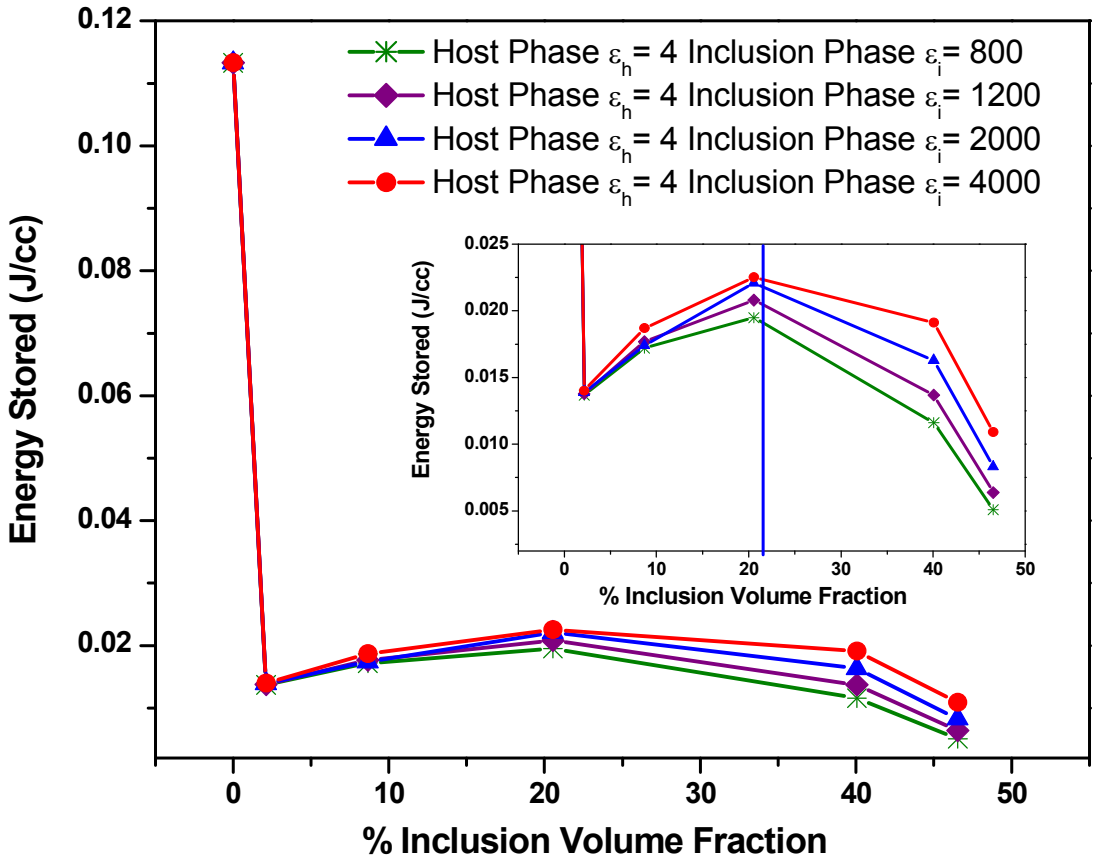

Fig. 2.4. Energy storage predictions for composite as a function of inclusion volume fraction and dielectric contrast.

From both cases it can be stated that at lower inclusion volume fractions (V_f < 20%), the effective permittivity of dielectric composite is more dominant, and at higher volume fractions (V_f> 20%) reduction in the inclusion proximity and the resultant increase in field enhancement is the more dominant parameter in determining energy storage. These results suggest how the properties of the phases (permittivities) and composite (inclusion volume fraction) may be tailored for optimization of energy storage density. Here, only the results for the composites are compared. The critical observations are:

- Increasing the host phase permittivity leads to a decrease in dielectric contrast, enhanced breakdown strength and higher energy stored.
- Inclusion volume fractions up to 20 vol% lead to an increase in energy stored.
- To investigate opportunities associated with dielectric nanocomposites, strategies to account for electron trapping and scattering processes must be developed. These nanocomposites have already been shown to demonstrate higher energy densities, and current simulation approaches cannot presently account for these observations. The capabilities of the simulation packages to incorporate interface and related effects should be explored to enable investigation of nano, as well as microcomposites.

2.1.2 Direction of Discretization. The equivalent capacitance model relies on its ability to discretize a diphasic composite body to predict the effective properties of composite. In order to validate the equivalent capacitance model, demonstration that the model predictions are independent of direction of the discretization is required. Two discretization pathways were identified to test the equivalent capacitance model. The first strategy is a horizontal discretization pathway and the second is vertical discretization

approach. Two dimensional views of these discretization schemes are presented in Fig. 2.5. As anticipated based on physical principles, it was found that the predictions of effective permittivity for both cases of horizontal as well vertical discretizations were similar. However, the integration schemes employed for calculation of the corner capacitances lead to minor discrepancies at low inclusion volume fractions.

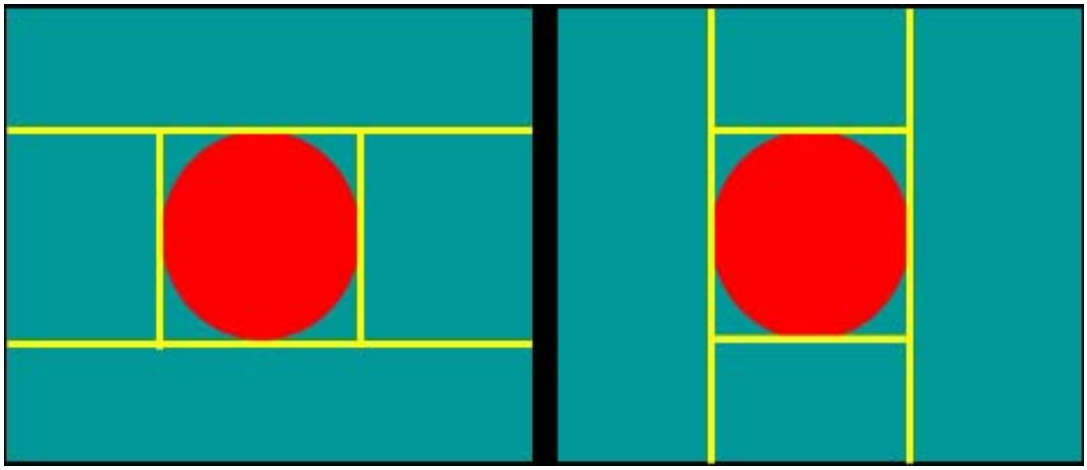

Fig. 2.5 Horizontal and vertical schemes of discretizations.

The effective permittivity predictions for a system of host phase permittivity of 4 and an inclusion phase permittivity of 1900 as a function of inclusion volume fraction are shown in Fig. 2.6. The primary condition that needs to be satisfied for predictions of the equivalent capacitance model to be independent of the discretization approach is that the permittivity of each phase is isotropic, as illustrated in the following equation:

$$\varepsilon(x,y,z) = \varepsilon_x(x) \cdot \varepsilon_y(y) \cdot \varepsilon_z(z). \tag{2}$$

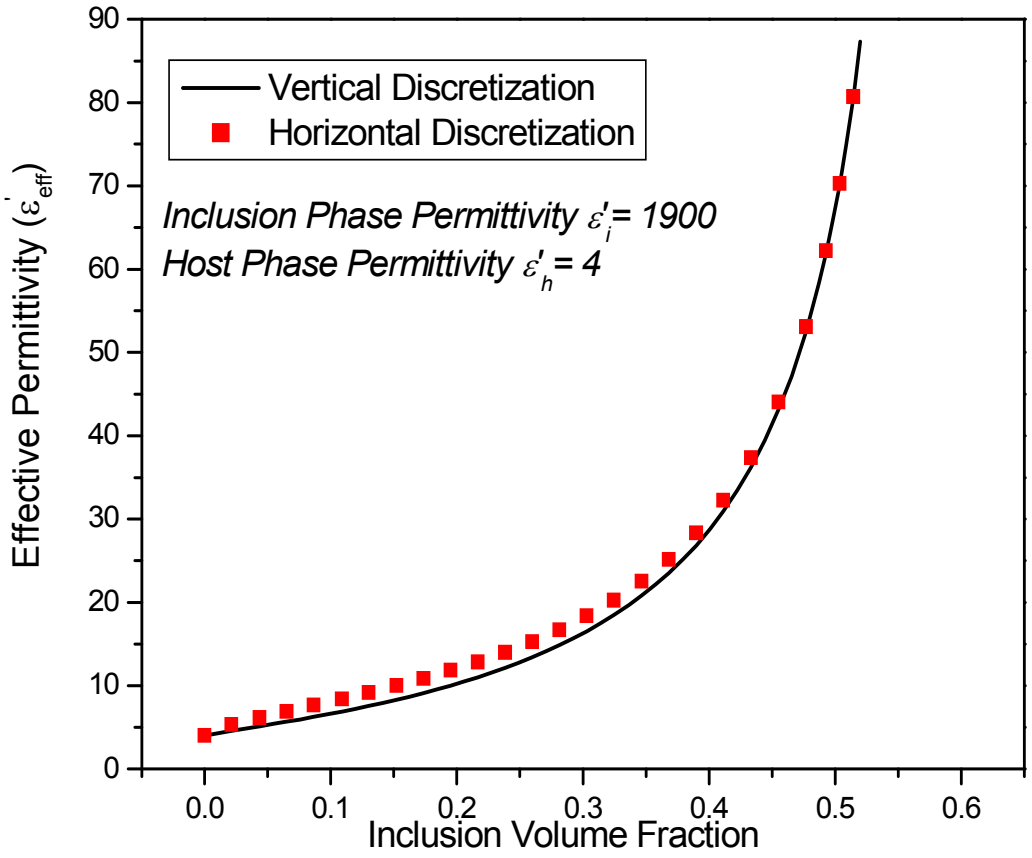

Fig. 2.6. Equivalent capacitance model predictions for effective permittivity as a function of inclusion volume fraction for both horizonta and vertical discretization approaches.

2.1.3 Orientation of Dependence of Permittivity. Recently, many experimental studies have investigated the impact of high aspect ratio inclusions on the effective permittivity. It is also important to verify that the equivalent capacitance model can account for orientation dependence, as for the case of 1-3 composites. A study was performed where an inclusion with an aspect ratio of 3:1 was assumed to be present in the host phase oriented in the vertical direction. In the second study, the inclusion orientation was in the horizontal direction. An enhancement in permittivity is expected for the vertically oriented inclusion, or for the case of spherical inclusions that are aligned with

the applied electric field, as illustrated in Fig. 2.7. This figure, which presents predictions of the equivalent circuit model, illustrates that the model can capture particle orientation effects. This capability of the model illustrates one of the benefits of the equivalent capacitance approach that has been developed compared to simple mixing rule methods. These later methods are typically limited to predictions of volume fraction effects and are incapable of predicting particle orientation effects.

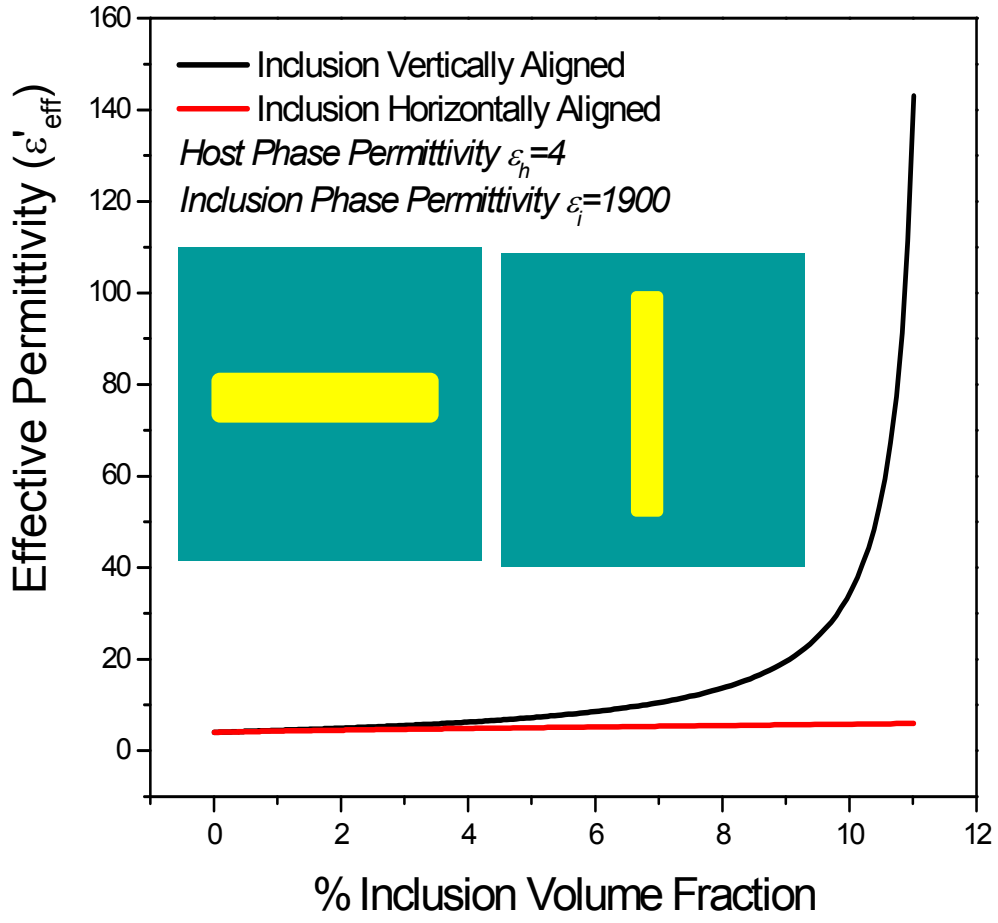

Fig. 2.7. Equivalent capacitance model predictions for effective permittivity as a function of inclusion orientation.

2.2 ELECTROSTATIC FIELD DISTRIBUTION IN RANDOM COMPOSITES AND ITS CORELATION TO BREAKDOWN

Recently, 0-3 high-permittivity polymer-based composites have been increasingly investigated, not only for comparatively low-energy embedded capacitor technology [55], but also for high-energy density applications for pulsed power capacitors [56]. The breakdown strength of the composite for high-energy applications is of special significance because of the important role of applied field in defining energy storage density. However, the relationship of local electric field distribution to dielectric breakdown in diphasic dielectrics is poorly understood.

Some of the possible mechanisms for breakdown in dielectric composites are intrinsic, thermal, and avalanche breakdown [57]. The nature of these mechanisms is complicated due to numerous events that trigger the breakdown process. One complicating factor in clarifying the breakdown mechanism is the fact that various extrinsic factors can influence the breakdown process. Also, the fact that breakdown depends not only on the intrinsic properties of the individual phases, but also on the composite as a whole complicates the understanding of dielectric breakdown. Possible important characteristics of a composite with regard to breakdown include:

- composite morphology (dispersion that dictates proximity of inclusion particles to one another, as well as inclusion shape, size, and mutual orientation);
- dielectric contrast between the phases (defined as the ratio of the inclusion phase permittivity to the permittivity of the host phase); and
- interfacial effects.

The impact of inclusion volume fraction on dielectric breakdown strength in metal-loaded polymer composites has been studied theoretically [58] and experimentally [55].

The objective of the present study was to establish a more quantitative correlation between inhomogenous local electric fields in 0-3 polymer system containing insulating high-permittivity inclusions and breakdown strength. Key goals include investigation of the impact of dielectric contrast, inclusion volume fraction and interfacial behavior on local electric field distribution, which is believed to influence the breakdown behavior of the composite.

2.2.1 Simulation Software. Simulations were carried out using the commercially available software *Coulomb* from Integrated Engineering Software (Winnipeg, Manitoba, Canada). *Coulomb* is a 3D code that uses a boundary element method (BEM) to solve a set of partial differential equations to describe the electrical potential behavior of the material. *Coulomb* allows for the construction of large 3D structures that contain periodically repeated cells with identical properties. An example of such a structure is shown in Fig. 2.8.

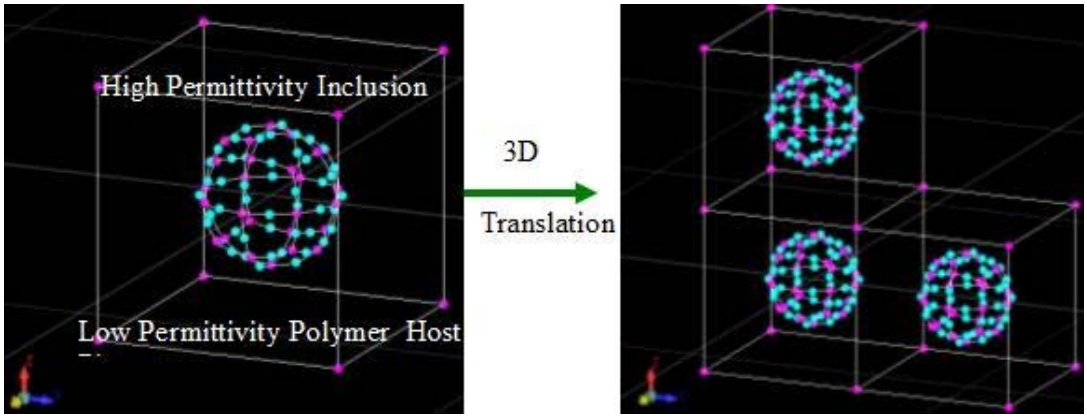

Fig. 2.8. Basic building block of composite sphere enclosed in cube and 3-D translation in x, y, z directions.

The geometry contains a cell with a sphere enclosed in a cube (SEC), and its 3D translation in x, y, and z directions and its translation into 3 directions. Similarly a random composite can be built in Coulomb.

2.2.2 Model Assumptions. The primary assumption is that macrosocpic breakdown originates through an intrinsic breakdown event, i.e., electrode, sample geometry, and sample size effects are not considered. Also, field characteristics, e.g., pulse rise time, pulse duration and temperature effects are neglected. By making these assumptions, it is possible to focus on the nature of dielectric. It is assumed that breakdown is electronic in origin. Another reasonable assumption is that *any* breakdown process eventually occurs in the host, *i.e.*, in the polymer phase. This means that breakdown either happens directly in the host phase, or it must pass through the host, even if it is triggered in the inclusion phase. The schematic in Fig. 2.9 elucidates one possible conduction path that would allow for electron transport between the electrodes would have to take to reach electrodes has to go through the host phase.

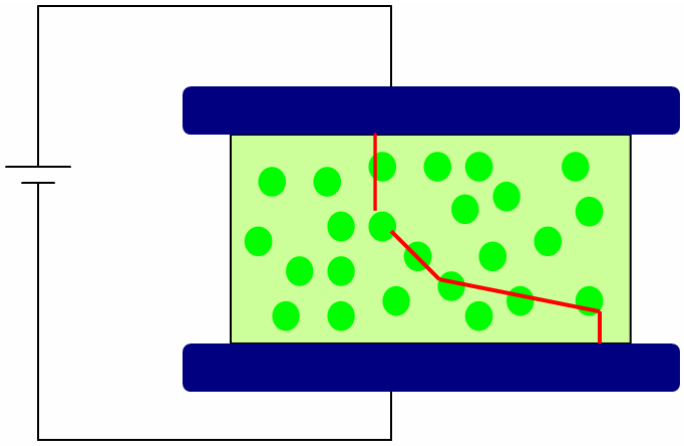

Fig. 2.9. One possible breakdown path in a diphasic dielectric composite.

It is also assumed that parallel plate electrodes are applied on the dielectric. The breakdown model employed herein is the intrinsic percolation breakdown model for insulating polymers proposed by Wu et al. [55]. This model suggests that, "an extended state for charge carriers can be formed due to a reduction of the trap barriers at sufficiently high electrical fields and that breakdown can be induced by the current multiplication in the extended state." The model further states that when the field exceeds a threshold value, a percolation path (or extended state) in an insulating polymer is formed in such a way that trap barriers are reduced to zero, leading to the development of a conductive path, or breakdown. Our ability to use the Coloumb software to predict local electric fields is ideally suited to the percolation model for the consideration of the development of a conductive path in the dielectric.

Potential barriers to charge transport between trap states, as reported by Wu et al. [55], may be interpreted in terms of:

$$\phi = \phi_0 - \left(\frac{e^3}{\pi \varepsilon \varepsilon_0} \right)^{1/2} \cdot E^{1/2} \qquad (3)$$

where ϕ and ϕ_o are the potential barriers with and without the presence of electric field, respectively, ε is host polymer relative permittivity, and ε_o is the free space permittivity. Using the local electric field distribution as calculated by *Coulomb* the electric fields leading to a decrease in the barrier to zero can be calculated using (3). When the potential falls to zero or below, this indicates that the composite is likely to undergo local conduction. When a sufficient number of local conduction events become "linked together" macroscopic breakdown occurs. Below, results from Coloumb on local electric

field behavior are presented. These results are then interpreted in the context of Wu's percolation model for breakdown.

2.2.3 The Role of Number of Inclusions on Electric Field Distribution. The first case studied was an electric field simulation carried out for a single inclusion with the radius of 0.204 μm, which is centered within an exterior cube having a side of 1.1 μm. Thus, the inclusion volume fraction is 2.69% (*the corresponding 2D plane surface fraction is 7.64%)*. The host phase permittivity is 4.9 (standard molded epoxy), and the inclusion phase permittivity is 1200 ($BaTiO_3$). The second case evaluated used the same parameters, except for the number of inclusions. For this simulations, 25 inclusions were randomly dispersed within the cube. This was made possible by choosing 25 random points in a plane within 3D space. The radius of each inclusion is 70 nm. The resultant inclusion volume fraction is the same as the first case: 2.69%. In both cases, the applied electric field between the top and bottom of the cube is 2500 kV/cm. By examining these cases, the role of inclusion proximity and size on composite breakdown can be understood.

The electrostatic field distribution maps for both cases are shown in Fig. 2.10. The maximum electric field can be determined from the color scale on the left of the image with the red color indicating the highest magnitude electric field and dark blue indicating the lowest magnitude electric field. The maximum electric field present for the single inclusion case is 7643 kV/cm for an applied field of 2500 kV/cm. This indicates that the field enhancement factor is approximately 3.05. In the second case with multiple inclusions 17520 kV/cm for the same applied field of 2500 kV/cm indicating a field enhancement factor of approximately 7.00.

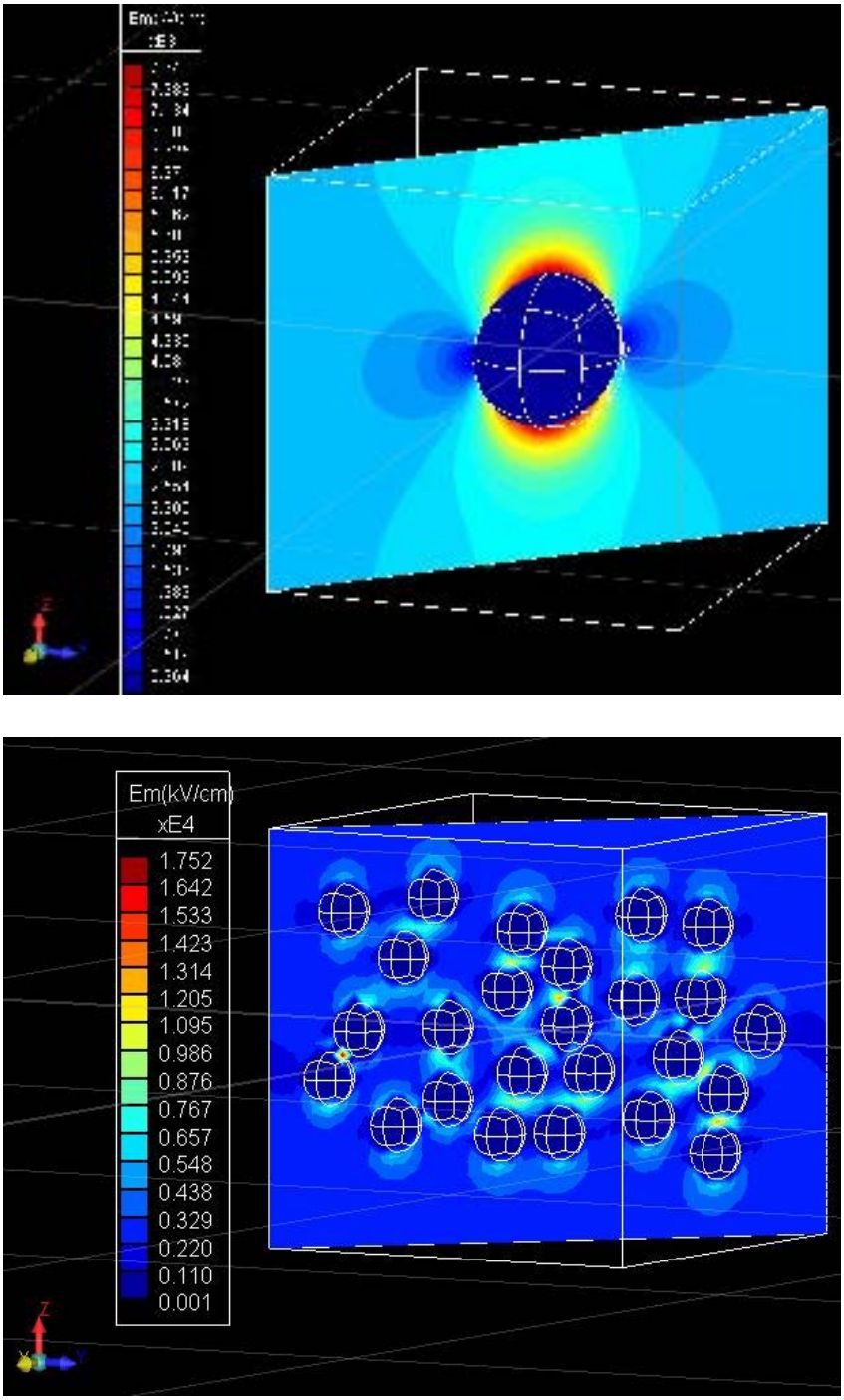

Fig. 2.10. Electrostatic field distribution map for single inclusion and 25 inclusions with applied electric field of 2500 kV/cm in both cases

The presence of multiple inclusions that are in close proximity to each other results in an increase in the local field enhancement factor.

2.2.4 Role of Inclusion Proximity/Inclusion Volume Fraction. The role of inclusion proximity/inclusion volume fraction in diphasic composites is a topic that requires careful construction of random systems. It is challenging to vary inclusion proximity in random systems. The approach that was chosen was to locate the the centers of inclusions using a mesh styled framework. The inclusion radii were varied from 30 to 60 nm. When the radii of the inclusions reached 60 nm, some inclusions were nearly touching. This is considered to be a limiting case for the investigations carried out. The total number of inclusions in the single cube were 25. Again the host phase permittivity was modeled with a permittivity of 4.9 and the inclusion phase was assumed to have permittivity of 1200. The simulation was carried out with an applied electric field of 2500 kV/cm in the z-direction.

The electrostatic field distribution maps for all cases are shown in Fig. 2.11. From the electrostatic field distribution maps it is seen that when interparticle separation (s) is high (on an average > 0.3 μm), as is the case of when radii of particle is 30 nm, the electric field enhancement is localized at the top and bottom of the inclusion sphere within the host phase. The electric field enhancement regions shows a marginal increase when the inclusion radius is increased from 30 nm to 40 nm. The maximum field present in the host phase for the 30 nm case is 7791 kV/cm for an applied field of 2500 kV/cm (*Field Enhancement Factor: 3.11*). The maximum field present in the host phase with 40 nm radii inclusions is 7958 kV/cm (*Field Enhancement Factor: 3.18*).

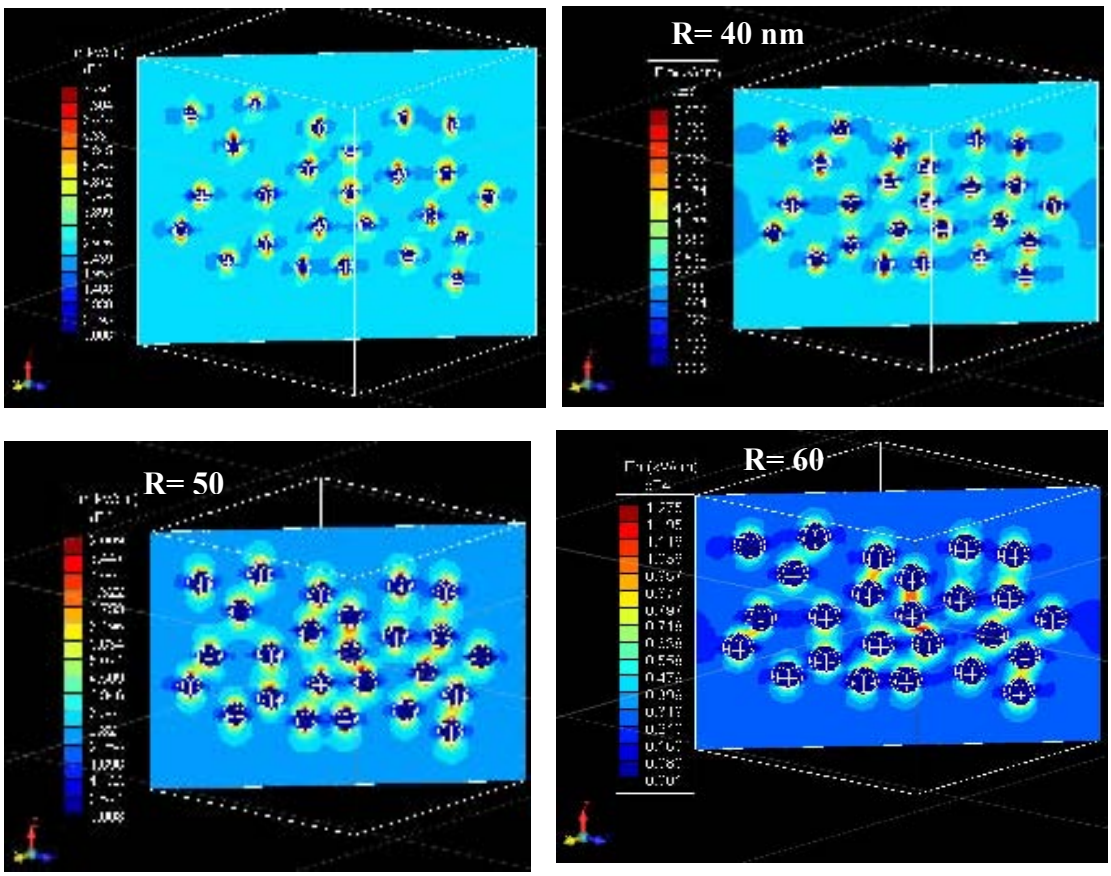

Fig. 2.11. Electrostatic field distribution maps of random composites each with 25 inclusions of radii 30 nm, 40 nm, 50 nm, 60 nm, respectively.

With the radii of the inclusions increasing to 50 nm a clear cut field enhancement path starts to form. This field enhancement path might be viewed as a percolative path where the field enhancement is sufficiently high that it would lead to current multiplication, and subsequently, breakdown. The maximum field present in the host phase is 9009 kV/cm (*Field Enhancement Factor: 3.6*). This field enhancement path becomes more pronounced with inclusion radii increasing to 60 nm. In this case, the inclusion proximity is considerably decreased (on an average less than 0.05 μm) compared to the earlier cases and it can be seen that the inclusions with closest proximity to each other result in

the formation of areas of maximum field enhancement. For the case with 60 nm inclusions the maximum field present in host polymer phase is 12750 (*Field Enhancement Factor:5.1*).

2.2.5 Relationship between Local Field Enhancement Factors on the Percolation Model of Breakdown. Wu's model discusses the role that an applied field can have on the potential barriers to conduction associated with the hopping conduction mechanism typically present in polymers. To begin to understand the correlation between the presence of inclusions, local field enhancements and Eq. 3, we examine both the ordered and random structures noted above, and relate the field distribution in these structures to calculated reduction in barrier height obtained from this equation. As the difference between ϕ and ϕ_o ($\delta\phi$) approaches zero (due to local field), local conduction results.

Local fields in ordered composites and their role on $\delta\phi$ are considered for a variety of typical potential barriers reported for polymers (1.2 eV > ϕ_o > 0.6 eV). A summary of these studies is presented in Fig. 2.12. This plot was obtained for an applied electric field of 800 kV/cm to a single inclusion in sphere geometry of varying inclusion radius, which results in a variation in inclusion volume fraction. As shown in Fig. 2.10, local fields of greater magnitude develop above and below the inclusion particle. Further, these local fields increase with increasing particle radius (volume fraction). All inclusion volume fractions result in a decrease in the potential barrier to conduction, with the greatest decrease being observed for the highest volume fraction. Assuming the polymer host phase is characterized by a potential barrier height of 0.6 eV, a volume fraction of 20% inclusion phase is sufficient to reduce the barrier height for charge

transport to 0. Under such conditions, local conduction will occur. Generally speaking, for polymers with higher potential barriers, higher local fields are required for conduction, as shown in the Fig. 2.12.

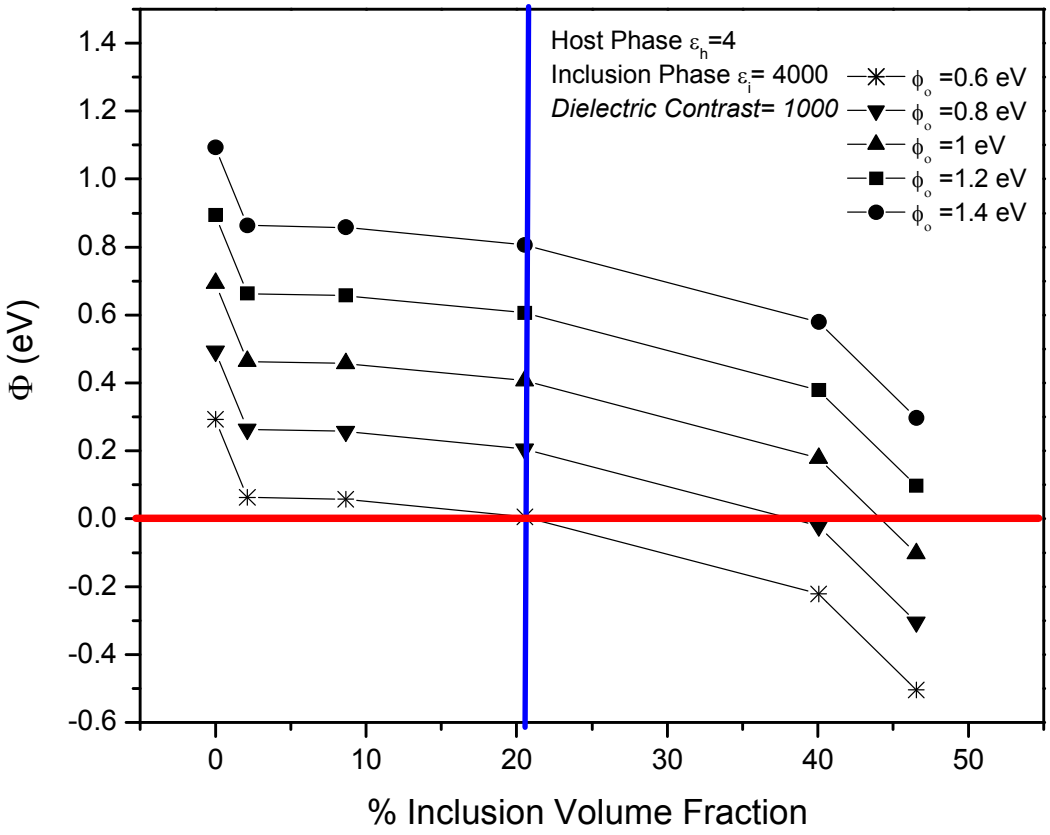

Fig. 2.12. Delta function as a function of inclusion volume fraction for diphasic composite with sphere enclosed in cube ordered geometry.

However, random composites are more commonly fabricated. To further explore macroscopic conduction across the dimensions of a sample (i.e., breakdown), local fields in random samples (e.g., Fig. 2.11) must be considered in detail. A representative perspective of a random and an ordered samples is illustrated in Fig. 2.13 and Fig. 2.14.

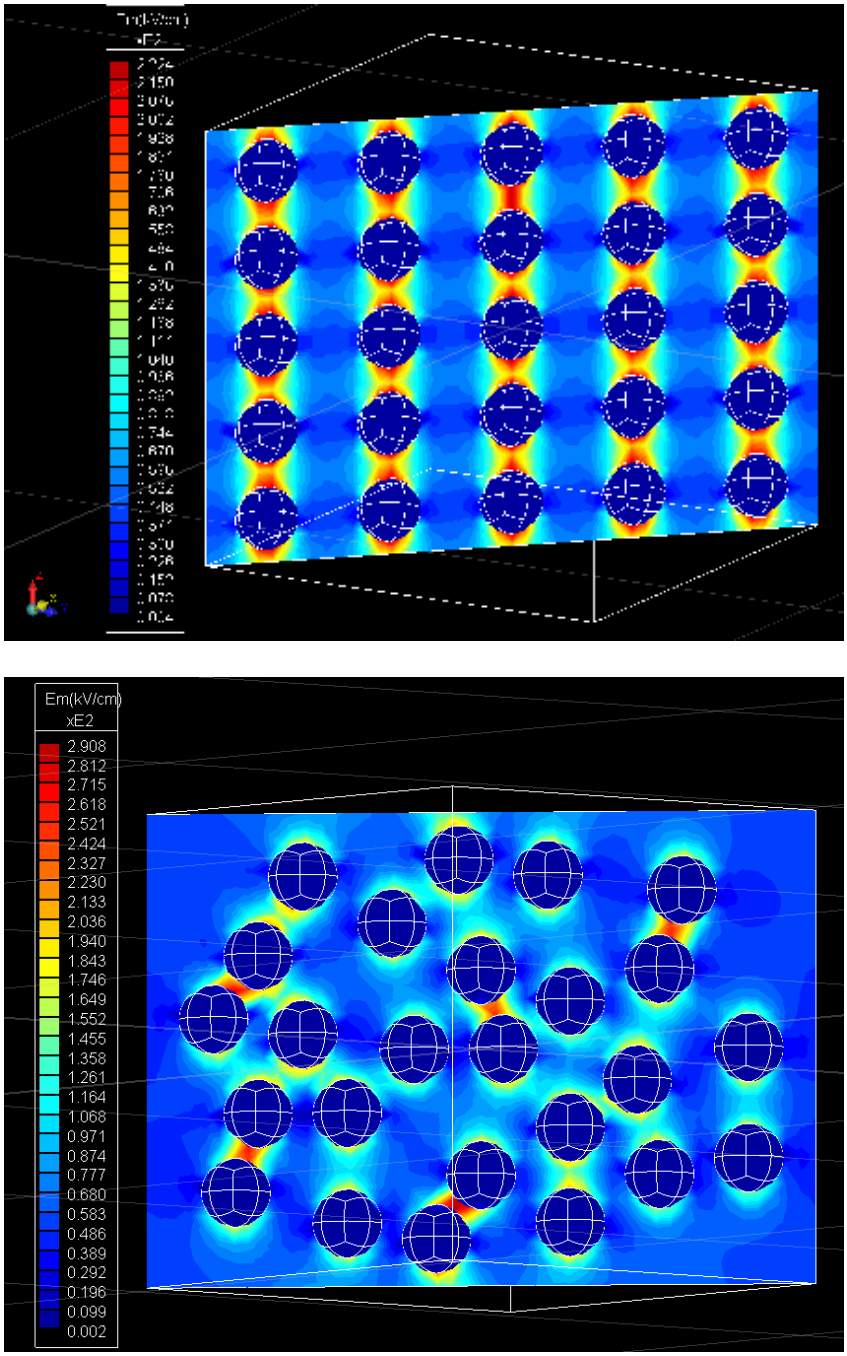

Fig. 2.13. Electrostatic field distribution maps of composite with ordered and random inclusions.

In this figure, both the ordered and random composite contain 4.02 vol% inclusion phase. The relative permittivity of the host phase is 4 and that of the inclusion

phase is 1200. The applied electric was 50 kV/cm. The field distribution data shown is for a vertical path through the center of the cube.

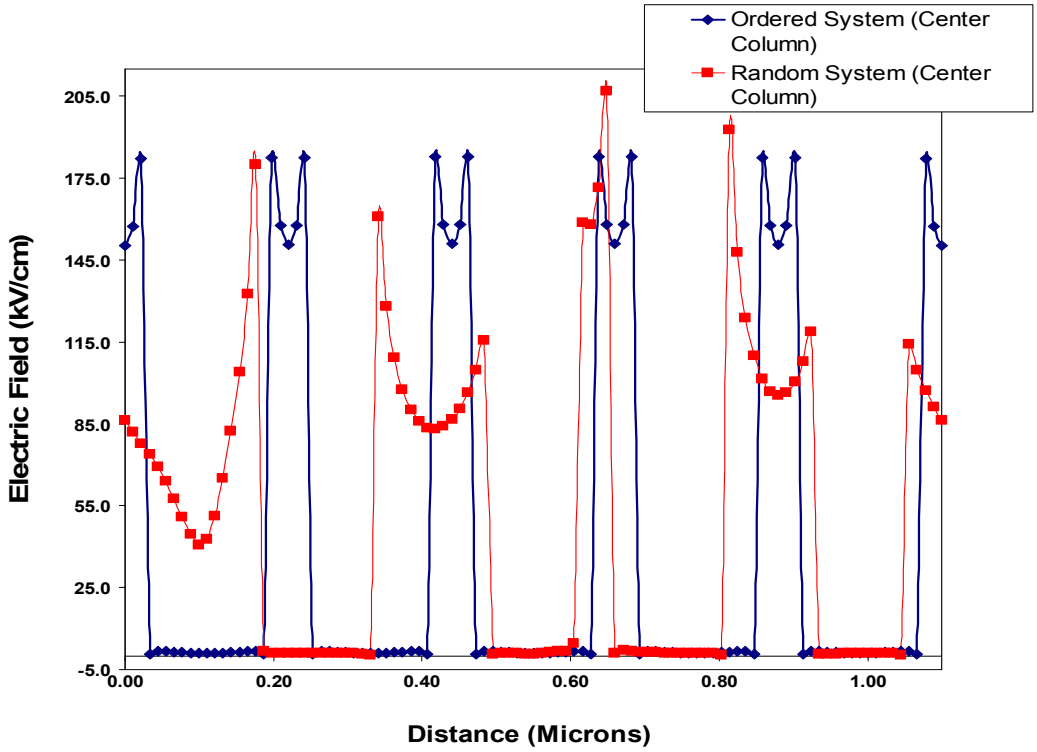

Fig. 2.14. Magnitude of electric field from top to bottom electrode for a vertical path through the center of the cube for both ordered and random composites.

This figure may, in general, be used to expand on the simple use of Eq. 3, which was employed above solely using the maximum local field as one point within the sample as determined through Coloumb simulations. Fig. 2.14 shows that periodic potentials exist within ordered composites and that a much more non-uniform potential distribution exists within the random composite. The highest peak field observed was 205 kV/cm, i.e., a local field enhancement of greater than 4. Using specific local field data at each

point across the sample allows enables the estimation of local potential barriers, invoking significant assumptions about the knowledge of ϕ_o.

Finally, the picture of breakdown in these materials based on the use of local electric fields and percolation models may be brought together. Breakdown occurs due to the linking together of local conduction regions throughout the dielectric. These regions are formed when the local potential barrier to conduction (ϕ) is reduced to zero due to the local electric field. The local fields are dictated by factors such as applied field, inclusion proximity and volume fraction, and dielectric contrast. Further, as inclusion volume fraction increases, additional regions of local conductivity are anticipated, due to the increase in field enhancement factors, and thus, local electrical fields.

However, the above parameters are only some of those that need to be considered for the full development of this model of breakdown. First, only one path through the dielectric has been considered, when in reality an infinite number of paths must be considered. Second, describing the potential barrier to local electron hopping by a single valued parameter may be inaccurate. In polymers, local heterogeneities will always exist that will contribute to a distribution of the potential barriers [59, 60]. Therefore, the specific field that will result in a reduction of ϕ to zero locally will be a function of the local polymer morphology. Third, the introduction of inclusions into a polymer will also contribute to the heterogeneous nature of the host material. This will also be expected to impact polymeric features such as free volume (nanopores), chain configurations, ionization behavior to form trap states, and of course, local potential barriers.

Despite the difficulty in identifying some of the specific characteristics of these materials that will certainly dictate their behavior, the basic framework of picturing

macroscopic breakdown from a percolation threshold perspective remains an attractive one. A key step in the development of this method is the acquistion of local field data, which has now been accomplished. Also accomplished is the general approach for the use of this data. What remains to be developed is the utilization of this information in a more statistical thermodynamic perspective, i.e., local heterogeniety effects on potential barrier distributions, probabilities of specific condution paths, etc. must be much more fully considered. However, significant steps have been taken in this work to provide the foundation for the full development of this picture of breakdown.

2.3. DEVITRIFICATION STUDIES OF HIGH REFRACTIVE INDEX MO-SCI COMPOSITIONS

Published data from the literature was used for verification of the analytical modeling results. For further verification of these results and those of the numerical simulations, attempts were made to synthesize composite materials, namely, glass-ceramic dielectrics. This material system was selected due to renewed interest in these materials. For example, recent studies have shown that these materials can demonstrate energy densities in the range of 4 J/cc.

The relationship between refractive index n and ε_r for non-magnetic dielectric materials (at optical frequencies) is given by the following expression.

$$\varepsilon_r = n^2 \tag{4}$$

This expression results from Maxwell's electromagnetic theory and it is valid only when the same polarization processes are active during measurement of both ε_r and n. The premise of this experimental work was that if devitrification of a high refractive index

glass was carefully carried out it would result in enhanced effective permittivity as there is a square relationship between refractive index and dielectric constant. By controlling devitrification, a residual glassy phase of high permittivity would be left behind, increasing the overall energy density of the composite, while at the same time reducing the dielectric contrast with the resulting crystalline phase. This would reduce the field enhancement factor, thereby enabling the application of higher electric fields. The objective of this work was to synthesize a high energy density *nanoscale glass ceramic* composite. Two glass compositions obtained from Mo Sci Corporation were studied (G 0175, G0176). The chemical composition of these MO-Sci glasses by weight are listed below. These glass systems were selected to devitrify the high dielectric constant phase, $BaTiO_3$.

MO-Sci Composition for High Index Glasses.
Chemical Composition by weight:
Silica (SiO_2)….....1~20%
Boron Oxide (B_2O_3).....1~20%
Zirconium oxide ZrO_2)….0~10%
Barium oxide (BaO)…...30~70%
Titanium oxide (TiO_2)…30~70%

Fig. 2.15 shows the thermogravimetric analysis (TGA) of both G-0175 and G-0176 and indicates there is no weight loss for either composition up to temperatures of at least 1000°C. This indicates that both compositions are highly stable. Differential thermal analysis (DTA) of the G-0175 and G-0176 compositions was also carried out and the plots are shown in Fig. 2.16. For the G-0175 composition, two peaks were observed, most likely indicating the onset of crystallization of two different phases at approximately 782 and 835^{o}C. DTA studies also showed the melting points of the two phases to be approximately 922^o and 938^{o}C. Based on the crystallization and melting temperatures, the processing window for devitrification of this compositions is narrow. DTA analysis

of the G-0176 composition revealed only one peak indicating onset of crystallization around 767°C.

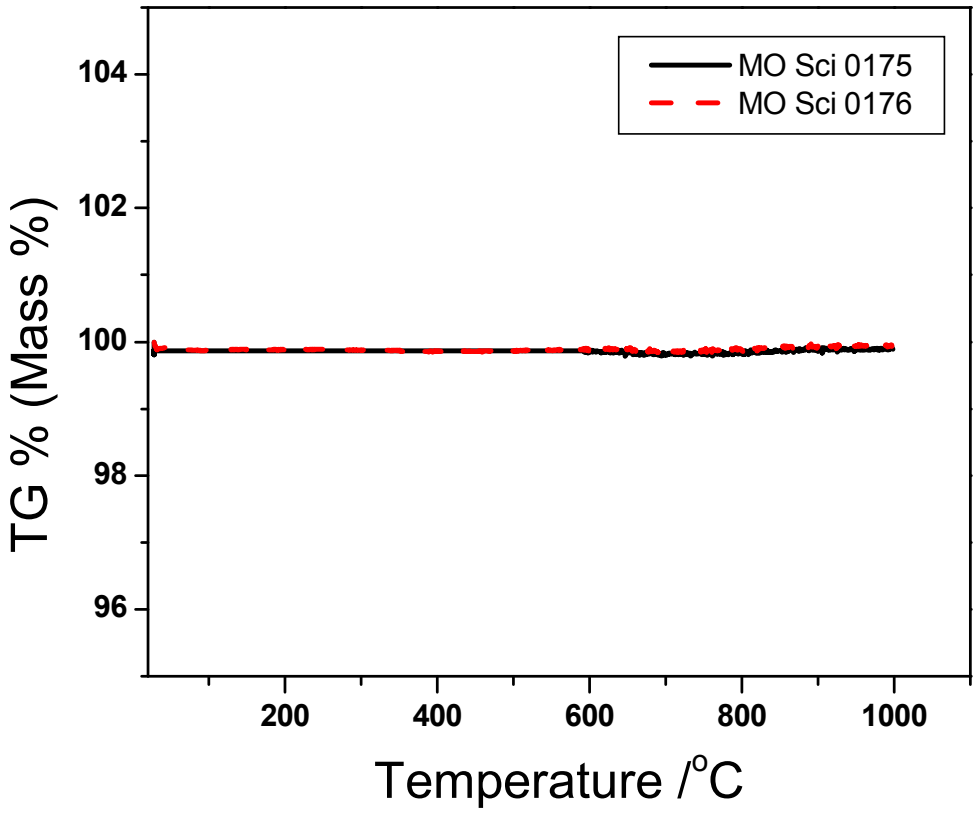

Fig. 2.15. TGA studies of MO-Sci compositions G-0175 and G-0176.

No melting was observed until 1000°C, the maximum temperature to which the analysis was performed. Based on the DTA analysis, it was expected that the G-0176 composition would sinter well compared to G-0175, as it was thought that processing of a composition with a single devitrified phase would be easier. Also, it was expected that the temperature window for devitrification would be greater as no melting was observed for temperatures up to 1000°C. A simple heat treatment procedure was applied which involved filling the two powder compositions in alumino-silicate molds followed by a

ramp rate of 10°C/min to 850°C. The hold time employed was 4 hours. After heat treatment, the furnace was cooled at a rate of 25°C/min.

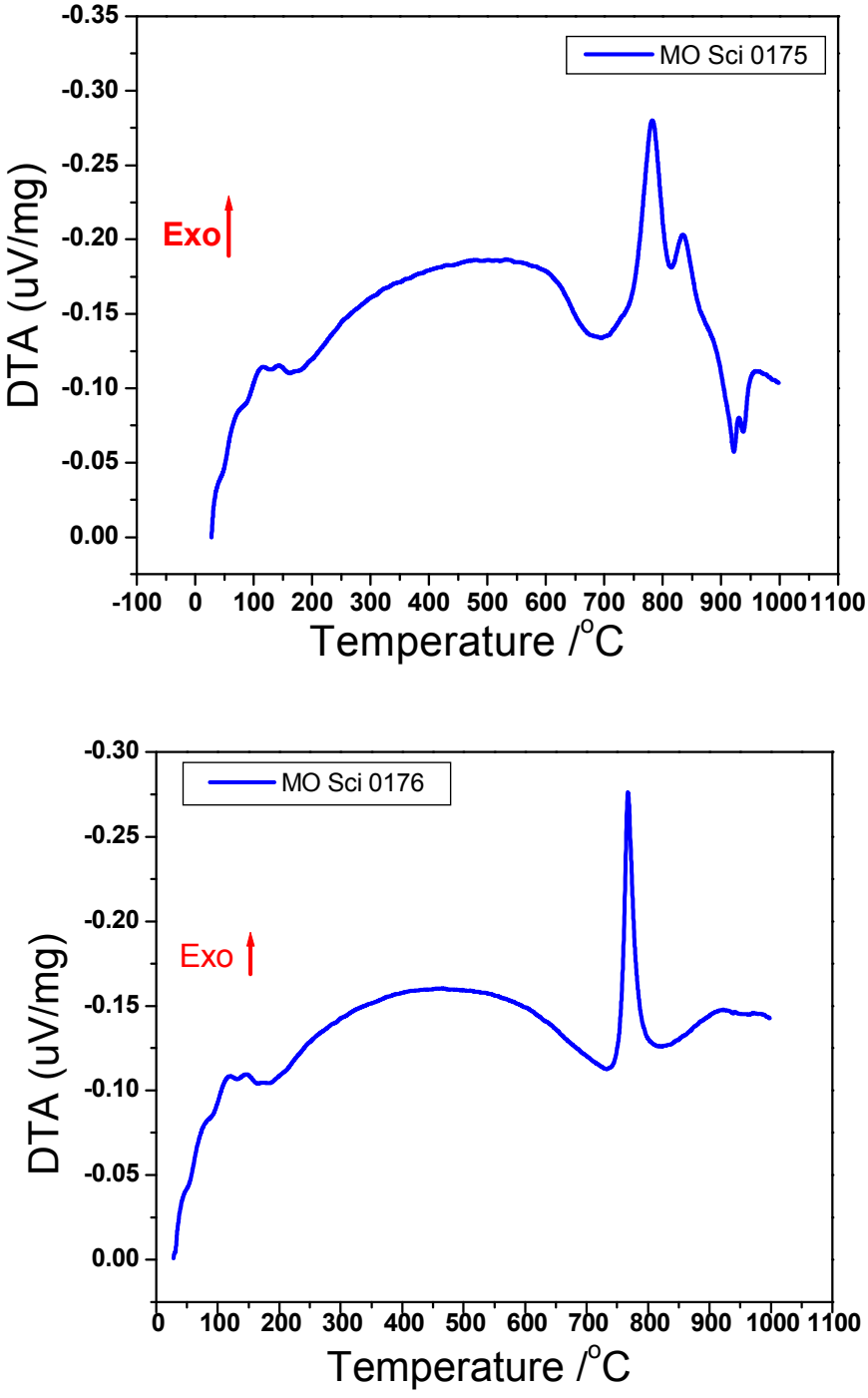

Fig. 2.16. DTA studies of Mo Sci compositions G-0175 and G-0176.

The alumino-silicate molds were prepared by machining to get requisite shape and fired to obtain molds.

The molded dielectric thickness was minimized to reduce requirements for post-processing to form samples for dielectric measurements. The alumino-silicate molds and sintered glass ceramics prepared from G0175 composition are shown in Fig. 2. 17.

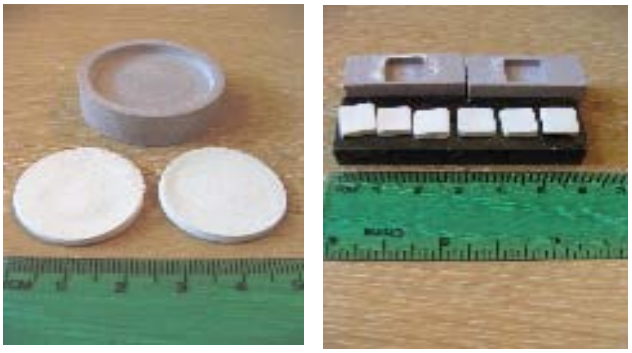

Fig. 2.17. Alumino-silicate molds and sintered glass ceramic dielectric compositions of G-0175.

Heat treatment resulted in the sintering of composition G-0175, however no densification was seen for composition G-0176. X-ray diffraction (XRD) analysis revealed the presence of two crystalline phases as seen in Fig. 2.18. For G-0175, the major crystalline phase is Barium titanium silicate" ($Ba_2TiSi_2O_8$) and small amounts of"Barium titanate ($BaTi_2O_5$)." The results of quantitative XRD analysis of devitrified G-0175 composition indicated the weight fractions of barium titanate silicate ($Ba_2TiSi_2O_8$) was 45.4 wt % and barium titanate ($BaTi_2O_5$) was approximately 54.6 wt%. Dielectric characterization of the sintered dielectric discs (G-0175) was carried out using an impedance analyzer (HP 4094A). The effective relative permittivity was found (at low frequency; 10^3 Hz) to be 140.

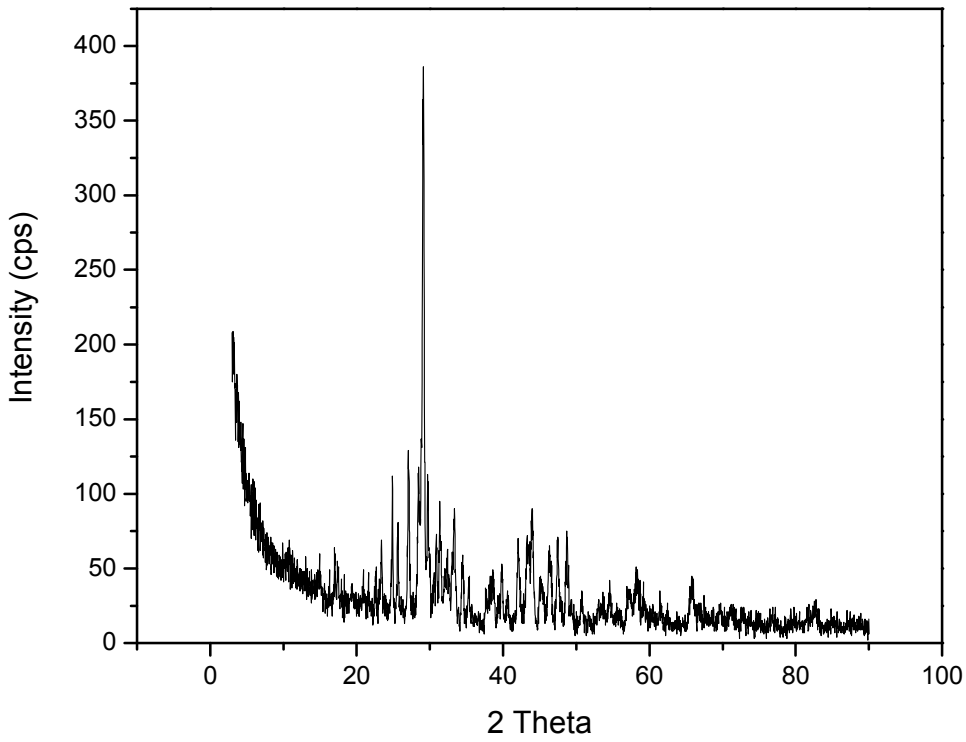

Fig. 2.18. XRD pattern of heat treated glass ceramic dielectric devitrified from G-0175.

The comparatively low permittivity of the glass ceramic compared to $BaTiO_3$ can be attributed to the presence of the high weight fractions of two low permittivity phases: $Ba_2TiSi_2O_8$ and $BaTi_2O_5$.

For breakdown measurements, samples were thinned using a surface grinder and polished. Samples were dimpled using a standard dimpler(Model D 500i) employed for TEM sample preparation and platinum was sputtered as electrodes. Fig. 2.18. shows representative dimpled samples used for breakdown testing. A high voltage source was used for measuring the breakdown strength of the samples, which was found to be approximately 510 kV/cm. Considering this value and the measured relative permittivity of 140, an energy density of 1.61 J/cc may be calculated.

Fig. 2.19. Dimpled glass ceramic dielectric composition prepared from G-0175.

Thus, even though a high permittivity $BaTiO_3$ phase was not formed, even these prelimary results suggest opportunities for glass-ceramic materials.

To initiate a more thorough comparison of the simulation results of diphasic dielectrics with experimental results of this type, further characterization of the phase assemblage of the glass-ceramics is required. Phase volume fractions and distribution need to be determined. It would also be desirable to develop a glass-ceramic system that demonstrates only a single crystalline phase, since such as system can serve as a more effective "model" system for simulation analysis. Finally, other measurements that need to be completed would include characterization of the relative permittivity of the residual glass phase so that dielectric contrast can be accurately estimated.

3. CONCLUSIONS

The area of diphasic composite research is a problem with many facets. The key properties and issues of interest in this area are listed in flow chart shown in Fig. 3.1

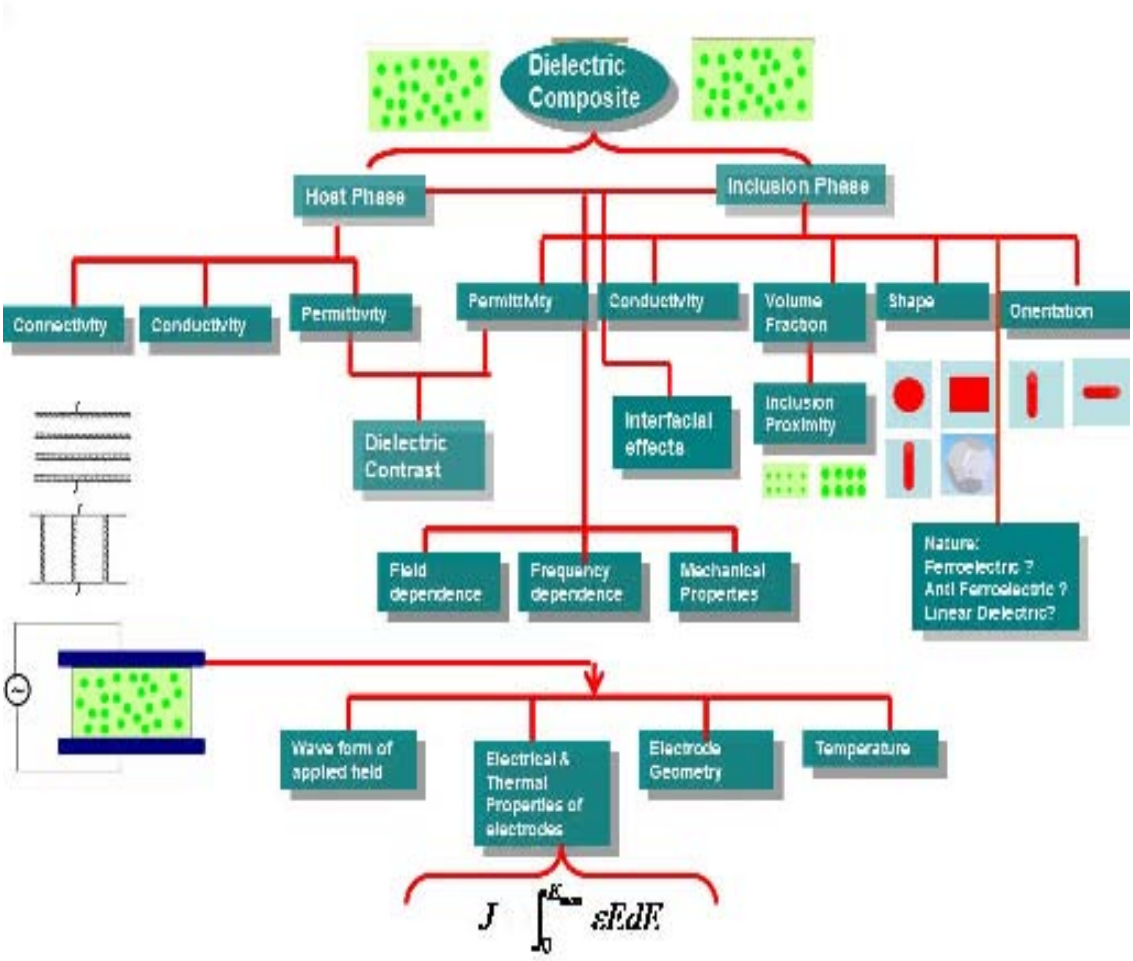

Fig. 3.1 Key issues in diphasic composites that may impact energy density.

This Ph.D. research has primarily focused on studying the intrinsic attributes of the diphasic composites system and evaluating their impact on energy density through

analytical and numerical modeling. In particular, an analytical method to predict effective permittivity and numerical approaches to evaluate local fields were developed.

The complexity of many-bodied interactions and the heterogeneous environment experienced by the charges and waves in a composite material under the action of applied electric field have made analytical studies of diphasic dielectrics notoriously difficult, in spite of the considerable number of studies aimed at understanding these materials. The aim of this research was to provide a simple solution to this complex problem. This research has resulted in the development of a new mixing rule. The mixing rule approach developed predicts effective permittivity of diphasic composites for both static, as well as dynamic cases, i.e., as a function of alternating electric field. A key feature of this model is its independence from the inclusion size limitations associated with traditional mixing theories, and the ability to uniformly apply this mixing theory to any composite dielectric architecture (0-3, 2-2, 1-3, 3-3). The equivalent capacitance/impedance model developed has also been extended to complex geometries (*High aspect ratio inclusions*) and high volume fractions of high phase permittivity systems.

To further understand composite dielectrics, numerical simulations were also carried out. These simulations have provided new insight into the electrostatic field distribution in diphasic dielectric systems and have enabled a perspective into the limitations of traditional mixing rules. To the best of my knowledge, for the first time, a comprehensive study of electrostatic field distribution in the three dimensional space of a diphasic dielectric has been carried out. This research has resulted in new understanding of dielectric contrast and volume fraction effects and has suggested opportunities for microstructural engineering of composites not previously considered.

The highlights of this research on analytical modeling include:

- ✓ Ability to account for any particle shape
- ✓ Able to handle many bodied interactions and heterogeneous environments
- ✓ Ability to model effective permittivity for both *DC as well as AC conditions*
- ✓ No need to approximate inclusion particle shape
- ✓ No volume fraction limitation
- ✓ Model can account for inclusion orientation

The highlights on the numerical modeling are:

- ✓ Quantified local field distribution in diphasic systems
- ✓ Evaluated effects of dielectric contrast and inclusion volume fraction on electric field enhancement in the host and electric field penetration into the inclusion
- ✓ Compared analytical modeling results to mixing theory predictions to identify inclusion volume fraction limitations of Maxwell Garnett theory
- ✓ Proposed new combinational approach of numerical modeling with percolation model for polymer phase to establish correlation between local electric field distribution in random systems with dielectric breakdown
- ✓ Developed insightful guidelines for microstructural opportunities

4. FUTURE WORK

This research has also laid the foundation for significant research investigations that could compliment the present work. Further studies that are recommended for future investigation in the area of analytical modeling are noted below.

(a) The equivalent capacitance/impedance model presented is for ordered diphasic composite systems. The similarities and differences between the macroscopic behavior of ordered and random composites is an ongoing area of research. A transmission electron microscope (TEM) photomicrograph of iron oxide particles in Vycor glass and its adaptation into random and ordered systems for modeling purposes is shown in Figure 4.1

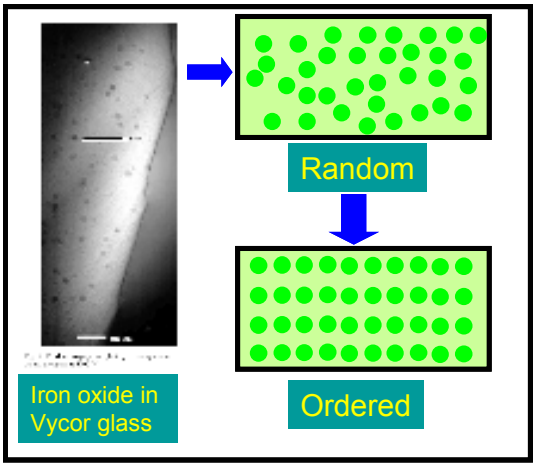

Figure 4.1 TEM micrograph of iron oxide in vycor glass and cartoon representing adaptation of the composite in random and ordered systems for computation purposes.

It is imperative that future studies include simulations of random inclusion geometries because these are more representative of real world systems. These studies could be achieved by consideration of a three dimensional array of cubes representing the host phase. By using probability theory, it is possible to allocate a particular probability of cells filled with inclusions as opposed to cells that are empty (i.e., host phase only). Thus, a random composite could be analytically created and then modeled. The equivalent capacitance/impedance model could then be applied to evaluate the effective properties of the composite and compare predicted properties with those of ordered systems and real world systems.

(b) The study of dielectric composites has been, unfortunately, divided between theorists and experimentalists. There is a need for a unified approach to examine dielectric composite electrical properties. Many investigators continue to apply effective medium theories and other analytical models without being cognizant of the fact that the relevance of these models, fitted to one data set, may not be applicable to other material or microstructural systems. This issue is complicated by the fact that the permittivity of the inclusion particle is a function of particle size, and this is often not measured, or is unknown. This results in the use of permittivity values that best fits the results. Theorists, on the other hand, continue to compare their mixing rule approaches with other models and bounds and not with experimental results. A joint approach needs to be adopted that would look at the following issues:

- Measurement of inclusion particle size distribution to account for the associated distribution in permittivity values expected for non-linear (ferroelectric) dielectrics
- Measurement of slurry properties, and thereby, deduction is of inclusion phase permittivity
- Impact of dispersant on composite polarization response, particularly at the interface between the particle and host phase
- Incorporation of this data into mixing models for both ordered and random systems to predict effective properties.

(c) It is known that the static permittivity, "ε'_{eff}" is a function of the intrinsic nature of the diphasic composite. Therefore, it is easier to model the behavior of ε'_{eff}. However, "ε''_{eff}" may be highly dependent on extrinsic parameters, like temperature. The equivalent capacitance/impedance model has not yet been developed to take into account temperature effects. Loss behavior can be modeled by taking the temperature dependence of dielectric loss.

(d) The equivalent capacitance/ impedance model approach needs to be extended to complex shapes and this would require development of integration methods which would account for shape characteristics.

BIBLIOGRAPHY

1. B. Chu, X. Zhou, K. Ren, B. Neese, M Lin, Q. Wang, F. Bauer and Q. M. Zhang, Science*.,* **313,** 5785 (2006

.2. W. J. Sarjeant, R. E. Dollinger, J. Macdougall, F. W. Goldberg in *Power Modulator Symposium* Boca Raton, FL, 1996, pp. 209-212.

3. Y. Tanaka, N. Ohnuma, K. Katsunami, and Y. Ohki, IEEE Trans. Electr. Insul. **26,** 258 (1991).

4. R. Hackam, IEEE Transactions on Dielectrics and Electrical Insulation **6,** 557 (1999).

5. M. Ieda, IEEE Transactions on Dielectrics and Electrical Insulation **21,** 793 (1986).

6. M. Lanagan, "Glass Ceramic Materials for Pulsed Power Capacitors," NSF Center for Dielectric Studies Meeting, Albuquerque, NM, May, 2004.

7. D. K. Dasgupta and K. Doughty, Thin Solid Films **158**, 93 (1988).

8. Y. Bai, Z. Y. Cheng, V. Bharti, H. S. Xu, and Q. M. Zhang, Appl. Phys. Lett. **76**, 3804 (2000).

9. Y. Rao, S. Ogitani, P. Kohl, and C. P. Wong, J. Appl. Polym. Sci. **83**, 1084 (2002).

10. Z. M. Dang, Y. H. Lin, and C. W. Nan, Adv. Mater. Weinheim, Ger. **15**, 1625 (2003).

11. C. Huang and Q. M. Zhang, Adv. Funct. Mater. **14**, 501 (2004).

12. C. Huang, Q. M. Zhang, J. Y. Li, and M. Rabeony, Appl. Phys. Lett. **87**, 182901 (2005).

13. T. J. Lewis, ''Nanometric Dielectrics,'' IEEE Trans. Dielectr. Electr. Insul., **1**, 812 (1994).

14. M. F. Frechette, M. Trudeu, H. D. Alamdari, S. Boily, Nanodielectrics, *IEEE Conf. Electr. Insul. Dielectr. Phenomena*, Kitchener, 2001, pp. 92-99.

15. J. K. Nelson, J. C. Fothergill, L.A. Dissado, and W. Peasgood, *IEEE Conf. Electr. Insul. Dielectr. Phenomena,* 2002, pp. 295-298.

16. Y. Cao and P. C. Irwin, *IEEE Conf. Electr. Insul. Dielectr. Phenomena*, Albuquerque, USA, 2003, pp. 116-119.

17. P. C. Irwin, Y. Cao, A. Bansal and L. S. Schadler, *IEEE Conf. Electr. Insul. Dielectr. Phenomena*, Albuquerque, USA, 2003, pp. 120-123.

18. B. Rangaranjan, B. Jones, T. Shrout, and M. Lanagan, J. Am. Ceram. Soc., **90,** 3 (2007).

19. C. T. Cheng, M. Lanagan, J. T. Lin, B. Jones, M. J. Pan, J. Mater. Res., **20,** 2 (2005).

20. McCauley J. W., Newnham R. E., and Randall, J. Am. Ceram. Soc., **81,** 979 (1998).

21. A. J. Moulson and J. M. Herbert, *Electroceramics*: *Materials, Properties, Applications* (2nd Edition John Wiley & Sons Limited, England, 2003), pp. 82-83.

22. R. E. Newnham, *Ann. Rev. Mat. Sci*., **16** 47 (1986).

23. D. Payne, "The Role of Internal Boundaries upon the Dielectric Properties of Polycrystalline Ferroelectric Materials," Ph.D. Thesis: The Pennsylvania State University (1973).

24. A. Sihvola, E*lectromagnetic Mixing Formulas and Applications* (IEE, London, UK, 1999).

25. O. F. Mossoti. "Discussione analitica sull'influenza che l'azione di un mezzo dielectrico ha sulla distribuzione dell'electtricita alla superfice di piu corpi electricdisseminati in ess," *Memorie di Matematica e di fisica della societa italiana dell science,* (Modena), 1850, XXIV, Parte Seconda, pp. 49-74.

26. R. J. E Clausius, R. J. E: "Die mechanische Behandlung de Electricitat," Abschinitt III F. Vieweg, Branschweig, 1879.

27. L. Lorenz,"Experimentale og theoretiske Undersoegelser over Legemernes Brydningsforhold", *Det Kongelige Danske Videnskabernes Selskabs Skrifter*, Naturvidenskabelig og mathematisk afde ling, 1869, Femte Raekke, Ottonde Bind, (8), pp. 205-248.

28. L. Lorenz, "Ueber die Refractionsconstante," *Annalen der Pphysik und Chemie,* 1880 **IX**, (9) pp. 70-103.

29. A. H. Lorentz," Ueber die Beziehung zwischen der Fortpflanzungsgeschwindigkeit des Lichtes und der Korperdichte," *Annalen der Physik und Chemie* 1880 IX, (4) pp. 641-665.

30. L. Rayleigh, "On the incidence of aerial and electric waves upon small obstacles in the form of ellipsoids or elliptic cylinders, and on the passage of electric waves through a circular aperture in a conducting screen," *Philosophical Magazine,* 1897, **44**, pp. 28-52.

31. J. C. Maxwell Garnett, “Colors in metal glass and metal films,” *Trans. Of the Royal Society,* (London), **CCIII**, 1904, pp.385-420.

32. D. A. G Bruggeman,“ Berechnun verschiedener physikalischer Konstanten von heterogenen Substanzen, I. Dielecktizitatskonstanten und Leitfahigkeiten der Mischkorper aus isotropen Substanzen,” *Annalen der Physik,*1935, Ser. 5, **24**, pp. 636-664.

33. T. C. Choy, *Effective Medium Theory, Principles and Applications* (Oxford University Press, Oxford, 1999).

34. G. W. Milton, *The Theory of Composites,* (Cambridge University Press, Oxford, 1999).

35. D. Bergman and D. Stroud, Solid State Phys. **46**, 147 (1992).

36. V. Myroshnychenko and C. Brosseau, J. Appl. Phys, **97**, 044101 (2005).

37. O. Weiner, Abh. Sachs.Akad.Wiss. 32:509 (1912).

38. D. F. Rushman, M. A. Striven, *Proc. Phys. Soc* **59**:1011 (1947).

39. D. Kingery, *Introduction to Ceramics,* (John Wiley and Sons, New York, 1960).

40. K. Lichtenecker, Phys. Z., **10**, 1005 (1909).

41. K. Wakino, T. Okada, N. Yoshida, and K. Tomono, J. Am. Ceram. Soc. **76,** 2588 (1993).

42. C. Brosseau and A. Beroual, Prog. Mater. Sci. 48, 373 (2003).

43. C. Ang, Z. Yu, R. Guo, and A. Bhalla, J. Appl. Phys. **93**, 3475 (2003).

44. A. H. Sihvola, and K.I. Nikoskinen, IEEE Trans. Geosco. Remote Sens. **38**, 1303 (2000).

45. B. Sareni, L. Krähenbühl, A. Beroual, and C. Brosseau J. Appl. Phys. **80**, 1688 (1996).

46. S. K. Patil and R. W. Schwartz, *12th US-Japan Seminar on Dielectric & Piezoelectric Ceramics*, Annapolis, MD, 2005, pp. 397 - 400.

47. B. Sareni, L. Krähenbühl, A. Beroual, and C. Brosseau, J. Appl. Phys. **81**, 2375 (1997).

48. B. Sareni, L. Krähenbühl, A. Beroual, and C. Brosseau, J. Appl. Phys. **80**, 4560 (1996).

49. A. Spanoudaki, Anna; R. Pelster, *Phys. Rev. B*: **64,** 064205 (2001).

50. M. Y. Koledintseva, J. Wu, J. Zhang, J. L. Drewniak, and K. N. Rozanov, in *Proc. IEEE Symp. Electromag. Compat.*, Santa Clara, CA, 2004, Vol. 1, pp. 309-314.

51. J. Avelin and A. Sihvola, Microwave and Optical Technology Letters, **32**, 1, (2002).

52. A. Lakhtakia, Microwave and Optical Technology Letters*.,* **17,** 4, (1998).

53. G. Goodman, R. C. Buchanan, and T. G. Reynolds, III *in Ceramic Materials for Electronics* 2nd Edition (Marcel Dekker Inc., New York, 1991) pp. 72.

54. Y. Cao, P. C. Irwin, K. Younsi, IEEE Trans. Dielectr. Electr. Insul.,**11**, 5, (2004).

55. K. Wu, T. Okamot, Y. Suzuoki, J. Appl. Phys., **98**, 114102, (2005).

56. J. J. O'Dwyer, *The Theory of Electrical Conduction and Breakdown in Solid Dielectrics,* Clarendon, Oxford, 1973.

57. P. D. Beale and P. M. Duxhury: Phys. Rev. B: Condensed Matter, **37**, 6, (1988).

58. T. Tomimura, N. Tanimoto, M. Hishida, S. Nakamura and T. Okamoto, *Proc. 7th Int. Conf. Properties and Applications of Dielectric Materials,* (2003), pp. 969-969.

59. P. K. Watson, IEEE Trans. Electr. Insul. **22**, 129 (1987).

60. G. Mazzanti, G. C. Montanari, and J. M. Alison, IEEE Trans. Electr. Insul. **10,** 187 (2003)

VITA

Sandeep Patil was born in Jalgaon, Maharashtra, India, on 4th February 1980. Sandeep graduated with Bachelor of Engineering degree in the field of Metallurgical Engineering from the College of Engineering, Pune in the year of 2001. Sandeep joined University of Missouri-Rolla (UMR) to pursue M.S. in Ceramic Engineering in fall of 2001. He worked on hydrothermal deposition of heteroepitaxial Barium Titanate thin films under the guidance of Dr. M. N. Rahaman. His Master's thesis resulted in 2 conference proceedings paper and 1 journal publication. After completion of his M.S. degree in 2003, he joined Dr. R. W. Schwartz to work as a Research Engineer on project jointly sponsored by UMR and Honeywell. Following this brief stint he worked with MO-Sci Corporation as a Process Engineer on fiber drawing process for development of composite materials. Sandeep also pursued internship opportunity with Brewer Science in the year of 2004 to work on bottom antireflective coating used in photolithography step of semiconductor manufacturing.

Sandeep joined Ph.D. program at UMR under the guidance of Dr. R. W. Schwartz in fall of 2004. His Ph.D. dissertation has resulted in 4 conference proceedings and submission of 3 journal publications. Sandeep received his Ph.D. in Materials Science & Engineering in May 2008. Sandeep will be joining Intel Corporation as a Senior Technology Development Engineer.